2018

REGULATION OF HCN CHANNEL FUNCTION BY DIRECT cAMP BINDING AND SINGLET OXYGEN

Vinaykumar Idikuda
Virginia Commonwealth University

REGULATION OF HCN CHANNEL FUNCTION BY DIRECT cAMP BINDING AND SINGLET OXYGEN

A dissertation submitted in partial fulfillment of the requirement for the degree of Doctor of Philosophy at Virginia Commonwealth University School of Medicine

By

Vinay Kumar Idikuda
M.S. Pharmaceutical Sciences, Idaho State University, 2011-2013
B.S, Pharmacy, Osmania University, 2007-2010

Director: Lei Zhou, Ph.D.
Associate Professor, Physiology and Biophysics

Virginia Commonwealth University
Richmond, Virginia
May 2018

Acknowledgements

I would like to take a moment and thank everyone who helped me in making my PhD journey a memorable one. Firstly, I would like to thank my advisor Dr. Zhou for his guidance and constant support and for being an outstanding mentor. Despite being a father of two children, the amount of time he spends in the lab speaks volumes of his work ethic. He was a constant source of inspiration for me to work hard. He would always be around if I had an issue with my experiments, I could go and knock his office door anytime of the day and ask even the most silliest of the questions. He always stressed the importance of being as careful as possible while doing experiments or in his own words "paying attention to detail". He emphasized the importance of spending time with my "electrophysiology rig" and knowing it inside-out or as Dr. Zhou would say "In order to juggle the ball, you need to first learn how to firmly hold it". These are the qualities that I learnt from him and I am sure they will help me at every stage of my career. He always encouraged me to think out of the box and to be independent as a scientist. I could go on and on but suffice to say that it was a great experience to get a PhD under him and I could not have asked for anything better.

I would like to thank my lab mates Jianbing Wang and Mengye Zhu for their support and friendship. They brought life into an otherwise very silent lab, and their energy and enthusiasm were infectious. I want to thank Nikhil Shah for being a great friend and lab-mate and also being a source inspiration for me in many ways. Let me thank Chris Waite, Hongtao Li, Weihua Gao and Jiao for all the help with the experiments. I would like to thank my department friends Sung Park for his support and also for teaching mammalian cell patch clamp, Guoqing Xiang for the constant support and friendship.

I would like to thank Late Dr. Louis DeFelice for his advice during the initial days of my PhD and always encouraging me to ask more questions. I would also like to thank Dr. Clive Baumgarten for his support in securing my “dissertation assistantship award”. I am grateful to Dr. Logothetis and Dr. John Bigbee for their constant care, support and guidance throughout. I would like to thank my PhD thesis committee members Dr. Liu, Dr. Akbarali and Dr. McQuiston for their constructive comments. I would like to express my deep sense of gratitude to Dr. Otilia Banji and Dr. David Banji for being my first mentors in science.

I am grateful for the support of my family, I could not have come this far without the never ending encouragement from them. Finally, I would like to thank a few more important people behind my success, my family away from home, and my friends - Satya, Kranthi, Naren, Sruthi, Tanya, Mauli, Bhanu, Ganesh and Rahul. All of them are not just my friends but fantastic human beings who had a great influence on my life. They have supported me, believed in me and never let me lose hope. Over the years, each of them have been part of some of the best moments of my life that I will cherish forever.

Table of Contents

LIST OF ABBREVIATIONS

ASD	Autism spectrum disorder
AchR	Acetyl choline receptor
bCNG	Brain cyclic nucleotide gated
cAMP	3', `5'-cyclic adenosine monophosphate
CALI	Chromophore assisted light inactivation
CAP	Catabolite activator protein
CCD	Charge coupled device
CCI	Chronic constriction injury
c-di-GMP	Cyclic di-guanylate
cDNA	Complimentary Deoxyribonucleic acid
CNG	Cyclic nucleotide gated ion channel
cGMP	Cyclic guanosine monophosphate
cRNA	Complimentary ribonucleic acid
DNA	Deoxyribonucleic acid
DRG	Dorsal root ganglion
EAG	Ether-a-go-go
EDTA	Ethylenediaminetetraacetic acid
EM	Electron microscopy
ESP	Excitatory postsynaptic potential
FDA	Food and Drug Administration
FITC	Fluorescein Isothiocyanate
GFP	Green fluorescent protein

HAC	Hyperpolarization activated channel
HEPES	(4-(2-hydroxyethyl)-1-piperazineethanesulfonic acid)
HH	Hodgkin and Huxley
ITC	Isothermal titration calorimetry
KO	Knockout
MAPK	Mitogen-activated protein kinase
mEPSC	miniature excitatory post synaptic currents
NADP	Nicotinamide adenine dinucleotide phosphate
NO	Nitric Oxide
NSNA	Non-stationary noise analysis
PDT	Photodynamic transformation
PGE2	Prostaglandin E2
PIP2	Phosphatidylinositol 4, 5-bisphosphate
Rab8	Ras related protein in brain
RMP	Resting membrane potential
RNA	Ribonucleic acid
ROS	Reactive oxygen species
RTN	Thalamic reticular neurons
SPR	Surface Plasmon resonance
SHANK3	SH3 and Ankyrin repeat domain 3
SA node	Sino atrial node
SEM	Standard error of mean
SNL	Spinal nerve ligation

TMD	Transmembrane domain
TPR	Tetratricopetide repeat
TRIP 8b	Tetratricopeptide containing rab8 interacting protein
TTL	Transistor-transistor logic
UVA	Ultraviolet A
VB	Ventro-basal
VGLUT	Vesicular glutamate transporter
WT	Wild type

List of Figures

Abstract

REGULATION OF HCN CHANNEL FUNCTION BY DIRECT cAMP BINDING AND SINGLET OXYGEN

By Vinay Kumar Idikuda, MS

A dissertation submitted in partial fulfillment of the requirement for the degree of Doctor of Philosophy at Virginia Commonwealth University School of Medicine**.**

Virginia Commonwealth University, 2018

Major Director: Lei Zhou, Ph.D., Associate Professor, Department of Physiology and Biophysics

Hyperpolarization-activated, cyclic-nucleotide gated ion channels (HCN channels) are activated by membrane hyperpolarization and modulated by cyclic nucleotides. HCN channels are important to maintain the resting membrane potential and input resistance in neurons and have important physiological functions in the brain and heart. Four mammalian HCN isoforms, HCN1-4, and the isoform cloned from sea urchin, spHCN, have been extensively studied. Among these, only spHCN channel shows a voltage dependent inactivation. Previous studies have shown that the ligand binding in mHCN2 channel is activity dependent: cAMP binding increases along with channel opening or channels in the open state have higher binding affinity for cAMP. But to date, information pertaining to the ligand binding to an inactivated ion channel or desensitized receptor is lacking. To address this gap, we used fluorescently labelled cAMP analogues in conjunction with patch clamp fluorometry (PCF) to study the ligand binding to the spHCN channel in various conformational states. We show that inactivated spHCN channel shows reduced binding affinity for cAMP, compared to that of the closed or open channel. Parallelly, we noticed significant changes to channel function when a combination of laser and photosensitizer was used to study

ligand binding. A reactive oxygen species called singlet oxygen has been confirmed to be the major player in this process. Both photo-dynamically generated and chemically generated singlet oxygen modifies spHCN channel by removing the inactivation. The effect of singlet oxygen on channel can be abolished by the mutation of a key histidine (H462) residue in the ion conducting pore. Taken together, these two projects expanded our understanding about the physicochemical nature of fluorophores from two aspects: (i) the release of photon as a valuable tool to study the conformational dynamics in proteins; (ii) the generation of singlet oxygen as an effective modulator of protein function.

CHAPTER 1
INTRODUCTION

A. Overview of HCN channels:

Hyperpolarization-activated, cyclic-nucleotide gated ion channels (HCN channels) belong to the superfamily of voltage gated potassium channels. In this superfamily, HCN channels along with cyclic nucleotide gated ion channels (CNG channels) and Ether-a-go-go channels (EAG channels) form the subgroup of cyclic nucleotide regulated ion channels. HCN channels have been identified in many vertebrates (e.g., human, mouse, rat, etc...) and invertebrates (sea urchins, cnidarians, lobsters, etc.), recently a prokaryotic channel with high sequence similarity to CNG and HCN channels has been identified. In the mammals, HCN channels are known to play important roles in cardiac and neuronal physiology. HCN channels are mixed cation conducting channels that open upon membrane hyperpolarization and in turn depolarize the membrane, hence they serve as a negative feedback mechanism. HCN channels are modulated by intracellular second messenger 3', 5' cyclic adenosine monophosphate (cAMP), which acts as co-agonist along with voltage to make the channel activation faster and more complete. This dual gating by voltage and ligand, makes HCN channels an exciting target molecule for the study of allosteric effects of voltage and ligand gating, two of the most intriguing questions in the ion channel biophysics.

B. I_f/I_h current - The historical perspective

In the late 1960's and 1970's, there was a quest to understand the electrical currents underlying the pace-making in the heart. The initial school of thought was that the pacemaker depolarization in the heart occurred concurrent to the decline in potassium conductance during a diastole (Weidmann, 1951). In 1969 Noble and Tsien showed that in sheep purkinje fibers, during a cardiac action potential, depolarization occurs due to a depletion of the outward potassium current [2] and

this was believed to be the pacemaker current or I_{k2}. This potassium current depletion hypothesis was further corroborated by various other studies. Although the experimental evidence for 'potassium-current' model proposed by Nobel and Tsien was strong enough, there were some apparent inexplicable observations in the above mentioned studies, such as (i) lack of a true current reversal at reversal potential (E_k) for potassium (ii) the disappearance of current in sodium [3,4] and (iii) presence of a biphasic current near E_k [4] Moreover, the decline in potassium currents would not lead to a depolarization per se. All these observations suggested that the pacemaker current may not be a pure potassium current.

The potassium current hypothesis prevailed until the hyperpolarization activated I_h or I_f cyclic nucleotide gated ion channel (HCN channels) mediated currents were first identified in rabbit sinoatrial nodal (SA node) cells. In 1976, a time dependent inward current was identified in the frog sinus-venosus preparations at voltages negative to the maximum diastolic potential, which was called the "pacemaker current" [5,6]. Similar observations were made in the rabbit SA node cells by Irisawa and Noma [7]. Although the ionic nature of this current that led to the "pacemaker potential" was still elusive at that point of time, the experimental evidence indicated that sodium could be one of the underlying charge carrier species. Later on, in 1979, Brown et al found an Ik_2 (inward or pacemaker current found in purkinje fibers) like component in the rabbit SA nodal preparation which was important not only for "pace-making" but also for modulation of heart rate by catecholamines like adrenaline [6,8,9]. For its funny behavior, this current component was called the funny current or I_f. Interestingly, striking similarities exist between the purkinje fiber Ik_2 and the SA nodal I_f. Similar to Ik_2, I_f also displayed a sodium dependence, could be blocked by Cesium (Cs^+) and showed a lack of reversal potential near the E_k (equilibrium potential for potassium) suggesting that these two were the same current component. Later on, the funny current I_f was also

termed as I_h (hyperpolarization activated currents) by Yanagihara and Irisawa [10]. Yet another feature that was notable with I_f was the modulation by adrenaline. Brown et al (1979) have identified that intracellular cAMP elevation by adrenaline causes the acceleration in the heart rate possibly by increasing I_f [9,11]. Conversely, muscarinic stimulation slows down the heart rate by decreasing the cAMP levels [12]. The modulation of I_h by hormones (adrenaline, acetylcholine and serotonin) was identified by many groups [13–15], and was speculated to be due to changes in intracellular cAMP concentration. Finally, using excised patches from cardiac pacemaker cells, DiFrancesco and Tortora showed that I_f current could be modulated directly by intracellular cAMP levels [16]. Thus, a possible molecular mechanism and putative substrate for heart rate modulation by autonomous nervous system was identified.

Subsequent to these findings, a reinterpretation of the Ik_2 current revealed that the pacemaker current was an inward activating current (based on the Cesium block of Ik_2). The reason for the misinterpretation was that this inward current was contaminated with the outward potassium current (mediated by inward rectifier potassium channels) which was active at the hyperpolarizing test voltages. The conundrum was finally solved by using Barium (a known inward rectifier blocker) to block the outward potassium current component and consequently resolving the underlying inward current component I_f/I_h. I_f was found to be a mixed cationic current with both sodium and potassium among the conducting species, this explained the observed sodium dependence of pacemaker current. The kinetics of I_f were found to be of hodgkin-huxley type [17,18]. Finally, I_f was established as the hyperpolarizing current that is activated during the diastolic depolarization. Nevertheless, the molecular substrate that led to this current was not known.

Despite many studies indicating the pace-making nature of the I_f, it is evident that I_f is not solely responsible for pace-making. Blocking I_f alone with cesium could not completely attenuate pace-

making ability of the heart, suggesting a much more complicated interplay of ionic currents during the cardiac action potential. I_f/I_h was also identified in various non-cardiac tissues as well. The most notable of these were the identification of I_h in the sensory neurons [19] and other neuronal cell types including thalamocortical neurons [20,21], photoreceptors of the salamanders [22] etc. Today, I_f has been identified in various tissues and is believed to play important roles in the oscillatory activity in the brain including regulation of sleep-wake cycle in the thalamus, pacemaking in the heart and cellular physiological functions such as the maintenance of resting membrane potential and input resistance in the neurons, etc. [23]. Some of these functions will be elaborated later in the text in detail. During the next decade with the advancement of molecular biology, the genes encoding the funny currents were unveiled and HCN channels were found to be the source or molecular correlate of I_f. This led to the opening of a new avenue at the molecular level for the study of structure and function of HCN channels.

C. The molecular identification of HCN channels:

In the late 1990's, HCN channel gene(s) have been cloned by several groups from various sources. It was initially identified from the mouse brain cDNA library using yeast two hybrid system and was named as *mBCNG-1* (Brain Cyclic nucleotide gated 1). Immunochemistry using mouse brain has shown that *BCNG-1* was expressed in the hippocampus, neocortex and cerebellar cortex [24]. Based on alignment of primary sequences *mBCNG*-1 was found to be part of a novel class of voltage gated potassium channels. Subsequently, partial cDNA clones of *mBCNG-2, 3, and 4* have also been reported and characterized by electrophysiology [25]. Simultaneously, Ludwig et al., have cloned three related genes encoding for hyperpolarization activated cation channel (HAC 1, 2, 3). Among these, HAC2 was identical to previously identified *BCNG-1*, and HAC-1 was identical to

BCNG-2 [26]. Later on, Ishii et al screened the rabbit SA node cDNA library and have cloned HAC-4 which showed 96% homology with *BCNG-3*. Electrophysiology studies have shown that HAC-4 was the molecular correlate of I_f or the pacemaker current in the heart [27]. Another notable contribution was the cloning of cDNA encoding SPIH from the cDNA library of sea urchin testes which had a sequence similarity with HCN channels and hence named as spHCN. Heterologous expression of spHCN channels in HEK cells produced a hyperpolarization dependent currents which were sensitive to intracellular cAMP [28], the biophysical properties of spHCN channel were strikingly unique. Later on, HCN channel homolog genes have been cloned from human brain, heart and testes [29,30] and also from other species including *Drosophila melanogaster* [31] and very recently from Aplysia [32]. To date four mammalian HCN channels have been cloned, HCN1-4. They show about 90% sequence similarity with each other. The cloning of HCN channel genes has given an opportunity to study the biophysical properties of the HCN channels at molecular level in heterologous expression systems.

D. The voltage-dependent gating in HCN channels

Four mammalian isoforms of HCN (1-4) channels have been characterized so far and have been studied very well in heterologous systems. Moreover, extensive biophysical characterization has also been done for the invertebrate spHCN channel owing to its unique properties. The biophysical properties of HCN channels are unique, with clear differences across different isoforms. The most unique property of HCN channels is the opening upon membrane hyperpolarization. Despite their structural similarity to potassium channels which are activated upon membrane depolarization, A closer look at the inward current that is generated by the activation of HCN channels, reveals two current components, one a fast activating but minor instantaneous current component (I_{inst}) and the other a slowly activating steady state hyperpolarizing current (I_h). The ionic nature and the physiological role of fast activating instantaneous current has been debatable and simultaneously very elusive. Further details regarding the instantaneous current are discussed in the next section of the text.

The half maximal activation voltage (the voltage potential at which half of the channel population is open) for HCN channels ranges from -70 to -100 mV. The wide range of activation voltages is a result of various factors including the source (native vs heterologous), the choice of expression system (oocytes, mammalian cell lines, stable cell lines) and the experimental conditions (pH, ionic composition of the solution, etc.).

The values of time constant of activation for the I_h were found to vary with different experimental conditions and the expression system from a few milliseconds to seconds. Among the mammalian HCN channels, HCN1 has fastest kinetics with HCN4 being the slowest [27,29,33] whereas, HCN2 and HCN3 show intermediary kinetics. For example, the heterologously expressed

hHCN2 and hHCN4 (both show expression in the SA node) in HEK cells show time constants of 179 ms and 679 ms, respectively in the absence of cAMP and at -140mV [33].

Stieber et al., have generated stably expressing HEK cell lines of all four human HCN isoforms and reported that the hHCN1 has the fastest kinetics whereas hHCN4 is the slowest isoform among the four, an observation that is consistent with the previous reports. The I_h from native cells like thalamocortical neurons, and SA nodal cells where HCN2 and HCN4 are the major isoforms, shows slower activation kinetics in the range of few hundreds of milliseconds, whereas in the hippocampal CA1 neurons, the T_{act} values were around 30 msec. Moreover, the kinetics were different between the currents from heterologous expression systems and the currents from the native systems [15,25,26,34]. This intrinsic variability and apparent inconsistency in kinetics could arise from the different subunit composition in native HCN channels and potential roles of auxiliary subunits and post translational modifications (glycosylation, phosphorylation, etc.). Heteromeric complex of HCN1 and HCN4 channels [35] and HCN 1 and HCN2 have also been reported [36].Taken together, the cellular microenvironment and subunit composition of HCN channels can result in differential biophysical properties that are tuned towards a specific function in a specific cell type.

E. The ligand-dependent gating in HCN channels: regulation by cyclic nucleotides

As mentioned earlier, in addition to membrane hyperpolarization, HCN channels can be regulated by direct binding of intracellular cyclic nucleotides like cAMP to the cyclic nucleotide binding domain (CNBD), which is a ligand-gating process and independent from the cyclic nucleotide dependent phosphorylation [16]. Membrane hyperpolarization alone is sufficient and necessary to open the HCN channels. However, the channel opening and kinetics can be fine-tuned depending

on the intracellular cAMP concentration. The CNBD is a highly conserved domain and has been previously identified in various other proteins including bacterial catabolite activating protein (CAP) [37], cGMP dependent protein kinases and the cyclic nucleotide gated ion channels (CNG channels). A highly conserved acidic arginine residue (R591 in mHCN2) in the CNBD is known to be critical for cyclic nucleotide binding[36,38–40]. Negatively charged phosphate group of the cyclic nucleotide interacts with this conserved residue[41,42]. Mutating R591 to an acidic glutamate residue (R591E) abolished cGMP effects in CNG channel and likewise abolished cAMP effect on HCN channel suggesting that the Arginine is critical for cAMP binding[36].

The extent and type of modulation that cAMP exerts on HCN channels is isoform specific. For example, in mammalian HCN, cAMP shifts the half maximal voltage of activation to positive voltages, whereas in the spHCN channel cAMP relieves the inactivation [25,28,43]. Among the four mammalian HCN isoforms, the effect of cAMP is variable. HCN2 and HCN4 show a strong response (about 12-15 mV shift toward positive voltages in V1/2) to cAMP compared to weak responses in HCN1 and HCN3 (2-7 mV shift).

The molecular mechanism underlying the cAMP dependent gating of HCN channels is intriguing. In the absence of cAMP, the CNBD of HCN channels has an auto-inhibitory effect on the channel opening. Binding of cAMP to this domain relieves this intrinsic inhibition and thereby facilitates channel opening by shifting the voltage dependent gating towards positive voltages. This inhibitory effect of CNBD has been elegantly demonstrated by deleting the CNBD from HCN1 and HCN2 (HCN1 ΔCNBD and HCN2 ΔCNBD), which led to activation at depolarized voltages (~24 mV). Furthermore, both the CNBD deletion mutants and the C-linker deletion mutants open upon hyperpolarization, suggesting that these domains are not essential elements of

voltage dependent gating in HCN channels but rather form an integral part of ligand dependent modulation of channel gating [44,45].

Experimental evidence suggests that the differences in the basic voltage dependent gating between HCN1 and HCN2 (HCN1 opening at more positive voltages than HCN2) are due to differences in the sequences in transmembrane core and the COOH terminus (both C-linker and CNBD together) of the channel together. Swapping the -COOH terminus and the transmembrane core of HCN1 with HCN2 could reverse the differences in basal voltage dependent gating between both the channels. On the other hand, differential sensitivity of different isoforms to cAMP is largely due to differences in COOH terminus. Swapping just the COOH terminus between HCN1 and HCN2 could completely reverse the cAMP effects on the channels[46]. These results were consistent with the observations from native HCN channels in SA nodal cells, where enzymatic digestion of the intracellular C-terminus using Pronase also accelerated the channel opening, suggesting that the C-terminus has an auto-inhibitory effect on the channel [47].

Cyclic Guanosine monophosphate (cGMP) can also facilitate HCN channel activation similar to that of cAMP. cGMP binding also shifts the activation curve of HCN2 by 12-14 mV towards positive voltages. Nevertheless, the apparent affinity for cAMP (K_a 0.6 M) was at least 10 fold greater compared to that of cGMP (K_a 6 µM) [26]. Surprisingly enough, cGMP does not activate currents in the spHCN channel [28]. cGMP binds to the channel through a hydrogen bond with a threonine residue in the beta roll of CNBD, the homologous residue in spHCN is a valine which explains the insensitivity of spHCN to cGMP [48,49]. Recently, it has been shown that cyclic dinucleotide (c-di-GMP and c-di-AMP) can bind to an allosteric site on the C-linker region of the channel and antagonize the effects of cAMP in hHCN4 and shift the half maximal voltage to the control levels [50]. However, surface plasmon resonance (SPR) studies and isothermal calorimetry

(ITC) with isolated C-linker/CNBD did not show any direct evidence of dinucleotide binding, suggesting that the intact/full length channel is probably necessary to see the allosteric effects of cyclic dinucleotides [51].

F. Ion selectivity and permeability of HCN channels:

Under physiological conditions, HCN channels are non-selective cation channels i.e., when they open, HCN channels permeate both sodium (Na^+) and potassium (K^+) into the cell [17,19,22,52]. Although HCN channels are mixed cation channels, they preferentially permeate K. The ratio of sodium to potassium permeability is approximately 1:3, this results in a reversal potential of -20 to -30 mV under physiological conditions [15,26,53–56]. Not just Na^+ and K^+, other monovalent cations like Lithium (Li^+), Rubidium (Rb^+) and Thallium (Tl^+) also permeate through the HCN channel albeit to a lesser extent [18,53,56]. On the contrary, large cation like Cesium (Cs^+) blocks the channel pore from the extracellular side[57].

The presence of potassium in the extracellular solution can affect the permeability of sodium. The lack of potassium in the extracellular solution shuts off sodium permeability and a corresponding increase in K results in an increased Na conductance suggesting a role of anomalous mole fraction i.e. interaction between the permeant ions [8,58,59]. Interestingly, there are some isolated reports of calcium entry through HCN channels in DRG neurons and rat ventricular myocytes. Furthermore, the entry of calcium through the HCN channels has been shown to be important for activity evoked neuronal secretion in the DRG neurons [60,61]. The precise physiological role(s) of calcium permeability is yet to be fully understood.

There have been many attempts to measure the single channel conductance of HCN channels. The challenge with HCN channels though is the small conductance and potentially slow

kinetics of opening and also significant run down in current with time making it difficult to get an accurate estimate [62]. Earlier studies on isolated SA nodal cells have estimated the conductance to be 0.97-1 pico-Siemens (pS). Adrenaline can increase the open probability of the channel [12]but not the single channel conductance. Similar values have been reported by various other studies. For example, ~ 0.67 pS for the native HCN channels in hippocampal neurons [63], 1.5pS for HCN2 channels heterologously expressed in HEK cells [64], 1.67 pS for HCN2 channels expressed in *Xenopus* oocytes [65] and -2.5 pS in HCN2 expressed in oocytes [66]. Interestingly, conductance values that are significantly higher than the values mentioned above have been reported by some studies. For example, heterologously expressed HCN channels in CHO cells have shown different conductance values when expressed alone (34.63 pS for HCN2, 17pS for HCN4) versus when expressed together (21pS for HCN2+ HCN4 together) suggesting a potential role for heteromerization. High conductance values have been reported from single channel recordings obtained from native tissues like atrial cardiomyocytes (~19 pS) [67] and 9.7 pS in hippocampal neurons [68] as well. Using a novel and interesting approach of employing patch clamp fluorometry to estimate single channel conductance in macro-patches, Chang et al have reported values of ~0.46 pS for HCN1, 1.46 pS for HCN2 and 0.8 pS for spHCN. These values were further confirmed using non stationary noise analysis (NSNA)[69]. Further studies are necessary to understand the underlying reasons for the vastly different values reported by various groups. One of the several reasons could be the tissue specific expression of some of the accessory proteins that can modulate the channel conductance. Some of the accessory proteins and modulating factors are discussed below.

G. Regulation of HCN channels by other factors:

In addition to voltage and cyclic nucleotides, the activity of HCN channels is modulated by other factors including pH, Phosphatidylinositol 4, 5-bisphosphate (PIP2), local microenvironment, etc., These factors add an extra layer of complexity by fine tuning the HCN channel activity as and when necessary to orchestrate a physiological process. Phosphatidylinositol 4, 5-bisphosphate (PIP2) is a membrane phospholipid that modulates activity of various ion channels including HCN channels [70–72]. Studies in both heterologously expressed HCN channels and native HCN channels have shown that PIP2 can right shift the activation curve (~20 mV shift in mammalian cells and ~10 mV shift in spHCN channel). Correspondingly, PIP2 presence slows down the channel activation and deactivation kinetics. The effects of PIP2 are independent of cAMP, although both cAMP effects and PIP2 effects seem to converge at some point mechanistically [73–76] Moreover, the rundown phenomenon observed in inside-out patches with HCN channels can be partly attributed to the loss of PIP2, because application of exogenous PIP2 delayed run down significantly but did not completely eliminate it [74].

HCN channels have are regulated by tyrosine kinases like Src kinases via phosphorylating Tyr476 in HCN2 and Tyr531 in HCN4. The Src kinase mediated modification has been shown in both native as well as recombinant HCN channels. Furthermore, Src directly interacts with HCN channels via SH3 domain [77–80]. Some Serine-Threonine kinases for example P38 MAP Kinase phosphorylate HCN channels [81] . Both these kinases shift the V0.5 to positive voltages but whether these observed effects are through direct phosphorylation is yet to be understood.

Protons are yet another important factor that regulates HCN channel function, pH mediated regulation of HCN channels has been first reported in thalamocortical neurons [82,83]. Intracellular alkaline pH potentiates the Ih current whereas acidification dampens it. Later on studies on HCN

channels heterologously expressed in HEK cells showed that an intracellular histidine (His 321, close to S4 region on cytosolic side) determined the pH sensitivity [84]. Intracellular acidification shifted V0.5 10 mV to hyperpolarized voltages whereas alkalization shifted the V0.5 10mV to depolarized voltages. In a more physiological context, activation of Ih in rat taste cells upon acidification of extracellular pH was reported. This was a proposed mechanism for sensing sour taste [85].

Among the co-factors that regulate HCN channels, the most significant one apart from PIP2 is TPR containing Rab8b interacting protein (TRIP8b). TRIP8b interacted with the C-terminus of HCN1 channel in yeast two hybrid screens [86]. Many splice variants of TRIP8b exist and have isoform specific effects on HCN channel function and expression. TRIP8b is expressed heavily in the layer V pyramidal neurons of neocortex and CA1 pyramidal neurons in hippocampus where they show a low to high expression gradient from soma to the dendrites [87,88]. Interestingly, HCN1 shows the same trend in expression gradient [86]. Furthermore, TRIP8b interacts with SNL tripeptide region of the channel and negatively regulates its expression[86,89]. Interestingly, similar to HCN1 knockout mice, brain specific knockout of TRIP8b produced an antidepressant effect in mice [90–92].

Recently, a neuronal scaffolding protein SH3 and Ankyrin repeat domain 3 (SHANK3) has been shown to modulate HCN channel expression in embryonic stem cell derived human neurons [93]. Loss of or mutations in Shank3 gene has been previously shown to be involved in the etiology of Autism spectrum disorder (ASD) and Phelan McDermid syndrome [94–98]. HCN channels co-immunoprecipitated with SHANK3 suggesting that they may be in physical contact with the Ankyrin repeat domain of SHANK3 protein. Loss of just a single copy (haploinsufficiency) of Shank3 gene was sufficient to affect HCN channel expression [93]. Recently, our lab has also shown

that two isoforms of Shank3 (Shank3A and Shank3C) when co-expressed with mHCN2 channel increase the expression of mHCN2 in *Xenopus* oocytes. Furthermore, Loss of a single copy of SHANK3 in mice led to an increase in excitatory/inhibitory balance ratio in ventro-basal (VB) thalamocortical neurons [99].

Apart from the factors mentioned above, HCN channels are regulated by extracellular chloride ions where lack of external chloride reduced the current amplitude significantly, an arginine residue is key to the binding of chloride to HCN channel on the extracellular side [100]. MiRP1 an auxiliary subunit increases the expression of HCN 1, 2 and 4 channel and has isoform specific effects on the activation kinetics [101–103] HCN1 interacts with cytoskeletal protein filamin A [104], whereas HCN4 was shown to interact with a lipid raft component Caveolin both these interactions modify the kinetics of the channel. Glycosylation has also been shown to affect the HCN channel subunit heteromerization [105,106] and surface expression [107]. Taken together, HCN channels are both spatially and temporally regulated by the tissue/cellular micro-environment according to the physiological need.

H. HCN channel structure:

Although the biophysical studies provided valuable mechanistic information, a holistic understanding can be gained with high resolution structural information. There have been many studies trying to tease out the structural details of the HCN channels and valuable information was also obtained. Recently, a high resolution 3.5 A Cryo-EM structure of full length human HCN1 channel was solved [108]. This has given the structural basis for understanding the unique biophysical properties of the HCN channel including gating and selectivity and ligand binding. Prior to the cryo-EM structure of the full length HCN1 channel, many groups have crystallized the C-terminal-

fragment (C-linker-CNBD) of various HCN channel isoforms [48–50,109]. The X-ray structure of the mHCN2 at 2.4A revealed that the C-Linker was primarily composed of six alpha helical domains connected through small loops. The CNBD on the other hand is made of alpha helical loops interspersed with an eight strand jelly roll like antiparallel β-roll. Addition of cAMP promoted the tetramerization of C-terminus. The cyclic nucleotides bind in the fold between the beta roll and the C-helix of the CNBD [48]. The phosphate group of the cAMP interacts with a conserved arginine residue in the β-roll [40,48], and the purine ring interacts with the C-helix, which correspond well with the functional studies. cAMP binds to the channel in anti-conformation, whereas cGMP binds the channel in Syn-conformation making a hydrogen bond with a threonine residue in the β-roll.

Similar structural arrangement was found in the crystal structure of HCN4 C-terminus solved at 2.4 A resolution and addition of cAMP promoted the tetramerization of HCN4 C-terminus similar to HCN2. Moreover, sequence alignment and mutational analysis has revealed a methionine residue (Met-572) between the β4 and β5 loops which was critical for stronger response of HCN2 to cAMP compared to HCN4 [109]. Following this, a comparative crystal structure analysis of cytosolic fragments of HCN1 (solved at 2.9A), HCN2 (solved at 2.3A) and HCN4 (solved at 2.5A) has shown that the HCN1 C-terminus tetramerizes at basal cAMP levels whereas HCN2 and HCN4 require saturating cAMP levels to tetramerize. These results suggest that HCN1 favors tetrameric form even in the apostate (absence of cAMP) which can at least in part explain the differential sensitivity of HCN isoforms to cAMP [50].

The cryo-EM structure of HCN1 channel has further confirmed the structure of the ligand binding pocket of the HCN channels which was consistent with the earlier studies. Moreover it appears that binding of cAMP leads to a rotation of CNBD to open the gate. As mentioned earlier, contrary to the other voltage gated potassium channels, HCN channels open upon membrane

hyperpolarization, the cryo EM structure of full length HCN1 shows that the S4 helix (voltage sensor) is unusually long which allows the S4-S5 linker in a depolarized state to contact C-linker and thereby forcing it to close the intracellular gate. In addition, the selectivity filter of HCN1 has only two ion binding sites due to a non-canonical confirmation thereby making it less selective compared to the KCsA channel with 4 ion binding sites [108].

I. Voltage-insensitive, instantaneous current (I_{inst}) conducted by HCN channels

In addition to the hyperpolarization-activated current, HCN channels also show a voltage independent component called instantaneous current. Native instantaneous HCN current (Iinst) was reported in some of the very early studies on these channels. The instantaneous component of HCN channels was observed in rod photoreceptors and was found to have an inward rectification as well as a potassium dependence. Both the components were found to be blocked by Cesium [58]. Subsequently, an instantaneous current component was reported in the interneurons of medicinal leech that could be blocked by cesium and sodium free saline [110]. I_{inst} was also observed in the rabbit SA nodal cells and initially was defined as the background current (I_b) or leak current [111]. An instantaneous current component was also reported in the rat midbrain dopaminergic neurons and could be blocked by Barium and Cesium by about 15-42% [55]. Notably, all these early observations were made in native tissues and there was a need to study the instantaneous current in heterologous systems to better understand its biophysics.

To this end, two studies have reported instantaneous current observed with mutant HCN2 channels expressed in heterologous systems. In the first study, the serine 306 residue in the voltage sensor (S4 domain) of mHCN2 was mutated to glutamine (S306Q), which resulted in a large instantaneous current. Usually the voltage sensor of voltage gated ion channels is made up of basic

residues. In mHCN2 channel a serine residue is present in between the 5th and 6th basic residues of S4 segment, rather than a basic residue in K_v channels. Mutation of this serine to a basic residue resulted in a complete loss of the channel function, which suggests that S306 is essential for channel [112,113]. In a subsequent study, the same group performed alanine scanning on the S4-S5 linker of mHCN2 and identified three residues to be important for channel gating. These three residues were mutated and among the mutants, Y331A was found to produce a large instantaneous current and also conducted an outward current even at potentials positive to the reversal potential [114]. Clearly, the channel's ability to close has been compromised in the mutant channel. Proenza et al. showed that instantaneous current can be found in both HCN2-GFP expressing HEK cells and also HEK cells just expressing GFP, but they should have different ion selectivity because of different reversal potentials. The study has also shown that the expression of instantaneous current was dependent on the chloride concentration and demonstrated a close correlation between Iinst and the expression of the HCN2 channel. One of the key findings of the study was the similar reversal potentials between Ih and Iinst (close to 16mV), suggesting that both these components are carried by the same channel and have similar ion selectivity [115].

In a study by Gary Yellen's group hinted that two distinct populations of HCN channels carry Iinst and Ih. Both spHCN and mHCN2 show a component of instantaneous current in heterologous expression systems. The instantaneous component of the current could be blocked by a known blocker of HCN channel ZD7288 at depolarizing voltages. Impressively, the blockade of the instantaneous component was immediate whereas the Ih reduction was progressive. This large difference in the blocking kinetics suggested that the instantaneous component of the current is carried by a distinct subset of channel populations. Nevertheless, the block of instantaneous current by pore blockers like Cesium suggests that the instantaneous current flows through the

same main conduction pathway as I_h [116]. It was also reported that the Iinst carried by spHCN could be modulated by cAMP but not the I_{inst} carried by mHCN2, which requires further clarification. Above all, the instantaneous current may be constitutively active at physiologically relevant voltages and might indeed play a major role in controlling cell excitability.

Recently, singlet oxygen (excited energy state of molecular oxygen) was shown to modify mHCN2 in a state-dependent manner. Singlet oxygen generated from photosensitizers (FITC-conjugated cAMP) modified mHCN2 channel in the open state, which leads to a substantial increase in the instantaneous current and a decrease in I_h, in addition to slowdown of the channel deactivation. Alanine replacement of a critical histidine (H432) near the intracellular gate in S6 abolished the effect of singlet oxygen, suggesting the possibility that this histidine residue is the target for singlet oxygen mediated modification and the key for generation of instantaneous current in the mouse HCN2 channel [117].

J. Physiological role of HCN channels- Insights from Knockout mouse models:

Early studies have shown that Ih isolated from neurons is a key determinant of the resting membrane potential (RMP) in neurons (Mayer & Westbrook, 1983; Pape, 1996). Negative feedback is a classic property of HCN channels [19,118]: it can oppose both depolarizing and hyperpolarizing voltage changes by activating at hyperpolarizing voltages and deactivating at depolarizing voltages. Blocking I_h with ZD7288 leads to a hyperpolarizing shift in the resting membrane potential in superior colliculus neurons [119], confirming the key role by Ih in maintaining the resting membrane potential. Yet another important role of Ih is to lower membrane input resistance. The presence of HCN channels on the dendrite will lead to dampening of the EPSPs by lowering the membrane resistance [120]. Thus, corresponding to the activation of HCN channels, a given current input leads to a smaller change in the membrane potential. Thus, Dual patch-clamp

recordings of the hippocampal CA1 neuron soma and dendrite shows a higher input resistance in dendrites compared with that of soma. This differential R_{input} correlated with the expression pattern of HCN channels (higher HCN expression in soma than dendrites. Blocking HCN channels with cesium increased the excitability of the neurons, most likely due to an increase in input resistance, and a larger voltage change with the same subthreshold current injections[87].

Tissue specific knockout mice are very useful tools for precise delineation of the physiological role of HCN channels especially its isoforms in the excitable tissues like neurons. Over the years, knockout models have provided valuable information regarding the isoform specific physiological role of the HCN channel. Neurons from various regions of the HCN1 knockout mice have shown a shift in the resting membrane potential towards the hyperpolarizing voltages. Concurrently, an increase in the input resistance was also observed. The lack of HCN1 isoform has altered the kinetics of I_h observed in the layer II stellate cells. Interestingly, HCN1 KO did not abolish Ih completely form these neurons, suggesting that in stellate cells, HCN1 is not the only isoform that is expressed and the I_h observed is a combination from different HCN channel isoforms. Furthermore, the altered kinetics in knockout neurons further strengthens this argument [118,121].

HCN1 knockout mice have been instrumental in our understanding of the role HCN channels play in motor learning. Global HCN1-/- have shown deficits in motor learning in visible platform water maze test and accelerating Rota-rod test, but these motor learning deficits were not observed when the HCN1 knockout was restricted just to the forebrain. These results suggest that the HCN1 expressed in the cerebellar purkinje cells is important for motor learning. Another hallmark observed in the mutant neurons was a decrease in the membrane conductance in the cerebellar purkinje cells (in other words an increase in R_{input}). The cells from the knockout mice

have an unstable membrane potential when hyperpolarization currents are injected. These findings reiterate that HCN channels regulate the resting membrane potential in the neurons by modulating the input resistance via a feedback mechanism. Consequently the membrane potential of the neurons from normal mice always stays closer to the threshold spike potential and also allows them to integrate the inhibitory and excitatory inputs [122].

Global HCN4 knockout was embryonically lethal in mice, which makes it harder to study the isoform specific role for HCN4. Embryonic lethality indicates the indispensable role of HCN4 in the generation of the cardiac rhythmic firing action potentials [123]. Nevertheless, this problem was circumvented by employing conditional knockouts by knocking down the HCN4 gene through a temporally controlled manner. It was striking that knocking out HCN4 only in the adults makes the mice viable.

Thalamo-cortical neurons from HCN2 global knockout mouse models show a shift in the resting membrane potential towards hyperpolarizing voltages. The HCN2-/- mice displayed whole body tremors. Neurons from these mice have shown an increased propensity for oscillations. The HCN2-/- neurons did not show the characteristic sag that is observed upon hyperpolarization in WT cells expressing HCN channels. Resting membrane potential in the thalamocortical neurons of HCN2-/- mice exhibited a hyperpolarizing shift of 12mV. On the other hand, cardiac specific HCN2 KO leads to the syndrome of sinus dysrhythmia [124], suggesting an important role by HCN2 in the cardiac tissue as well.

HCN's role in neuropathic pain: In addition to being a key component in regulating working memory and other essential neuronal functions in the central nervous system, HCN channels also play important roles in the peripheral nervous system. One of the most studied roles of HCN is the

sensation of neuropathic pain. In a spinal nerve ligation (SNL) rat model for the study of pain, an increase in the HCN magnitude was observed in injured neurons compared to that of the control neurons. This increase in Ih was attributed to the increase in the open probability of the HCN channels through a 10 mV shift towards depolarizing voltages in the voltage-dependent channel activation. Simultaneously, a 10 mV shift in depolarizing direction was observed in the resting membrane potential of SNL neurons, suggesting that HCN channels regulate the membrane potential in these neurons. Blocking the HCN channels by employing ZD7288 resulted in the allodynia which suggests that the increased Ih in the neurons forms the molecular basis for neuropathic pain. However, the specific HCN isoform that is responsible for the pain sensation could not be dissected due to non-discriminative blocking of all HCN isoforms by ZD7288 [125]. Subsequently, many other studies have employed blockers like cesium, Ivabradine and ZD72888 in various pain models and confirmed the importance of the HCN channels in sensing neuropathic pain [126–130].

HCN knockout mice helped identify the specific HCN isoform involved in mediating neuropathic pain. HCN2 tissue-specific KO from the nociceptive small somatosensory neurons caused a dramatic decrease in the pain related behavior such as the hind paw withdrawal test upon injection of formalin, PGE2, or Carrageenan and in chronic constriction injury model (CCI model), confirming the importance of HCN2 in regulating pain in peripheral neurons. In all these behavior tests, blocking of Ih by ZD7288 resulted in reduced pain sensation in the WT mice. A still mysterious observation was that the membrane properties of the mutant neurons remained unaltered [131].

In contrast to HCN2, the expression of HCN1 is more specific to the large somatosensory neurons. Specifically knocking out HCN1 from the large somatosensory neurons resulted in lack

of cold allodynia in mice. The response to heat and inflammatory allodynia was similar to the wild-type, suggesting a specific role for the HCN1 in mediating cold allodynia. Moreover, HCN1 plays an important role in regulating the frequency of action potential firing in small somatosensory neurons [132]. Pathological conditions inducing neuropathic pain lead to the activation of HCN (either by increased open probability or increased expression) in the peripheral neurons, which leads to depolarizing shift in RMP and thereby causing hyper excitability in these neurons.

Role in neurotransmitter vesicle filling: In a recent study, HCN channels were shown to regulate the vesicular neurotransmitter levels in a squid giant glutamatergic neuronal synapse, the calyx of held. The inward current through the HCN channel located in the dendritic terminal of presynaptic neurons (leads to an increase in the local sodium concentration in the presynaptic terminal. This sodium gradient is necessary for the vesicular transporters to replenish their proton gradient and thereby keep their VGLUT activated. Blocking the presynaptic HCN channels leads to small mEPSC whereas in the absence of the blocker the mEPSCs were larger on average [133]. Thus it would be interesting to see if similar to the giant squid system, in the mammalian nervous system, HCN channels are present on the presynaptic terminal could be regulating the neurotransmitter levels in the vesicles.

K. Overview of research directions:

1. cAMP-binding to spHCN channel:

A simple implementation of ligand-gating is that the open channel has a higher binding affinity for the ligand than the closed channel does, which had been confirmed in mammalian HCN2 channel. Different from mammalian HCN isoforms, the spHCN channel exhibits strong voltage-dependent inactivation which can be abolished by cAMP binding. Here we report that the inactivated spHCN channel shows reduced binding affinity for cAMP, compared to that of the closed channel. The decrease in cAMP binding is voltage-dependent but proceeds a much slower rate than the voltage sensor moves. A single point mutation near the channel's gate, F459L, abolishes inactivation and concurrently reverses the profile of cAMP binding. Finally, locked-open and locked-closed spHCN channel show opposite changes in cAMP binding. Taken together, our study demonstrates intricate communications between the channel's gate at different conformations and the ligand binding and thus provides new insights for channel inactivation.

2. Modification of spHCN (m2, CNG) channel by 1O2:

Photochemically or metabolically generated singlet oxygen ($^1O_2$) broadly reacts with macromolecules in the cell. Because of its short life time and working distance, $^1O_2$ holds the potential as an effective and precise tool at nanoscale for basic research and clinical practice. However, a working model for $^1O_2$ modification at the molecular level has been unavailable. Here we investigate the modification of spHCN channel by photochemically and chemically produced $^1O_2$. In a state-dependent manner, millisecond-long laser pulses transform the gating properties of the spHCN channel in complex with photosensitizers. Alanine replacement of a histidine residue located near the activation gate within the channel's pore abolishes key modification effects.

Application of a consortium of chemicals including $^1O_2$ scavengers or generators supports the involvement of $^1O_2$ and excludes other reactive oxygen species. This study provides a much-needed working model and essential insights for $^1O_2$–mediated modification of bio-macromolecules.

3. HCN-Shank3 interactions

Shank3, a scaffolding protein highly enriched in excitatory synapses, has been linked to neuropsychiatric disorders. Shank3 deficiency is known to cause impairments in synaptic transmission, but its effects on neuronal electrical properties remain unclear. Here we focus on thalamocortical neurons in the ventrobasal (VB) nucleus in the thalamus. We found that Shank3 deficiency leads to decreases in the expression of hyperpolarization-activated, cyclic-nucleotide-gated (HCN) channels. VB neurons from the Shank3 knockout mouse strain that displays more severe behavioral phenotypes demonstrate increased input resistance, negatively shifted resting membrane potential, and abnormal spike firing in both tonic and burst modes. Impressively, these changes closely resemble those of HCN2-/- VB neurons. Additionally, Shank3 deficiency impairs the excitatory/inhibitory balance in VB neurons but has a limited impact on the thalamic reticular (RTN) neurons. Therefore, HCN channelopathy plays an instructive and more direct causal role downstream from defective Shank3 in altering basic electrical properties of affect

CHAPTER 2

Materials and Methods:

Functional expression in Xenopus oocytes and electrophysiological characterization

The cDNA sequence encoding spHCN was generously provided by Drs. Reinhard Seifert and U. Benjamin Kaupp from the Center of Advanced European Studies and Research (caesar) (Gauss et al., 1998). The spHCN cDNA was inserted into the pGEM-HE vector for expression in Xenopus oocytes (Liman and Buck, 1994). mMessage machine (Ambion) was used for cRNA synthesis. 25-30 ng of cRNA encoding the spHCN channel was injected into each oocyte at stage VI. For patch-clamp recording, the electrode solution (extracellular) and bath solution (intracellular) were symmetrical and contained 110 KCl, 2 NaCl, 10 HEPES, and 1 EDTA (all in mM; pH 7.4 adjusted by KOH). A Model 2400 patch clamp amplifier (A-M Systems) was used in all voltage-clamp recordings. Current signals were filtered at 5 kHz and digitized by Digidata 1320A (Axon Instruments) at 10 kHz. The WinWCP program was used for data acquisition (http://spider.science.strath.ac.uk/sipbs/software_ses.htm). All experiments were carried out at room temperature.

For the voltage-dependent channel activation curve shown in Fig. 4B, the Boltzmann equation was used to fit the normalized Ih (tail) amplitudes:

〖Normalized I〗_h=A2+ (A1-A2)/ (1+exp ((V-V_□ (1/2))/slope))

, where A1 and A2 represent the peak and the offset values, respectively.

For the measurement of K+/Na+ selectivity, K+ ions in the bath solution (in contact with the intracellular side of the membrane) were replaced by Na+. Na+ in the pipette solution was also replaced by K+. We used the following equation to calculate the ratio of K+/Na+ selectivity:

$$\frac{P_K}{P_{Na}} = \frac{[Na]_o - \exp^{\frac{REV}{RT/F}} \cdot [Na]_i}{\exp^{\frac{REV}{RT/F}} \cdot [K]_i - [K]_o}$$

, where REV is the reversal potential. [K]i and $[Na]_O$ are both zero.

Patch-clamp fluorometry (PCF)

The PCF setup was assembled based on an Olympus IX71 microscope equipped with a 100X oil lens (Olympus, Plan N 100X, N.A. 1.25). A 473-nm Diode-pumped solid-state (DPSS) laser (Ultralasers Inc.) was used as the excitation light source. The following filter set was used for the recording of FITC fluorescence signal: exciter, D480/30; dichroic mirror, DC505LP; emitter, D510LP (Chroma Technology). Optical signals were detected by a 16-bit EMCCD camera (Cascade 1K by Photometrics Inc.). The laser light source, the CCD camera exposure, and the amplifier for patch-clamp recording were synchronized by TTL signals. As confirmed by histogram of the intensities of all pixels, the optical signals were collected within the linear range of the CCD camera. The ImageJ program was used to analyze the fluorescence images (Schneider et al., 2012).

For routine quantification of the intensity profile of the excitation light, a fluorescent plate (Chroma Technology Corp.) was mounted at the focal plane of the objective lens. The fluorescence image of the plate was recorded with the same optical configuration (473 nm laser, filter sets and dichroic mirror, EMCCD camera). Exposure time and gain of the camera were reduced to prevent saturation (65,535 for a 16-bit camera). The peak area of the excitation light was marked on the computer monitor to help position the membrane patch held within the glass pipette

Chemicals

All chemicals were ordered from Sigma-Aldrich or Fisher Scientific unless otherwise specifically noted. 8-FITC-cAMP (Fig. 1B) was ordered from Biolog.de (Catalog number: F002). The stock solution (1 mM) was made by adding 1 ml ddH2O to the vial containing 1 µmol 8-FITC-cAMP. The stock solution of Rose Bengal (1 mM) was made by adding ddH2O and stored as aliquots at -20oC. The stock solution was protested from light and diluted in the bath solution just prior to the experiments. Hydrogen peroxide was diluted in the bath solution to a final concentration of 10 mM just before experiments. Sodium hypochlorite was also diluted directly in the bath solution to obtain a final concentration of 10 mM. Both hydrogen peroxide and hypochlorite have to be freshly prepared just before experiments. Stock solution of Xanthine was made in NaOH and diluted to 5 mM in bath solution. 15 mU of Xanthine oxidase in bath solution was added through a separate perfusion line. Hydroxyl radical was generated by mixing 1 mM FeSO4 with 15 mM hydrogen peroxide which were also delivered to the recording chamber through separate perfusion lines. Stock solution of FeSO4 was prepared in ddH2O.

The experimental configuration for solution mixing is shown in Fig. 25. Briefly, the solutions containing H2O2 and ClO- were delivered through a double-barrel glass pipette. The tip of the glass pipette was positioned as a distance from the double-barrel as indicated. For the adjustment in the Z-dimension, the lower edge of the double barrel and the pipette tip are adjusted to the same focal plane.

List of related chemicals:

Rose Bengal (Fisher Scientific # R323-25);

H2O2 (Fisher scientific # BP2633);

Iron (II) sulfate heptahydrate (Acros Organics; #423731000);

Sodium hypochlorite (Alga Aesar; #3336936);

Potassium superoxide (Acros Organics; #AC325501000);

Xanthine (Alfa Aesar; #A1107714);

Xanthine oxidase (EMD Millipore; #68215110U).

STATISTICS

All statistical tests were performed using the OriginPro program. Error bars in the graph represent the amplitude of one standard error of the mean (SEM). Data were presented as mean ± SEM. Standard t-test was used to evaluate the statistical significance of the results of two independently collected pools of data (unpaired; for example, cAMP vs. FITC-cAMP) or a group of data before and after certain treatments (paired; for example, before and after laser pulses). $p > 0.05$ was considered as statistically non-significant (n.s.). ***, $p<0.001$; **, $p<0.01$; *, $p<0.05$.

CHAPTER 3

Inactivated channel gate allosterically reduces ligand binding in sea urchin spHCN channel

Vinay Idikuda, Weihua Gao, Zhuocheng Su, Qinglian Liu, and Lei Zhou
Department of Physiology and Biophysics, School of Medicine, Virginia Commonwealth University, Richmond, VA, USA

2.1 Abstract:

A simple interpretation of ligand-gating is that the open channel has a higher binding affinity for the ligand than the closed channel does, which had been confirmed in mammalian HCN2 channel. Different from mammalian HCN isoforms, the spHCN channel exhibits strong voltage-dependent inactivation which can be abolished by cAMP binding. Here, we report that the inactivated spHCN channel shows reduced binding affinity for cAMP, compared to that of the closed channel. The decrease in cAMP binding is voltage-dependent but proceeds a much slower rate than the voltage sensor moves. A single point mutation near the channel's gate, F459L, abolishes inactivation and concurrently reverses the profile of cAMP binding. Finally, locked-open and locked-closed spHCN channel show opposite changes in cAMP binding. Taken together, our study demonstrates intricate communications between the channel's gate at different conformations and the ligand binding and thus provides new insights for channel inactivation.

2.2 Introduction:

HCN channels encode the I_f or I_h current isolated from cardiac myocytes and neurons from the nervous systems. Four mammalian HCN isoforms, HCN1-HCN4, and the isoform cloned from sea urchin, spHCN, have been extensively studied. Both heterologously expressed and native HCN channels show unique biophysical properties including the channel activation upon membrane hyperpolarization, a mixture of permeability for K+ and Na+ ions, and the direct sensitivity to intracellular cAMP. At the cellular level, HCN channels contribute to the maintenance of resting membrane potential, synaptic transmission, dendritic signaling integration, action potential generation and propagation. At the physiological level, HCN channel are involved in maintenance of normal heart rate, working memory and motor learning, sensation of inflammatory and neuropathic pain etc.

The biophysics of HCN channels matches well the organization of the channel. Each functional HCN channel contains four subunits. Within each subunit, there is a transmembrane (TM) domain, homologous to that of the Kv channel, and the C-linker (CL) and the CNBD. Crystal structures of CL-CNBD provide an atomic view over the local interactions between cAMP and CNBD and the assembly of four protomers [48,50,109]. Recent publication of the cryo-EM structure of HCN1 provides the first atomic view over the whole molecule. These structures provide a static view over the conformations adopted by protein at certain energy minima and can be used as a solid and trustable starting point for computational and theoretical investigations. Undoubtedly, these structural advances are important step stones towards the understanding of the biophysics of ion channel.

But the allosteric communications between subdomains within the whole channel molecule in response to external stimuli, mainly voltage and ligand (cyclic nucleotides), remains to be

uncovered. To interpret the cAMP-dependent gating in HCN channels, we adopted the notion that the dynamic, state-dependent interaction between ligand and the full-length channel protein holds the key. This fits with the contemporary model for protein allostery, namely the pre-existing equilibrium or the conformation selection model, that incorporates both protein structure and protein dynamics in the interpretation of protein function [134–138]. Technically, we used the method of patch-clamp fluorometry (PCF) which enables simultaneous monitoring of the channel activity and the binding of the fluorescently labeled cAMP [139,140]. We showed that the open HCN2 channel binds to cAMP with higher affinity than the closed channel [141]. Moreover, by combining the evidence from an open channel blocker and mutagenesis experiments, we confirmed that the rotation of the last transmembrane segment S6 controls the opening of the gate and at the same time modulates the binding of cAMP through the coupling mechanism involving the elongated α-helix from S6 to the C-linker region [142].

spHCN shares key biophysical features with mammalian HCN channels [29] in the presence of cAMP. Researches on spHCN channel have provided important insights into the structure-function relationship of HCN channel, such as the movement of S4 during channel activation, the recording of gating current, the hysteresis or mode shift in channel gating, and the coupling between the gate and movement of S4 and the binding of cAMP [43,143–145] . However, in the absence of cAMP, spHCN goes through a fast voltage-dependent inactivation process, which has been attributed to a "slippery" coupling between the gate and the movement of the voltage sensor. Here we utilized the PCF method to investigate the binding of cAMP to inactivated spHCN channel and the intriguing allosteric communication between the gate and the cAMP binding domain.

2.3 Results:

Inactivated spHCN channel show decreased binding of cAMP than closed channel does

In the absence of cAMP, the spHCN channel briefly opens in response to hyperpolarizing voltage steps and then quickly inactivates (Fig. 1a, black trace). Application of cAMP removes this voltage-dependent inactivation and makes the spHCN channel behave like HCN1 or HCN2 channel (Fig. 1b and 1a red trace) [28]. To monitor the dynamic interaction between cAMP and the spHCN channel, we used 8-NBD-cAMP as the fluorescent marker. The fluorescence intensity of NBD increases over 90 folds upon the binding of 8-NBD-cAMP to the hydrophobic CNBD [141]. After the start of the optical recording, we consistently observed a rundown of the fluorescence intensity without applying any voltage-step (Fig. 1c), accompanied by a change in the channel behavior. Results using cAMP labelled with a different fluorophore, FITC-cAMP, show a similar trend of change upon a hyperpolarizing voltage step (Fig. 2). To circumvent the issue of photodynamic modification of the channel, we applied 2 mM of Trolox to the bath solution when collecting the results shown in c and d. Furthermore we used a photodynamic transformation resistant mutant spHCN channel, spHCN/H464A to further confirm the observation (Fig3).

Moreover, to ensure that most of the channels were in the closed state and to approach a more stable recording of the optical signal, we continued the optical recording and laser pulses at the holding potential of +80 mV for 7 seconds before applying the hyperpolarizing voltage step to -100 mV. Impressively, corresponding to the voltage-dependent channel inactivation, the binding of cAMP was significantly reduced compared to the cAMP binding to the closed channel (Fig. 1d). Following experiments were repeated in the absence of Trolox but still with the 8-second continuous optical recording at the holding potential of +80 mV. Averaged results show that upon

the voltage-step to -80 mV, the cAMP binding was decreased by 31.4 ± 0.02 % compared to that of the closed state. The process is time-dependent and can be fit by a single-exponential function (Fig. 1e). Conversely, corresponding to a depolarizing voltage step from -80 to +80 mV, the binding of cAMP recovered back to the level of the closed state (Fig. 1f). These changes in the binding of spHCN channel to cAMP in response to voltage steps are totally opposite to those of the mHCN2 channel, which does not show any voltage-dependent inactivation.

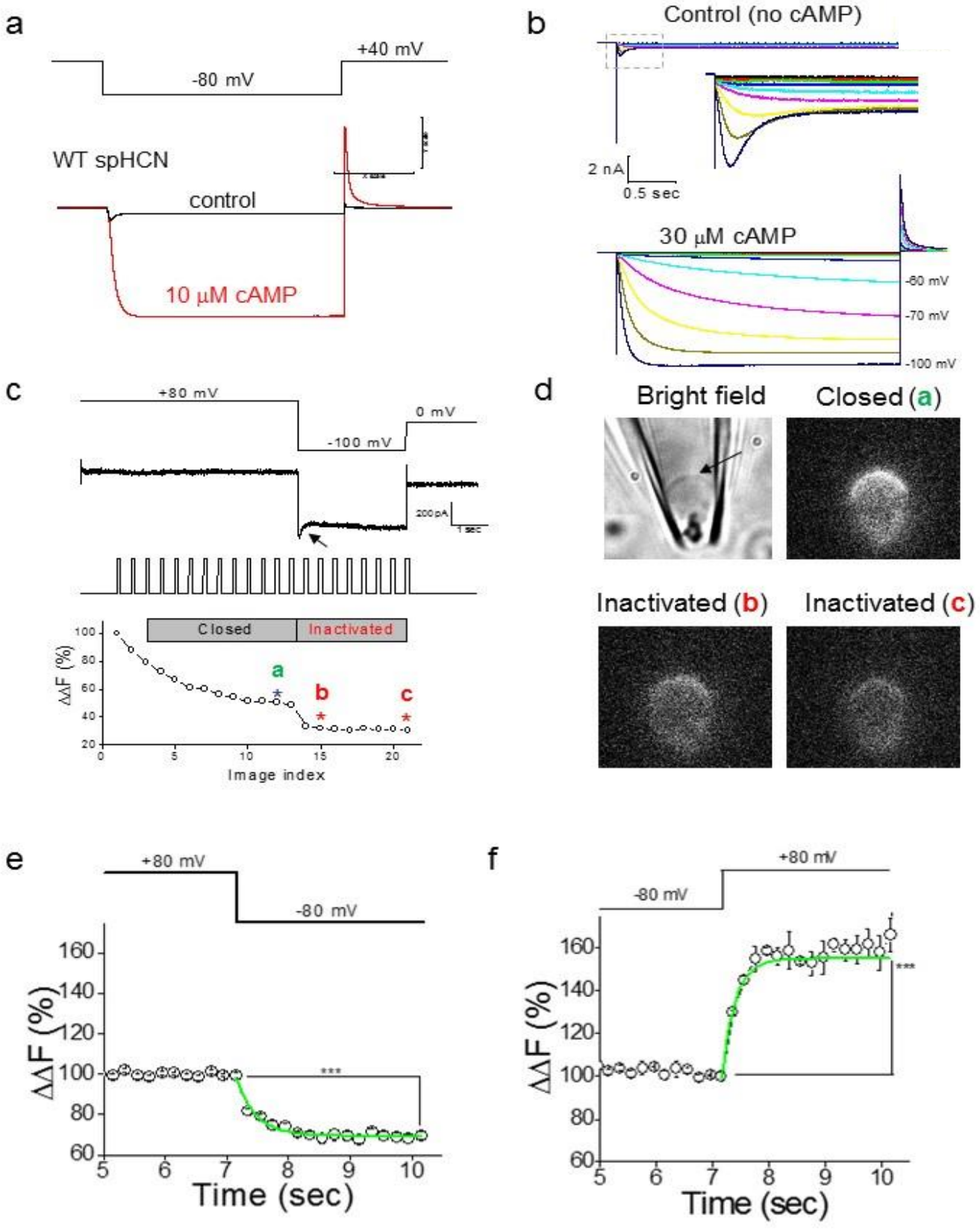
a
+40 mV
-80 mV
WT spHCN
control
10 µM cAMP
b
Control (no cAMP)
2 nA
0.5 sec
30 µM cAMP
-60 mV
-70 mV
-100 mV
c
+80 mV
0 mV
-100 mV
200 pA
1 sec
Closed
Inactivated
ΔΔF (%)
a
b
c
Image index
d
Bright field
Closed (a)
Inactivated (b)
Inactivated (c)
e
+80 mV
-80 mV
ΔΔF (%)
***
Time (sec)
f
+80 mV
-80 mV
ΔΔF (%)
***
Time (sec)

Fig. 1. Inactivated spHCN channel shows decreased binding of cAMP.

A. In response to a hyperpolarizing voltage step from +40 mV to -80 mV, the WT spHCN channel transiently opens and then inactivates (black trace; no cAMP). Adding cAMP (10 μM) to the bath solution abolishes the inactivation so that the channel shows typical voltage-dependent activation and deactivation (red). **B**. Current traces of the WT spHCN channel in response to a series of voltage steps from -40 to -130 mV at a -10 mV interval. Top, current traces in the absence of cAMP. Inset shows zoomed view over the transient activation-inactivation. Bottom, current traces with cAMP. **C**. Raw PCF results of the WT spHCN channel. 2 mM Trolox was added to bath solution to alleviate photo bleaching and photodynamic modification of the channel. The membrane patch was held at +80 mV for 6 seconds to stabilize the optical signal preceding the hyperpolarizing voltage step from +80 to -100 mV. From top to bottom, voltage protocol, current trace, laser pulses and exposure of fluorescence image collection, normalized fluorescence intensity. Three representative images (a, b, c) are shown in D. **D**. Raw fluorescence images of the membrane patch along the hyperpolarization voltage step (a, b, c in C). **E.** Averaged results showing the significant reduction in cAMP binding (31.4 ± 0.02%; paired t-test; $p<0.0001$; n=12) upon the voltage step from +80 to -80 mV. The fluorescence intensity was normalized to the averaged value of the last three images before the voltage step. Green trace shows the single-exponential fit of the time-dependent decrease in cAMP binding. **F** .Averaged results showing a significant recovery in cAMP binding (51.1 ± 0.03%; paired t-test; $p<0.0001$; n=12) upon the depolarization voltage step from -80 to +80 mV. Green trace shows the single-exponential fit of the time-dependent increase in cAMP binding.

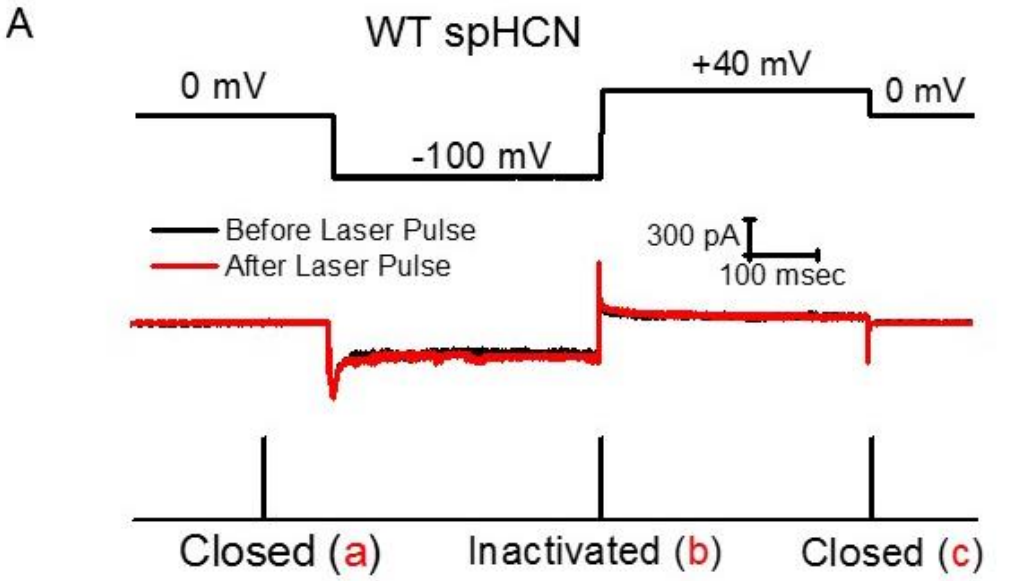
A
WT spHCN
0 mV
-100 mV
+40 mV
0 mV
Before Laser Pulse
After Laser Pulse
300 pA
100 msec
Closed (a)
Inactivated (b)
Closed (c)

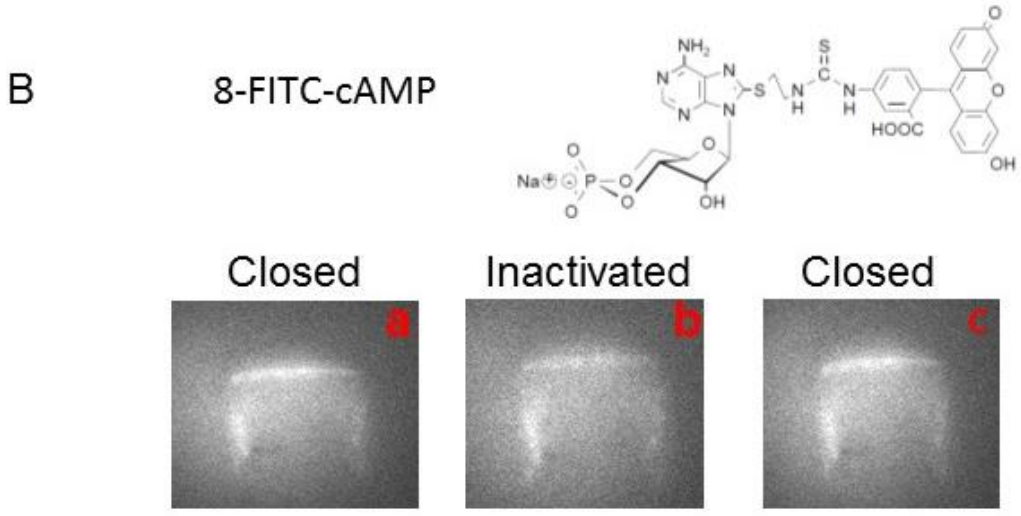
B
8-FITC-cAMP
Closed
Inactivated
Closed
a
b
c

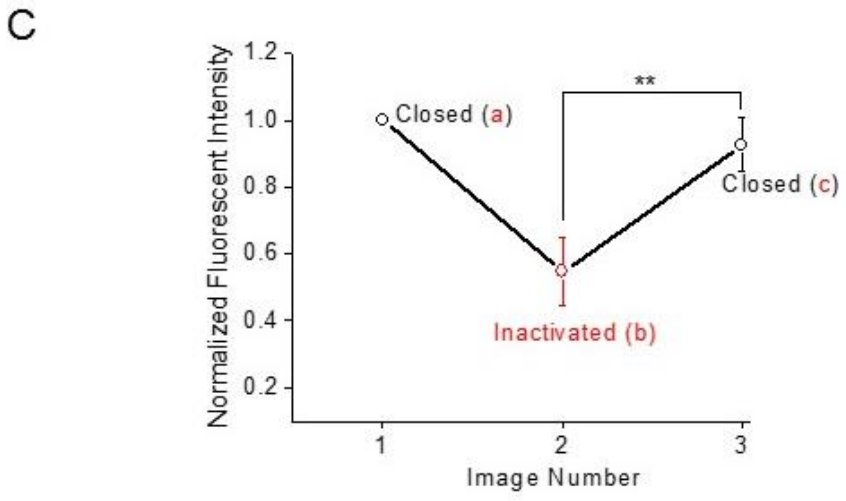
C
Normalized Fluorescent Intensity
1.2
1.0
0.8
0.6
0.4
0.2
1
2
3
Image Number
Closed (a)
Inactivated (b)
Closed (c)
**

Fig. 2. Measuring cAMP binding to the WT spHCN channel using FITC-cAMP, a fluorescent cAMP labeled with a different fluorophore than NBD-cAMP

A. Top, voltage protocol. Middle, current traces of the WT spHCN channel in the absence (black) and presence of 1 μM FITC-cAMP (red) in the bath solution. Bottom, protocol of laser pulse and image collection. 10 msec laser pulses were used to minimize the photodynamic modification of the spHCN channel. **B**. Top, chemical structure of the FITC-cAMP. Bottom, fluorescence images showing the binding of FITC-cAMP to the WT spHCN channel. Timing of the image collection is shown in A **C**. Normalized fluorescence intensities show a significant reduction in cAMP binding upon the voltage step from 0 mV to -100 mV and a significant recovery ($N=8$; $P<0.001$) of cAMP binding upon the voltage step from -100 to +40 mV. Fluorescence intensities were normalized to the value of image a.

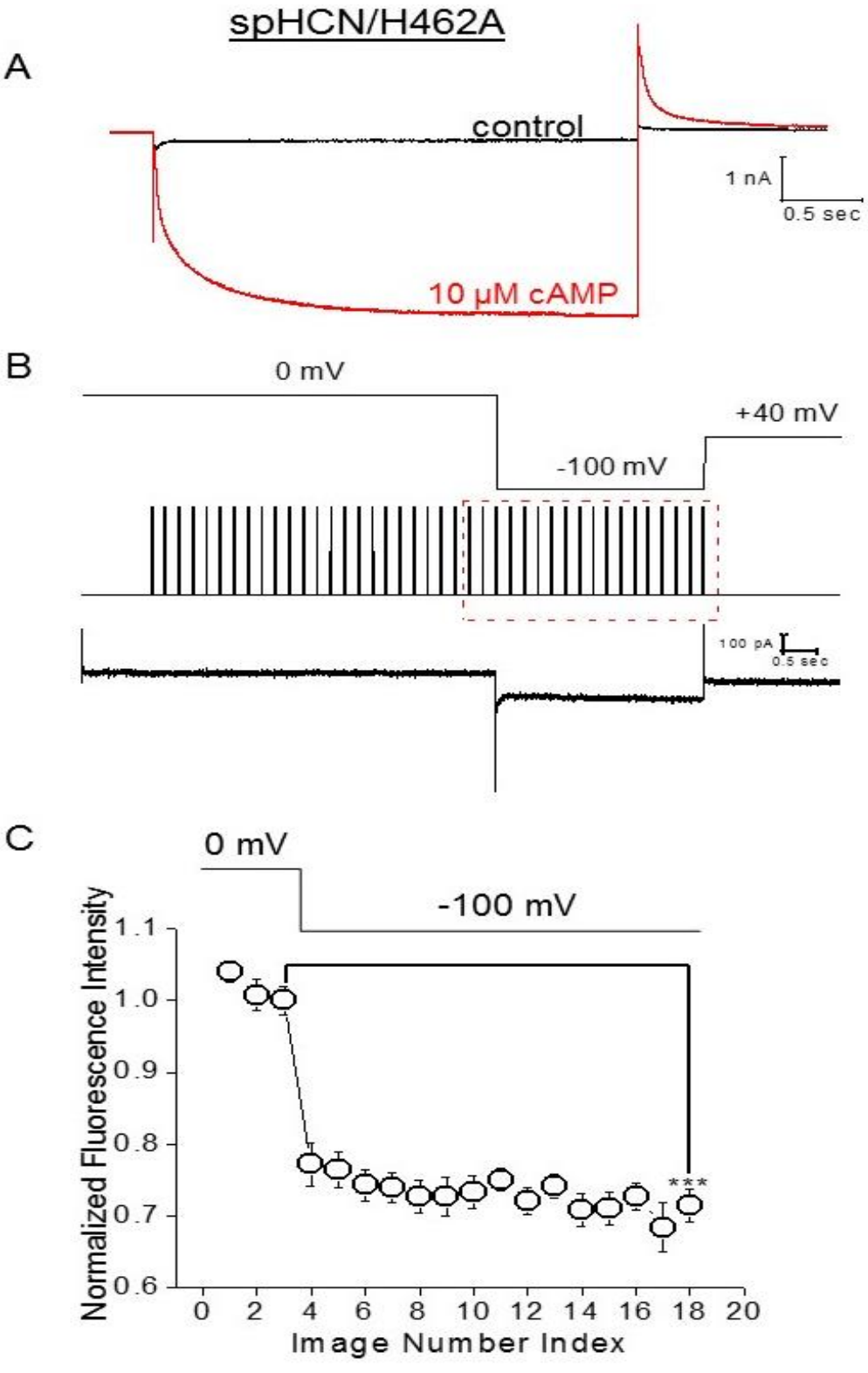
spHCN/H462A
A
control
1 nA
0.5 sec
10 μM cAMP
B
0 mV
+40 mV
-100 mV
100 pA
0.5 sec
C
0 mV
-100 mV
Normalized Fluorescence Intensity
1.1
1.0
0.9
0.8
0.7
0.6
***
0 2 4 6 8 10 12 14 16 18 20
Image Number Index

Fig. 3. Inactivated spHCN channel shows reduced binding of cAMP in a photodynamic effect resistant spHCN/H462A mutant.

A. In response to a hyperpolarizing step from 0 mV to -100 mV, spHCN/H462A channel transiently opens and then inactivates (black trace; no cAMP), Adding cAMP (10uM) abolishes the inactivation (red). **B.** Top, Voltage command and image collection protocol. Bottom, current traces of spHCN/H462A channel in the presence of 0.5 µM 8-NBD-cAMP to a hyperpolarizing voltage steps from 0mV to -100 mV. The current trace shows inactivation even after a series of laser pulses. **C.** Averaged results showing the reduction in cAMP binding upon the voltage step from 0 to -100 mV. A significant reduction (39.6±0.03%; N=8, $P<0.0001$) in fluorescent intensity was observed in response to a hyperpolarizing voltage step. The fluorescence intensity was normalized to the averaged value of the last three images before the voltage step.

F459L abolishes channel inactivation and reverses the decrease in cAMP binding to increase

F459 is located in the S6 of spHCN and aligned precisely to the first proline of the PVP motif in voltage-gated potassium channel. It was reported previously that replacing F459 by leucine (F459L) effectively abolished the voltage-dependent inactivation of spHCN. Noticeably, spHCN/F459L also responds to cAMP, reflected in the faster channel activation and slower channel deactivation (Fig. 4a, 4b). Next, we studied the binding of cAMP to spHCN/F459L mutant channel during the processes of activation (Fig. 4c) and deactivation (Fig. 4d), using the same protocol as used for the WT spHCN channel. Indeed, the binding of cAMP to spHCN/F459L channel was increased by 51.1 ± 0.03% during channel activation, in contrast to the decrease in cAMP binding observed in the WT spHCN channel (Fig. 4e). In contrast, cAMP binding decreased (34.78 ± 0.03 %) during the deactivation of spHCN/F459L (Fig. 4f), comparable to that of mHCN2 channel but again opposite to that of WT spHCN channel. Thus, the F459L mutation by itself makes the spHCN channel behave just like mHCN2, in the aspects of voltage-dependent activation in the absence of cAMP and the dynamic increase in cAMP binding during channel activation.

For both WT spHCN and spHCN/F459L channels, the time course of the changes in cAMP binding in response to voltage can be fit with a single exponential function (Fig. 5; Fig. 6). For the WT spHCN channel, corresponding to more negative hyperpolarizing voltage steps, the time constant of the decrease in cAMP binding decreases by ~3 folds, from 3.02 ± 0.21 seconds at -60 mV to 1.075 ± 0.19 seconds at -120 mV, which supports the decrease in cAMP binding as a voltage-driven process. As indicated by the value of $\Delta\Delta F$, the relative decrease in cAMP binding reaches a plateau at the voltage of -80 mV. For the spHCN/F459L channel, although the direction of the change in cAMP binding is opposite to that of the WT channel, the time constant of the change in cAMP binding is also voltage-dependent: from 6.96 ± 0.94 seconds at -60 mV to 4.14 ±

0.89 seconds at -120 mV. Again, the relative increase in cAMP binding reaches a plateau at the voltage of -80 mV. Noticeably, the absolute value of the time-constants of cAMP binding are in seconds, much longer than that of the movement of voltage sensor which largely finishes within 50 msec after the voltage step [146].

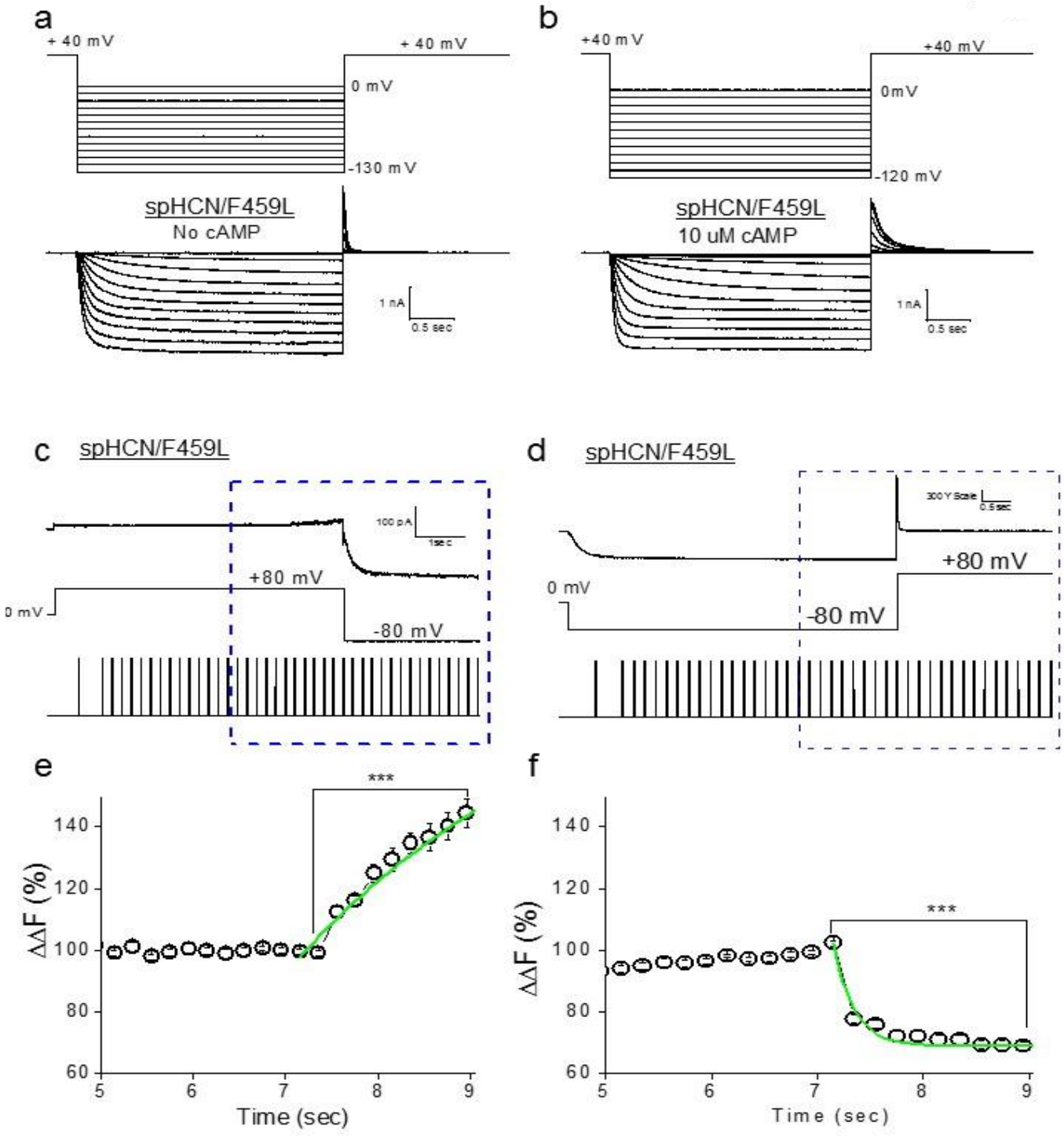
a
+ 40 mV
+ 40 mV
0 mV
-130 mV
spHCN/F459L
No cAMP
1 nA
0.5 sec
b
+40 mV
+40 mV
0mV
-120 mV
spHCN/F459L
10 uM cAMP
1 nA
0.5 sec
c
spHCN/F459L
100 pA
1sec
+80 mV
0 mV
-80 mV
d
spHCN/F459L
300 Y Scale
0.5sec
+80 mV
0 mV
-80 mV
e
***
ΔΔF (%)
140
120
100
80
60
5
6
7
8
9
Time (sec)
f
***
ΔΔF (%)
140
120
100
80
60
5
6
7
8
9
Time (sec)

Fig. 4. A single point mutation in S6, F459L, abolishes the channel inactivation and reverses the decrease in cAMP binding upon membrane hyperpolarization.

A. Current traces of the spHCN/F459L mutant channel recorded in response to a series of hyperpolarization voltage steps (no cAMP). **B**. Current traces of the spHCN/F459L channel recorded in the presence of 10 µM cAMP. Notice the changes in channel kinetics (faster activation and slower deactivation) compared to the traces shown in A. **C**. Top, current traces of spHCN/F459L in response to the hyperpolarization voltage step from +80 to -80 mV. To approach more stable optical recording results, laser pulses and image collection were started before the hyperpolarization voltage step. Bottom, averaged results corresponding to the dashed blue box shown in C indicate a significant increase upon the voltage step from +80 to -80 mV. (58.4 ± 0.05%; paired t-test; $p<0.0001$; n=12) in ΔΔF. **D**. Top, current traces of spHCN/F459L in response to the depolarization voltage step from -80 to +80 mV**. E and F**. Averaged results corresponding to the dashed blue box shown in D indicate a significant decrease in ΔΔF upon the voltage step from -80 to +80 mV (34.78 ± 0.03%; paired t-test; $p<0.0001$, n=12).

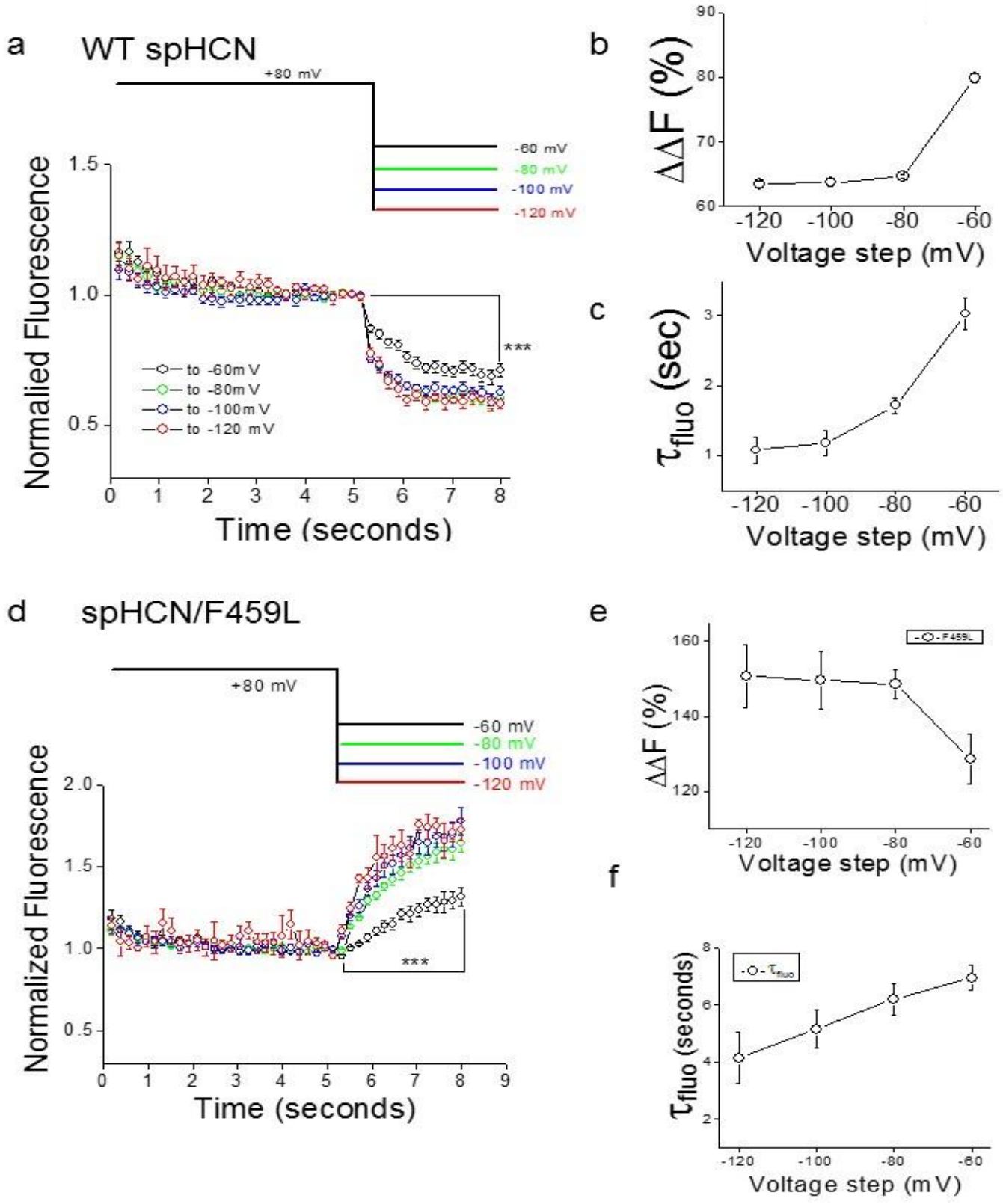
a
WT spHCN
+80 mV
-60 mV
-80 mV
-100 mV
-120 mV
Normalied Fluorescence
1.5
1.0
0.5
0
1
2
3
4
5
6
7
8
Time (seconds)
***
to -60mV
to -80mV
to -100mV
to -120 mV
b
ΔΔF (%)
90
80
70
60
-120
-100
-80
-60
Voltage step (mV)
c
τfluo (sec)
3
2
1
-120
-100
-80
-60
Voltage step (mV)
d
spHCN/F459L
+80 mV
-60 mV
-80 mV
-100 mV
-120 mV
Normalized Fluorescence
2.0
1.5
1.0
0.5
0
1
2
3
4
5
6
7
8
9
Time (seconds)
***
e
ΔΔF (%)
160
140
120
-120
-100
-80
-60
Voltage step (mV)
F459L
f
τfluo (seconds)
8
6
4
2
-120
-100
-80
-60
Voltage step (mV)
τfluo

Fig. 5. Comparing the decrease (WT spHCN) or increase (spHCN/F459L) in cAMP binding in response to the same set of hyperpolarization voltage steps.

A. The membrane patches were held at +80 mV for 5 seconds before the application of hyperpolarization voltage steps from -60 to -120 mV at a -20 mV interval. Fluorescence intensities for each patch were normalized to the value of the last three images just before the voltage steps. At -60mV, paired t-test: $p<0.0001$, n=12. **B**. Percentage of the decreases in fluorescence intensity vs. hyperpolarization voltage steps. Averaged results of the WT spHCN channel shown in A are used in the calculation. **C**. Time constant of the decrease in fluorescence intensity of the WT spHCN channel vs. hyperpolarization voltage steps. The profiles of the decrease in fluorescence intensity after the hyperpolarization voltage steps shown in A were fitted by a single exponential function. **D.** Normalized fluorescence intensity for the spHCN/F459L mutant channel. At -60mV, paired t-test: $p<0.0001$, n=13**. E.** Percentage of the increases in fluorescence intensity of the spHCN/H462A mutant channel vs. hyperpolarization voltage steps. Averaged results shown in D are used in the calculation**. F.** Time constant of the increase in fluorescence intensity of the spHCN/H462A channel vs. hyperpolarization voltage steps. The profiles of the increase in fluorescence intensity after the hyperpolarization voltage steps shown in D were fitted by a single exponential function.

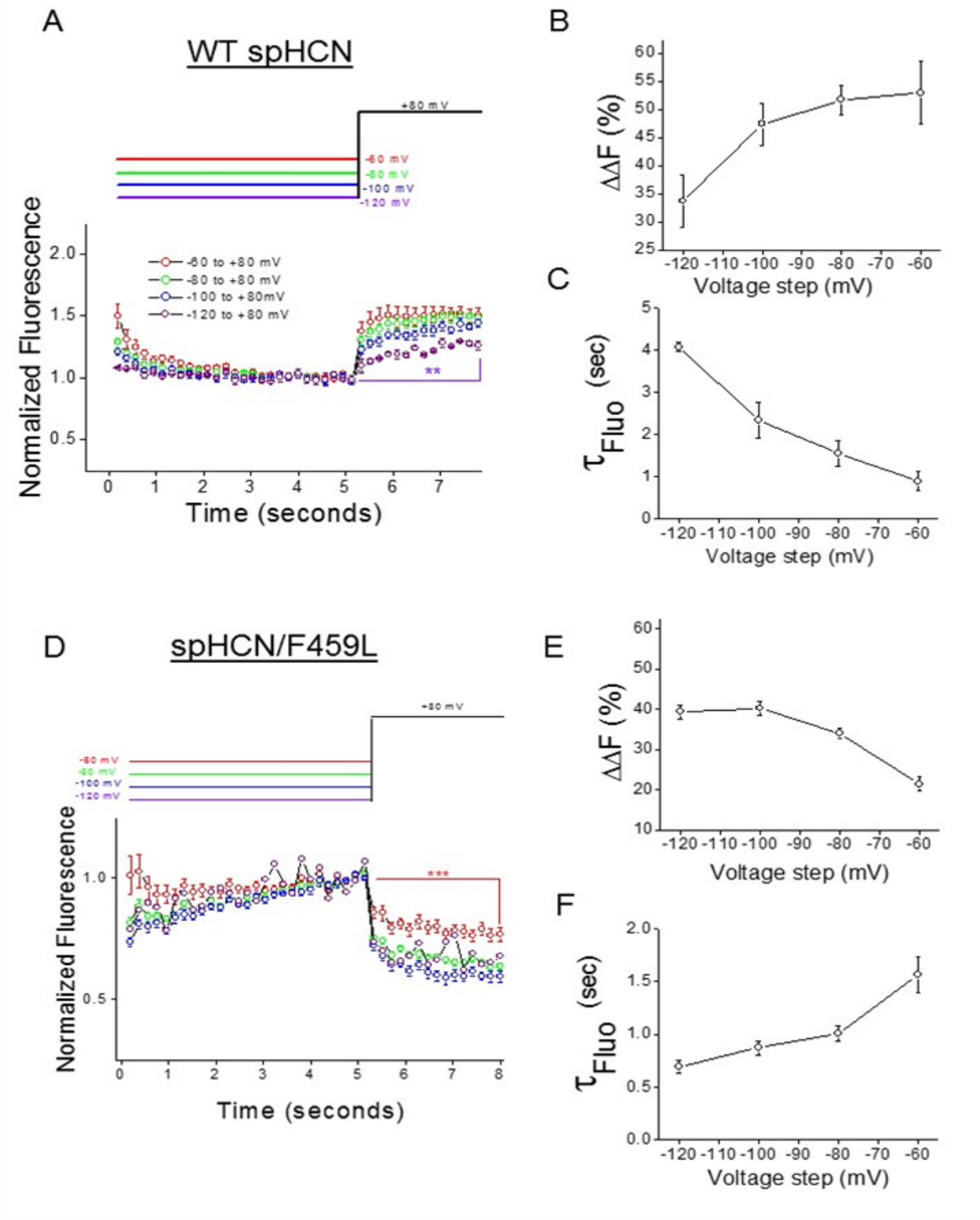
A
WT spHCN
+80 mV
-60 mV
-80 mV
-100 mV
-120 mV
-60 to +80 mV
-80 to +80 mV
-100 to +80mV
-120 to +80 mV
**
Normalized Fluorescence
Time (seconds)
B
ΔΔF (%)
Voltage step (mV)
C
τFluo (sec)
Voltage step (mV)
D
spHCN/F459L
+80 mV
-60 mV
-80 mV
-100 mV
-120 mV
***
Normalized Fluorescence
Time (seconds)
E
ΔΔF (%)
Voltage step (mV)
F
τFluo (sec)
Voltage step (mV)

Fig. 6. Comparing the increase (WT spHCN) or decrease (spHCN/F459L) in cAMP binding in response to the same set of depolarization voltage steps.

A. The membrane patches were held at hyperpolarized potentials from -60 to -120 mV for 5 seconds before the application of the depolarization voltage step to +80 mV. Fluorescence intensities for each patch were normalized to the value of the last three images just before the voltage steps. **B**. Percentage of the increases in fluorescence intensity vs. hyperpolarized holding potentials. Averaged results of the WT spHCN channel shown in A are used in the calculation. **C**. Time constant of the increase in fluorescence intensity of the WT spHCN channel vs. hyperpolarized holding potentials. The profiles of the increase in fluorescence intensity after the depolarization voltage step shown in A were fitted by a single exponential function **D.** Normalized fluorescence intensity for the spHCN/F459L mutant channel. **E.** Percentage of the decreases in fluorescence intensity of the spHCN/H462A mutant channel vs. hyperpolarized holding potentials. Averaged results shown in D are used in the calculation. **F.** Time constant of the decrease in the fluorescence intensity of the spHCN/H462A channel vs. hyperpolarized holding potentials. The profiles of the decreases in fluorescence intensity after the depolarization voltage step shown in D were fitted by a single exponential function**.**

ZD7288 but not Cs blocked the decrease in cAMP binding to inactivated spHCN channel

Since F459 is located in the S6 and close to the activation gate in spHCN channel, the above results of cAMP binding suggest that the movement of the gate might be allosterically coupled to the binding of cAMP. Previously, we had investigated such a mechanism for mHCN2 channel [142]. To introduce local structural perturbations in the vicinity of the activation gate, we used a specific HCN channel blocker, ZD7288, which is a commonly used blocker for HCN channels [147]. Previous studies have mapped the binding site of ZD7288 to the inner activation gate in the S6 of spHCN channel [43,148,149]. To probe any putative allosteric effects between the movement of the gate and cAMP binding, we applied 60 μM ZD to the bath solution of excised patches and measured the profile of cAMP binding in response to hyperpolarizing voltage steps (Fig 7a). Indeed, in the presence of ZD7288, the reduction in cAMP binding was significantly dampened (~10% with ZD7288 vs. ~40% in the absence of ZD7288 at the voltage of -80 mV (Fig. 7b and 7c).

Other than ZD7288, Cs+ in the milli-molar range is another popularly used blocker for HCN channels [57,150]. The binding site for Cs+ has been mapped to the region near the extracellular opening of the ion conducting pore [151,152]. But Cs+ needs to be applied from the extracellular side so that we added 2 mM Cs+ to the pipette solution, which is in contact with the extracellular side of the membrane. Opposite to the observation with ZD728 8, no apparent changes in the profile of cAMP binding was observed (Fig. 7e and 7f). These observations strengthened the notion that the movement of the inner activation gate is allosterically coupled to the binding of cAMP to the binding domain.

Locked-open and locked-close spHCN channels show opposite changes in cAMP binding

In spHCN channel, inactivation occurs via the closure of the same activation gate near S6 [43]. The decrease in the cAMP binding in spHCN channel could be a direct consequence of this rapid re-

closure of the gate. Moreover, we need to establish the relative binding affinity to cAMP between closed and open spHCN channel. To address these questions, we adopted the strategy of "locking" the spHCN channel specifically in the open or closed state though applying Cd2+ to cysteine-replacement mutant channels (spHCN/H462C-L466C for locked open or spHCN/H462Y-Q468C for locked closed) [148,153] (Fig. 8a, 8b). For the WT channel, cAMP is required to maintain the close-to-normal open state in the presence of 1µM Cd2+ (on top of cAMP) (Fig. 8c). For the lock-open or lock-closed channel, exposure to Cd2+ traps the channel either in the open or closed state, in the absence of cAMP (Fig. 8d & 8e).

Next, we investigated the binding of cAMP to the lock-open or lock-closed channel. Because of the instability of the membrane seal in the presence of Cd2+ and also to avoid photo bleaching of the dye, we started from a simple protocol of collecting three images along the -100 mV voltage step, before and after application of Cd2+ (Fig. 9a). For the WT spHCN channel, we observed a decrease in cAMP binding during the -100 mV voltage step and some recovery upon the voltage-step back to 0 mV, before and after exposure to 1 µM Cd2+. Impressively, for the lock-open channel, exposure to 1 µM Cd2+ switched the direction of the change in cAMP binding from decrease to increase (Fig. 9b). In contrast, for the lock-close channel, application of 2 µM Cd2+ locked the channels in closed state but did not change the decrease in cAMP binding (9d and 9e). Similar changes in cAMP binding were observed when we used a long duration pulse protocol (Fig 10).These results provide further support for the allosteric communication between the status of the activation gate and the binding of cAMP to the binding domain.

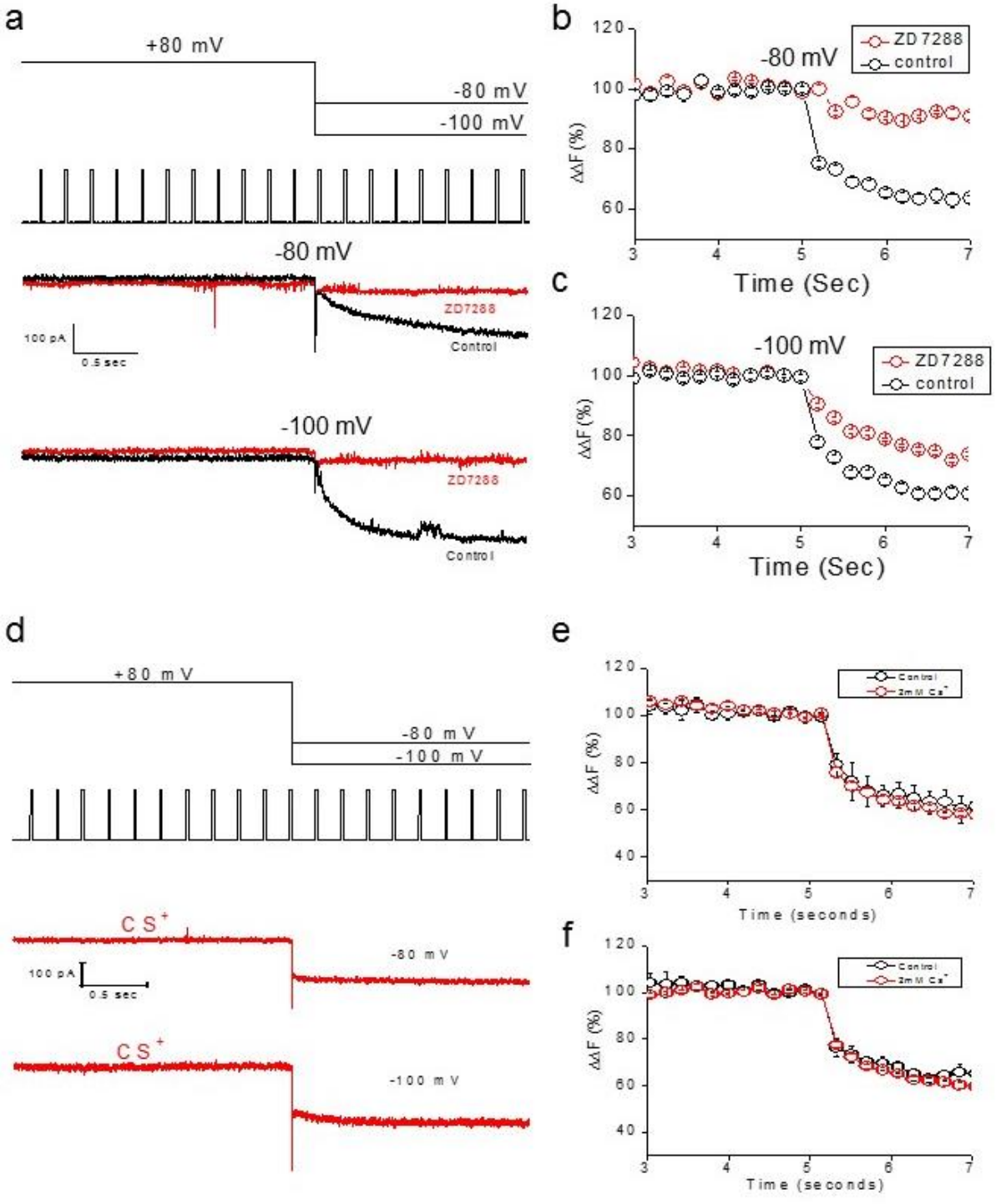
a
+80 mV
-80 mV
-100 mV
-80 mV
ZD7288
Control
100 pA
0.5 sec
-100 mV
ZD7288
Control
b
-80 mV
ZD 7288
control
ΔΔF (%)
Time (Sec)
c
-100 mV
ZD7288
control
ΔΔF (%)
Time (Sec)
d
+80 mV
-80 mV
-100 mV
CS+
100 pA
0.5 sec
-80 mV
CS+
-100 mV
e
Control
2mM Ca2+
ΔΔF (%)
Time (seconds)
f
Control
2mM Ca2+
ΔΔF (%)
Time (seconds)

Fig. 7. Both ZD7288 and Cs+ can block the spHCN current but only ZD7288 affects the binding of cAMP.

A. ZD7288 blocks the currents of the WT spHCN channel. Top, voltage step, laser pulse, and image collection protocol. Bottom, current traces before (black) and after (red) 60 μM ZD7288. **B**. Normalized fluorescence intensity before (black) and after (red) ZD7288 application. Voltage step, +80 to -80 mV. **C**. Normalized fluorescence intensity before (black) and after (red) ZD7288 application. Voltage step, +80 to -100 mV. **D.** 2 mM Cs+ was added to the pipette solution to block the WT spHCN current from the extracellular side. Top, voltage step, laser pulse, and image collection protocol. Bottom, current traces collected with Cs+ added to the pipette solution. **E.** Normalized fluorescence intensity without (black) or with Cs+ (red). Voltage step, +80 to -80 mV. Because the pipette solution was not exchanged during the experiments, control results and Cs+ results were collected from different patches. **F.** Normalized fluorescence intensity without (black) or with Cs+ (red). Voltage step, +80 to -80 mV.

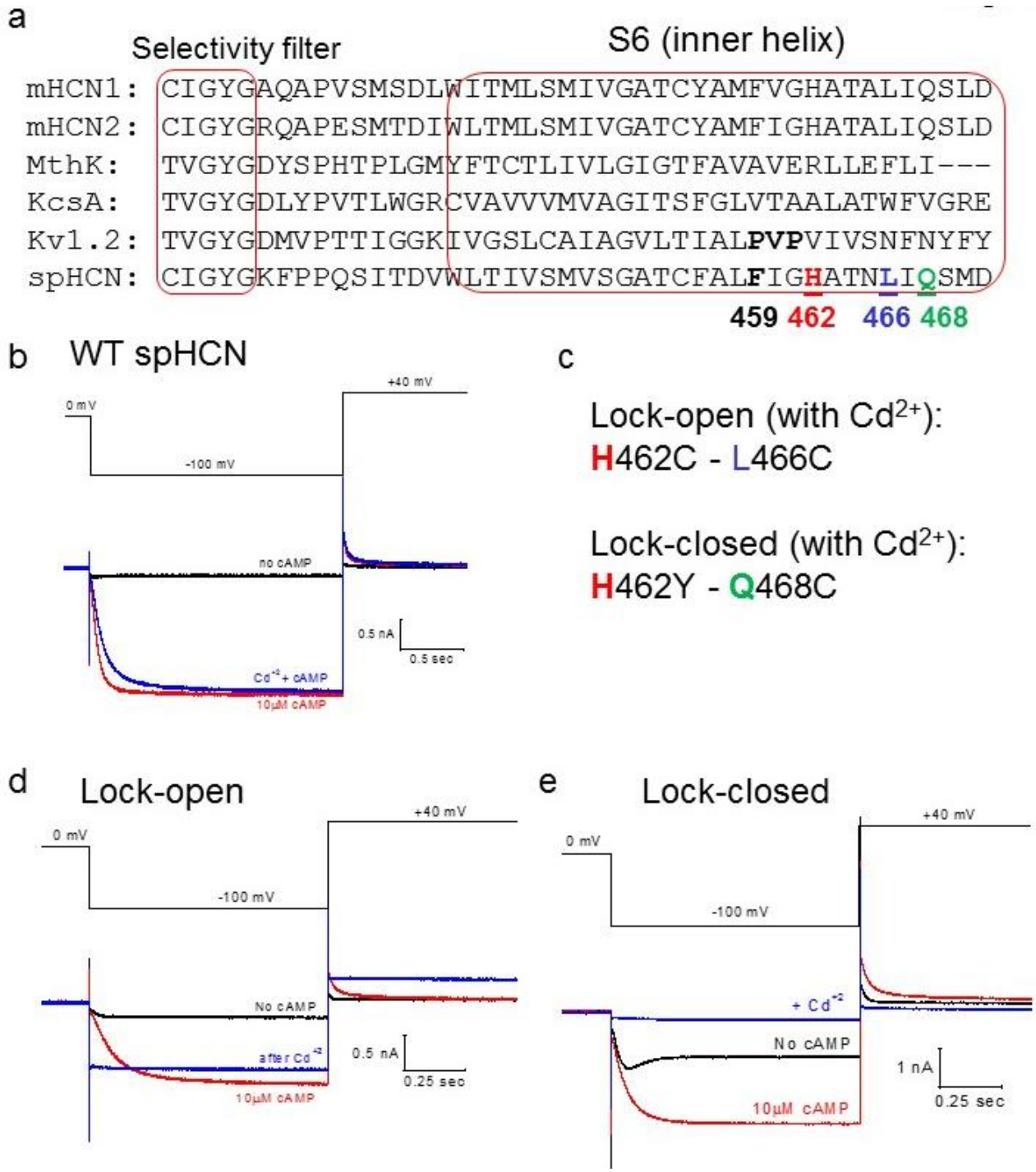
a
Selectivity filter
S6 (inner helix)
mHCN1: CIGYGAQAPVSMSDLWITMLSMIVGATCYAMFVGHATALIQSLD
mHCN2: CIGYGRQAPESMTDIWLTMLSMIVGATCYAMFIGHATALIQSLD
MthK: TVGYGDYSPHTPLGMYFTCTLIVLGIGTFAVAVERLLEFLI---
KcsA: TVGYGDLYPVTLWGRCVAVVVMVAGITSFGLVTAALATWFVGRE
Kv1.2: TVGYGDMVPTTIGGKIVGSLCAIAGVLTIALPVPVIVSNFNYFY
spHCN: CIGYGKFPPQSITDVWLTIVSMVSGATCFALFIGHATNLIQSMD
459 462 466 468
b WT spHCN
+40 mV
0 mV
-100 mV
no cAMP
0.5 nA
0.5 sec
Cd+2 + cAMP
10µM cAMP
c
Lock-open (with Cd2+):
H462C - L466C
Lock-closed (with Cd2+):
H462Y - Q468C
d Lock-open
+40 mV
0 mV
-100 mV
No cAMP
after Cd+2
0.5 nA
0.25 sec
10µM cAMP
e Lock-closed
+40 mV
0 mV
-100 mV
+ Cd+2
No cAMP
1 nA
0.25 sec
10µM cAMP

Fig. 8. Strategy to specifically lock the spHCN channel in either open or closed state.

A. Alignment of primary protein sequences of representative HCN and other potassium channels in the region encompassing the selectivity filter and the last transmembrane segment (S2 in KcsA or S6 in other channels). Relevant residues are shown in bold and marked with different color. **B**. Current traces of the WT spHCN channel. Black, control in the absence of cAMP and Cd2+. Red, 10 μM cAMP. Blue, 10 μM cAMP and 1μM Cd2+. **C.** Mutations introduced to the S6 of the spHCN channel to make the lock-open (H462C-L466C) or lock-closed (H462Y-Q468C) channel. **D.** Current traces of the lock-open spHCN channel. Black, control in the absence of cAMP and Cd2+. Red, 10 μM cAMP. Blue, 1 μM free Cd2+ without cAMP. The lock-open effect was persistent after the washing off of cAMP with bath solution containing Cd2+ **E.** Current traces of the lock-closed spHCN channel. Black, control in the absence of cAMP and Cd2+. Red, 10 μM cAMP. Blue, 2 μM Cd+2 and 10μM cAMP.

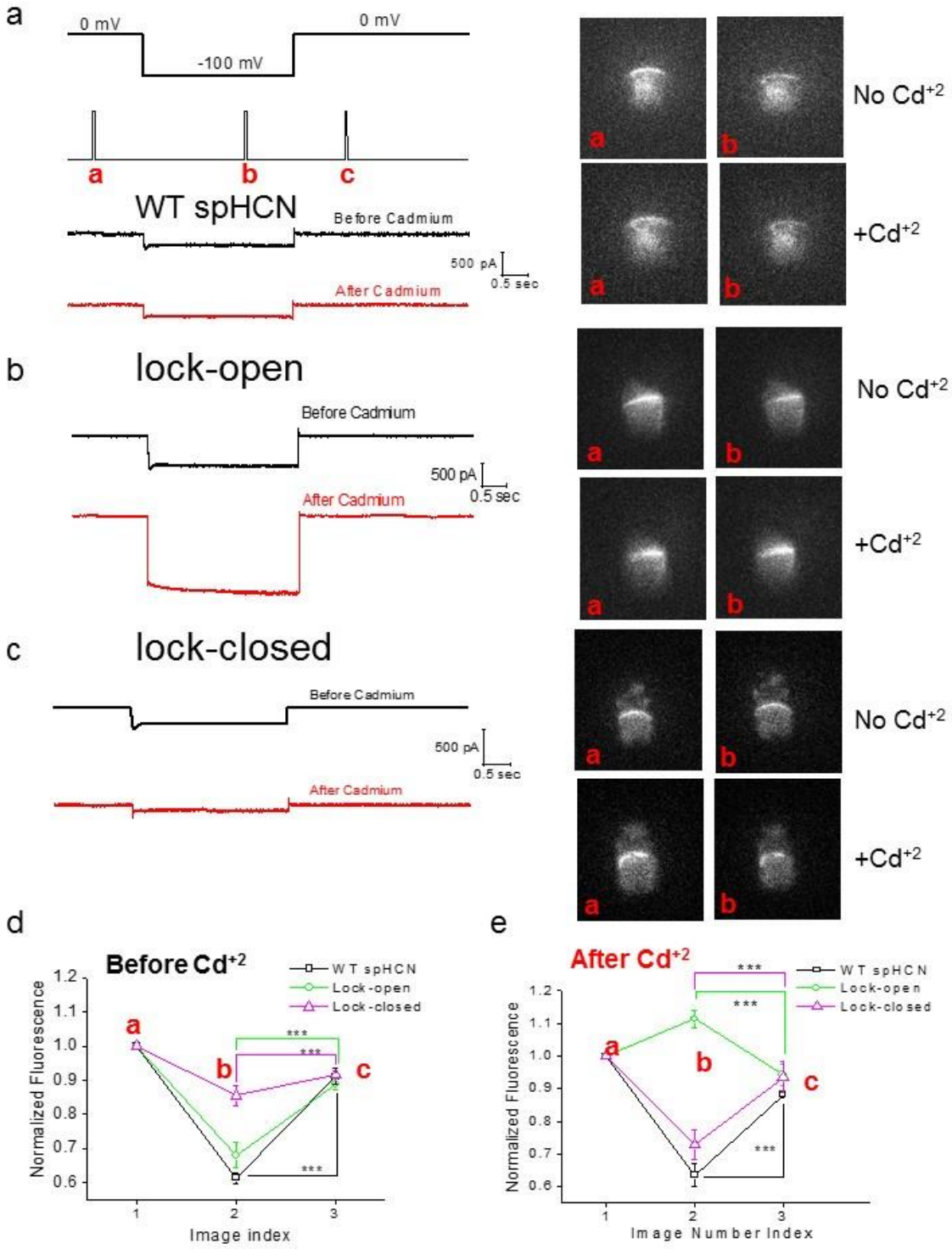
a
0 mV
-100 mV
0 mV
a
b
c
WT spHCN
Before Cadmium
500 pA
0.5 sec
After Cadmium
No Cd+2
+Cd+2
b
lock-open
Before Cadmium
500 pA
0.5 sec
After Cadmium
No Cd+2
+Cd+2
c
lock-closed
Before Cadmium
500 pA
0.5 sec
After Cadmium
No Cd+2
+Cd+2
d
Before Cd+2
WT spHCN
Lock-open
Lock-closed
Normalized Fluorescence
Image index
e
After Cd+2
WT spHCN
Lock-open
Lock-closed
Normalized Fluorescence
Image Number Index

Fig. 9. The inactivated WT spHCN channel, the lock-open and the lock-closed spHCN channels show three different levels of cAMP binding.

A. ZD7288 blocks the currents of the WT spHCN channel. Top, voltage step, laser pulse, and image collection protocol. Bottom, current traces before (black) and after (red) 60 μM ZD7288. **B**. Normalized fluorescence intensity before (black) and after (red) ZD7288 application. Voltage step, +80 to -80 mV. **C**. Normalized fluorescence intensity before (black) and after (red) ZD7288 application. Voltage step, +80 to -100 mV. **D.** 2 mM Cs+ was added to the pipette solution to block the WT spHCN current from the extracellular side. Top, voltage step, laser pulse, and image collection protocol. Bottom, current traces collected with Cs+ added to the pipette solution. **E.** Normalized fluorescence intensity without (black) or with Cs+ (red). Voltage step, +80 to -80 mV. Because the pipette solution was not exchanged during the experiments, control results and Cs+ results were collected from different patches. **F.** Normalized fluorescence intensity without (black) or with Cs+ (red). Voltage step, +80 to -80 mV.

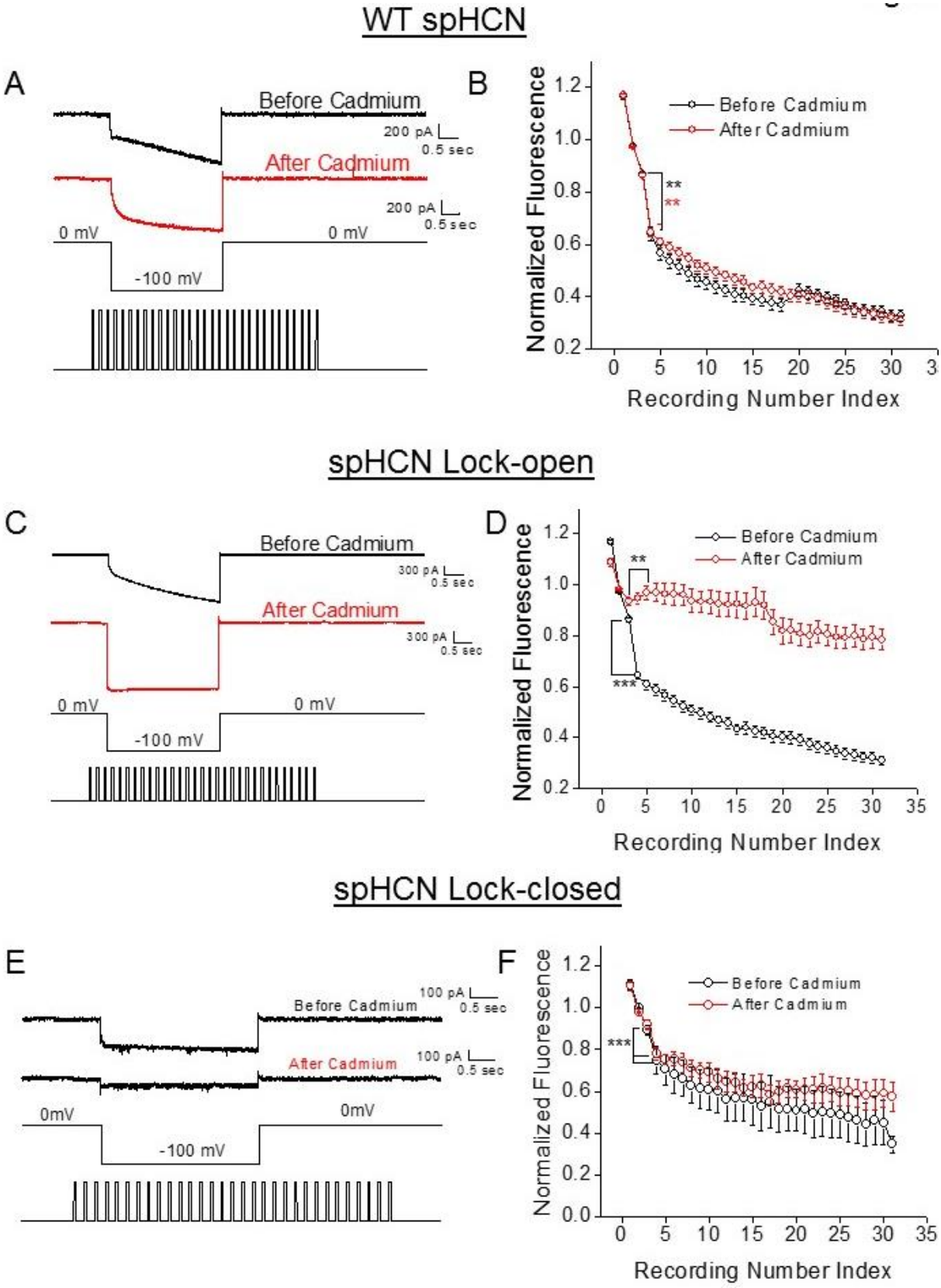
WT spHCN
A
Before Cadmium
200 pA
0.5 sec
After Cadmium
200 pA
0.5 sec
0 mV
0 mV
-100 mV
B
Normalized Fluorescence
Before Cadmium
After Cadmium
**
**
Recording Number Index
spHCN Lock-open
C
Before Cadmium
300 pA
0.5 sec
After Cadmium
300 pA
0.5 sec
0 mV
0 mV
-100 mV
D
Normalized Fluorescence
Before Cadmium
After Cadmium
**
***
Recording Number Index
spHCN Lock-closed
E
Before Cadmium
100 pA
0.5 sec
After Cadmium
100 pA
0.5 sec
0mV
0mV
-100 mV
F
Normalized Fluorescence
Before Cadmium
After Cadmium
***
Recording Number Index

Fig. 10. Profiles of cAMP binding to the lock-open and lock-closed spHCN channel along a hyperpolarization voltage step.

A. Top, current traces of the WT spHCN channel in the presence of 1 μM 8-NBD-cAMP, before (black) and after (red) the application of 1 μM Cd^{+2} to the bath solution. Bottom, protocol of voltage step, laser pulse, and image collection. The membrane patches were held at 0 mV for 1 second before the application of a hyperpolarization voltage step to -100 mV **B**. Normalized fluorescence intensity of the WT spHCN channel. Fluorescence intensities are normalized to the averaged intensity of first three images collected before the hyperpolarization voltage step. A significant decrease in fluorescence intensity was observed before (black; N=10, $p<0.001$) and after (red; N=9; $P<0.001$) the application of Cd^{+2} **C**. Current traces of the lock-open spHCN channel in the presence of 1 μM 8-NBD-cAMP, before (black) and after (red) the application of 1μM Cd^{+2} **D.** Normalized fluorescence intensities for the lock-open spHCN channel show a decrease in cAMP binding before the application of Cd^{+2} (black). But after the channel being locked in the open state by Cd^{+2}, a significant increase in fluorescence intensity indicating an increase in cAMP binding was observed (red) (P=0.0066; N=8). The fluorescence intensity was normalized to the average intensity of first three images collected before the hyperpolarizing voltage step. **E.** Current traces of the lock-closed spHCN channel in the presence of 1 μM 8-NBD-cAMP, before (black) and after (red) the application of 2 μM intracellular cadmium (Cd^{+2}). **F.** Normalized fluorescence intensity for the lock-closed spHCN channel showing a significant decrease in fluorescence intensity both before (black; n=4; paired t-test, $p<0.01$) and after (red; n=4; paired t-test, $p<0.01$) the application of Cd^{+2}. The fluorescence intensity was normalized to the average intensity of first three images collected before the hyperpolarizing voltage step.

2.4 Discussion:

HCN channel bridges membrane excitability with intracellular signaling pathways and thus plays important roles in the nervous and cardiovascular systems. At the molecular level, dually regulated by voltage and ligand, HCN channels exist as an elegant model for studying ion channel related protein allostery. Here we addressed the coupling of the activation/inactivation gate with the binding of cAMP in the full-length spHCN channel. Surprisingly, cAMP binding to spHCN channels decreases in response to the hyperpolarizing voltage step. We tackled the allosteric communication between the gate and cAMP binding in spHCN channels by from three directions: 1) The spHCN/F459L mutant channel that does not show inactivation; 2) Cs+ and ZD7288, two different blockers that act on different regions in the ion conducting pore; and 3) The strategy of locking the channel in either open or closed state. The experimental results provide direct support for the allosteric communication between the activation gate and the binding of cAMP.

Clearly, the decrease in cAMP binding is a voltage-dependent process, as indicated the gradual decrease in the time constant from ~3 seconds at -60 mV to ~1 second at -120 mV (Fig. 6C). Thus, a coupling mechanism should exist between the movement of the voltage sensor and the binding of cAMP. However, the S4 does not seem to directly communicate with the CNBD, because the kinetics of the decrease in cAMP binding upon membrane hyperpolarization is much slower than the movement of the voltage sensor. Previous recording of gating current from spHCN channel showed that majority of charge displacements finishes within 50 msec [145]. It is likely that certain structural rearrangements downstream from the movement of S4 affect the binding of cAMP. As supported by our results, the activation/inactivation gate in S6 plays a critical role in the allosteric modulation of the cAMP binding and at the same time controls the opening or closing of the ion conducting pathway.

Without cAMP, the spHCN/F459L channel still behaves like mHCN1 or mHCN2 channel. Sequence alignment shows that F459 is aligned to the first Proline in the critical "PVP" motif in the S6 of K_v channels and very close to the proposed activation gate for HCN channels [148,153–157]. The observations with the F459L mutant channel is quite intriguing because a single mutation effectively abolishes the voltage-dependent inactivation and switches the direction of cAMP binding. Alanine replacement of the corresponding residue in the mHCN2 channel, F431A, reduced cAMP binding and prolonged channel deactivation, which might share certain mechanistic connections with spHCN/F459L [142]. The location of F459, close to the activation gate and in contact with a critical hydrophobic pocket that involves residues from the S4-S5 linker of a neighboring subunit, and together with the impacts on gating by F459L, are comparable to a disease-causing L269F mutation in the muscle-type nicotinic AChR epsilon subunit . L269F causes pathologic channel openings in the absence of Ach and excessive Ca2+ entry. Interestingly, L269 is located in the m2 segment that corresponds to the S6 helix in Kv or HCN channels and engages in hydrophobic interactions with neighboring subunits [158–160].

To further delineate the binding of cAMP in various conformational states, we adopted the strategy of locking the spHCN channel in either open or closed state which was first developed by Gary Yellen's lab. They reported that the gating currents recorded from these gate-locked channels still show certain dependency on voltage, which indicates a relatively free movement of the S4 from the gate and thus a weak coupling between the voltage sensor and the gate in HCN channels [146]. On the other hand, the Q-V curves of the lock-open or lock-closed channel do shift in opposite directions, supporting the retrograde communication between the gate and the movement of the voltage sensor. Such retrograde communication has been reported for other types of ion channels like Na channel [161]. From the angle of gate - ligand binding, our measurements of the cAMP

binding to locked-open or locked-close spHCN channels, together with previous study of state-dependent binding of cAMP to mHCN2 channel, complement well to the study addressing the gate - voltage sensor communications in more traditional voltage-gate K or Na channels.

As an important negative feedback mechanism, voltage-dependent inactivation and ligand-dependent desensitization are gating mechanisms frequently adopted by different types of ion channels. From the aspect of the ligand binding in inactivated spHCN channels, our study provides useful insights for the interpretation of inactivation and desensitization. We confirmed that the interaction between cAMP and spHCN channel is dynamic and depends on the functional state: closed, inactivated, and open, and obtained direct evidence for the involvement of the activation/inactivation gate located near the intracellular end of S6. Therefore, for the study of protein allostery, the intimate coordination among adjacent and discrete domains and the interpretation at the whole molecule level should still be an important direction to pursue.

CHAPTER 4

Singlet oxygen modification abolishes voltage-dependent inactivation in a sea-urchin hyperpolarization-activated cyclic nucleotide-gated (spHCN) channel

Vinay Idikuda*, Weihua Gao*, Khade Grant, Zhuocheng Su, Qinglian Liu, and Lei Zhou

3.1 ABSTRACT

Photo-chemically or metabolically generated singlet oxygen ($^1O_2$) broadly reacts with macromolecules in the cell. Because of its short lifetime and working distance, $^1O_2$ holds the potential to be an effective and precise tool at the nanoscale level for basic research and clinical practice. Here we investigate the modification of the spHCN channel by photo-chemically and chemically produced $^1O_2$. The spHCN channel shows strong voltage-dependent inactivation in the absence of cAMP. Millisecond-long laser pulses transform the gating properties of the spHCN channel in complex with photosensitizers by abolishing the channel inactivation and increasing the voltage-insensitive current component. Alanine replacement of a histidine residue located near the activation gate within the channel's pore eliminates key modification effects. Application of a variety of chemicals including $^1O_2$ scavengers or $^1O_2$ generators supports the involvement of $^1O_2$ and excludes other reactive oxygen species. This study provides new insights into the photodynamic modification of ion channels by $^1O_2$.

Running Title: Singlet oxygen abolishes voltage-dependent inactivation in spHCN channel.

* contributed equally

3.2 INTRODUCTION

Molecular oxygen (O2) is indispensable for sustaining most forms of life on earth. Molecular oxygen has three electronic configurations, the triplet ground state ($^3\Sigma$) and the first and the second singlet excited states ($^1\Delta$ and $^1\Sigma$) [162,163]. Singlet oxygen ($^1O_2$, mainly referring to the $^1\Delta$ state because of the longer lifetime) is highly reactive and oxidizes a wide range of molecules from pollutants in the water/air to most macromolecules in the cell, including DNA, protein, and unsaturated lipids. Biological production of $^1O_2$ can occur through photochemical processes which involves three elements: photosensitizer, oxygen, and light [164], or metabolic processes without light [165,166]. In cells from the skin and the eye, intracellular compounds including flavins and NADH/NADPH are efficient photosensitizers [167]. $^1O_2$ can be generated under sunlight, especially UVA light (320-400 nm). This process has been linked to the aging and the development of cancer in these cells [168,169]. In liver tissues, $^1O_2$ can be generated in the dark through the oxidation of triplet carbonyls catalyzed by peroxidase [170]. Enzymatic generation of $^1O_2$ has also been observed in stimulated neutrophils, macrophages, and plants [171,172].

$^1O_2$ is very unstable in aqueous solution, with its lifetime in microseconds and effective range in nanometers. Low levels of $^1O_2$ may function as an intriguing intracellular second messenger by modifying the function of molecules in the vicinity [162,172]. High-levels of $^1O_2$ can used to specifically ablate the function of certain biomolecules and cells. $^1O_2$ holds the potential as a powerful tool with high spatial and temporal precision. For example, commonly used fluorescent molecules, such as fluorescein (FITC) and certain fluorescent proteins, are effective photosensitizers. In chromophore assisted light inactivation (CALI), fluorophore-tagged antibody recognizes and forms a complex with the target protein [173]. Upon light illumination, $^1O_2$ is generated and specifically abolishes the function of the proteins in close vicinity [173,174]. Similarly,

in photodynamic therapy (PDT), light is guided to the target tissue to excite the pre-administered photosensitizers. Target cells are damaged by $^1O_2$ but are eventually killed through a combination of apoptosis, necrosis, and acutely triggered local immune response. PDT has been approved by FDA to treat cancers of the esophagus, lung and skin, and other diseases related with the skin and eyes [175].

In spite of its broad application potential, little is known about how $^1O_2$ modifies targets at the molecular level. $^1O_2$ is not a radical and does not share similar chemical mechanisms with well-studied reactive oxygen species including hydrogen peroxide (H_2O_2), superoxide and hydroxyl radical, and nitric oxide (NO) [176]. The volatile chemical nature of $^1O_2$, the wide range of molecules that react with $^1O_2$, and the heterogeneous distributions of oxygen and photosensitizer together make $^1O_2$ a challenging research target. Most of the research on $^1O_2$ have been carried out at cellular and tissue levels in the presence of complex intracellular signaling pathways, including several studies on the modification of ion channels and transporters by $^1O_2$ [177–180]. To produce observable effects, these photodynamic studies often require long light exposure - up to minutes, in contrast to the extreme short life of $^1O_2$ in microseconds. A sensitive and well-defined working system for studying $^1O_2$ becomes necessary.

The hyperpolarization-activated, cyclic-nucleotide regulated (HCN) channels encodes the I_h (or I_f) current that was originally isolated from neurons and cardiac cells [23,181]. Four mammalian isoforms, HCN1 to HCN4, and an isoform from sea urchin, spHCN, have been cloned and extensively studied[25,26,28]. Each functional HCN channel contains four subunits, with each subunit having a six-helix transmembrane domain that is homologous to that of the voltage-gated K channel and a canonical cyclic-nucleotide binding domain (CNBD) in the C-terminus. Thus, HCN channels are equipped with the gating machinery for both voltage- and ligand-dependent gating

processes. In our study of the dynamic and state-dependent interaction between cAMP and full-length HCN channel, we applied the patch-clamp fluorometry technique and used different fluorescently labeled cAMP molecules [141,142]. We have previously shown that laser pulses applied to the mHCN2 channel in complex with FITC-cAMP prolonged the channel deactivation and introduced a prominent expression of voltage-insensitive, instantaneous (I_{inst}) current [115,117]. This observation leads us eventually to the establishment of $^1O_2$ as the major player and the identification of a critical histidine residue near the activation gate in S6. The I_{inst} carried by the HCN channel refers to the increase in current amplitude after the voltage step, without the typical time-dependency as observed with most voltage-gated ion channels. I_{inst} refers to the increase in current amplitude immediately after the voltage step, without the typical time-dependency as observed with most types of voltage-gated conductance. The I_{inst} carried by the HCN channel has been detected in both native and heterologous expression systems, but the corresponding molecular basis for the decoupling between the gate and the voltage sensor remains unclear.

Here we expand the investigation to spHCN channel, which shows strong voltage-dependent inactivation in the absence of cAMP, a unique feature that differentiates it from the mammalian forms. cAMP binding removes the inactivation in spHCN channel so that it behaves similarly to HCN1 or HCN2 channel. We found that $^1O_2$ modification removes the voltage-dependent inactivation of spHCN channel. This photodynamic modification is state-dependent and relies on the same homologous histidine residue near the activation gate. Finally, a consortium of chemical processes that generate or quench $^1O_2$ were used to establish the involvement of $^1O_2$ as the major player.

3.4 RESULTS:

Laser pulses abolish the voltage-dependent inactivation of the spHCN channel

We used the inside-out configuration of the patch-clamp technique to record currents from spHCN channels expressed in Xenopus oocytes. The intracellular side of the channel is exposed to the bath solution whereas the extracellular side is contact with the pipette solution. Unlike the mammalian HCN isoforms, the spHCN undergoes significant voltage-dependent inactivation which can be removed by the addition of cAMP (10 μM) to the bath solution (Fig. 11A; 12A), with an EC50 of 0.74 μM (Gauss et al., 1998). The definitions of Iinst, Ih, the macroscopic current (Imacro; I_h+I_{inst}), Ih (tail) (Ih or the voltage-sensitive component within the tail current), and the steady-state current (I_{ss}) are illustrated. Using patch-clamp fluorometry, we found that the fluorescent cAMP analog 8-FITC-cAMP bound to spHCN (Fig. 11B, 11C) but had minimal impacts on channel gating, most likely due to the bulky and charged FITC group. Therefore, in the presence of 1 μM 8-FITC-cAMP, spHCN channels showed strong voltage-dependent inactivation (trace 0 in Fig. 11D; the last trace before laser pulses).

As shown in the zoomed view during the 100 msec laser pulse (Fig. 11E; within the dashed red box), increases in the total or microscopic (Imacro) current were observed. After the laser pulse, the Imacro amplitude continued to increase, indicating a continuing shift of the equilibrium from the closed or inactivated state to the open state. The FITC moiety was required for the photodynamic transformation process because the same laser pulse applied to the spHCN channel in complex with cAMP did not increase current (Fig. 11F; 11G). In addition, light-activated current was not observed in patches from cells which contained no spHCN channel but were exposed to FITC-cAMP, indicating that spHCN was required (Fig12C)

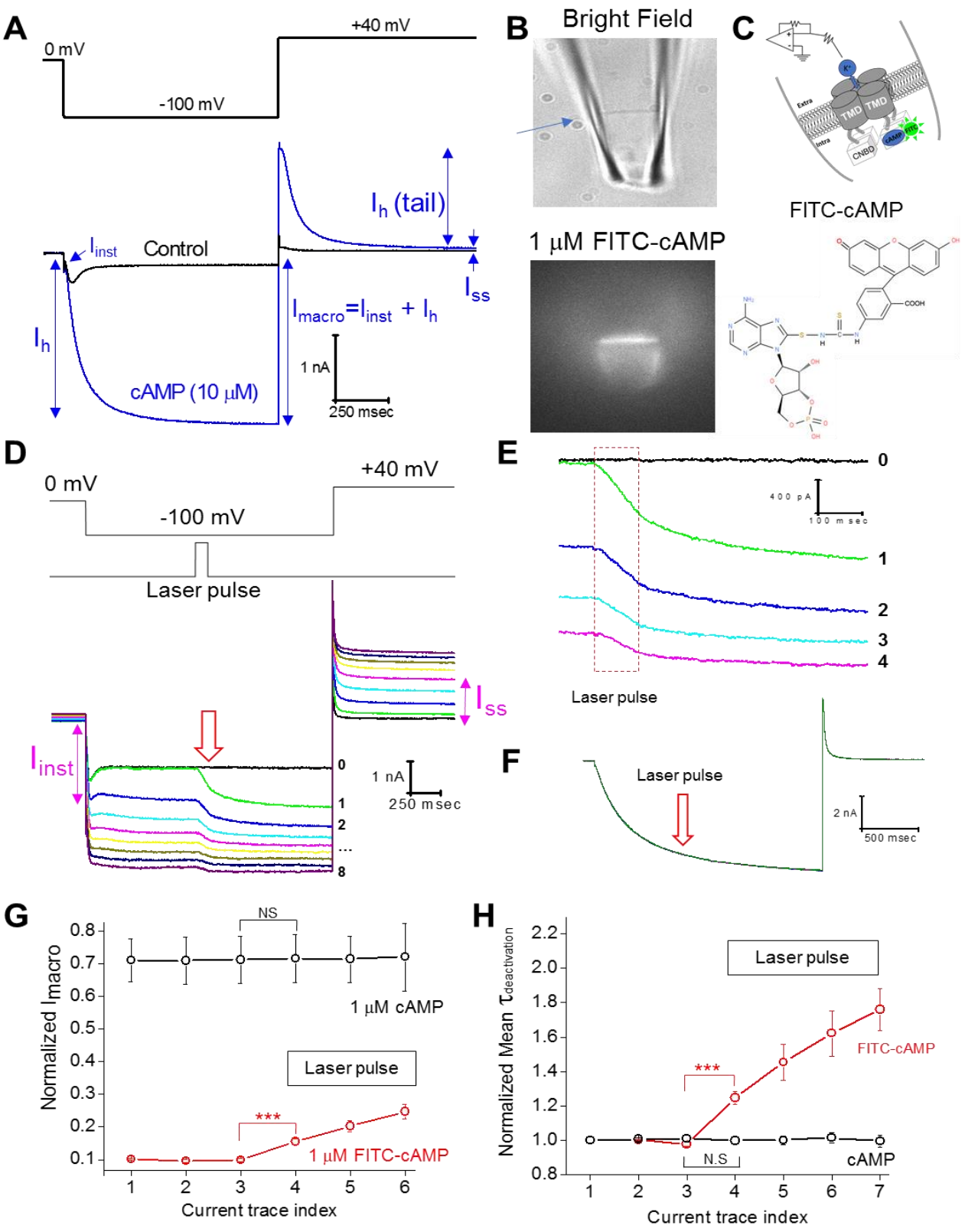
A
0 mV
+40 mV
-100 mV
I_h (tail)
I_{inst}
Control
I_{ss}
$I_{macro}=I_{inst}+I_h$
I_h
cAMP (10 μM)
1 nA
250 msec
B
Bright Field
1 μM FITC-cAMP
C
FITC-cAMP
D
0 mV
+40 mV
-100 mV
Laser pulse
I_{ss}
I_{inst}
0
1
2
...
8
1 nA
250 msec
E
0
400 pA
100 msec
1
2
3
4
Laser pulse
F
Laser pulse
2 nA
500 msec
G
NS
1 μM cAMP
Laser pulse
***
1 μM FITC-cAMP
Normalized Imacro
Current trace index
H
Laser pulse
FITC-cAMP
***
N.S
cAMP
Normalized Mean τdeactivation
Current trace index

Figure 11. Photodynamic modification of spHCN channel in complex with 8-FITC-cAMP

A. voltage command for channel activation (-100 mV) and tail current recording (+40 mV). Bottom, WT spHCN channel shows strong voltage-dependent inactivation (black) which can be abolished by cAMP binding. **B.** Top, bright field image of a piece of membrane patch (indicated by an arrow) held within the glass recording pipette. Bottom, fluorescence signal from the 8-FITC-cAMP in complex with the spHCN channel. Membrane from uninjected oocytes (no channel expressed) only shows fluorescence intensity at background level. **C.** Top, schematic drawing of the patch-clamp recording at inside-out configuration. Bottom, chemical structure of FITC. **D.** Top, voltage command and timing of laser pulse. Bottom: current traces before and after laser pulse application. Control trace before laser pulses (labeled 0) is shown in black. Numbers represent the order of applied laser pulses. **E.** A zoomed view over the moment when laser pulses were applied. Red box in dash represents the 100 msec laser pulses. **F.** Laser pulses have no effect on the spHCN in complex with regular cAMP. **G.** Averaged results (N=8) showing the effect of laser pulses on the amplitude of macroscopic current measured at -100 mV (see Fig. S1D for the description regarding macroscopic current, I_h, and I_{inst}). The horizontal box with the label of laser pulse indicates the episodes with laser pulses. The data points represent the index of current trace and are slightly behind the laser pulse in terms of timing. Current amplitudes were normalized to the maximal current measured in the presence of 10 □M cAMP. The first trace after laser pulse with FITC-cAMP is already significantly different from the last control trace (P= 0.0003, Paired T-test). NS, not significant. **H.** Averaged results (N=10) showing the effect of laser pulses on the time constant of deactivation. The first trace after laser pulse with FITC-cAMP is already significantly different from the last control trace (P= 0.00007, Paired T-test). NS, not significant.

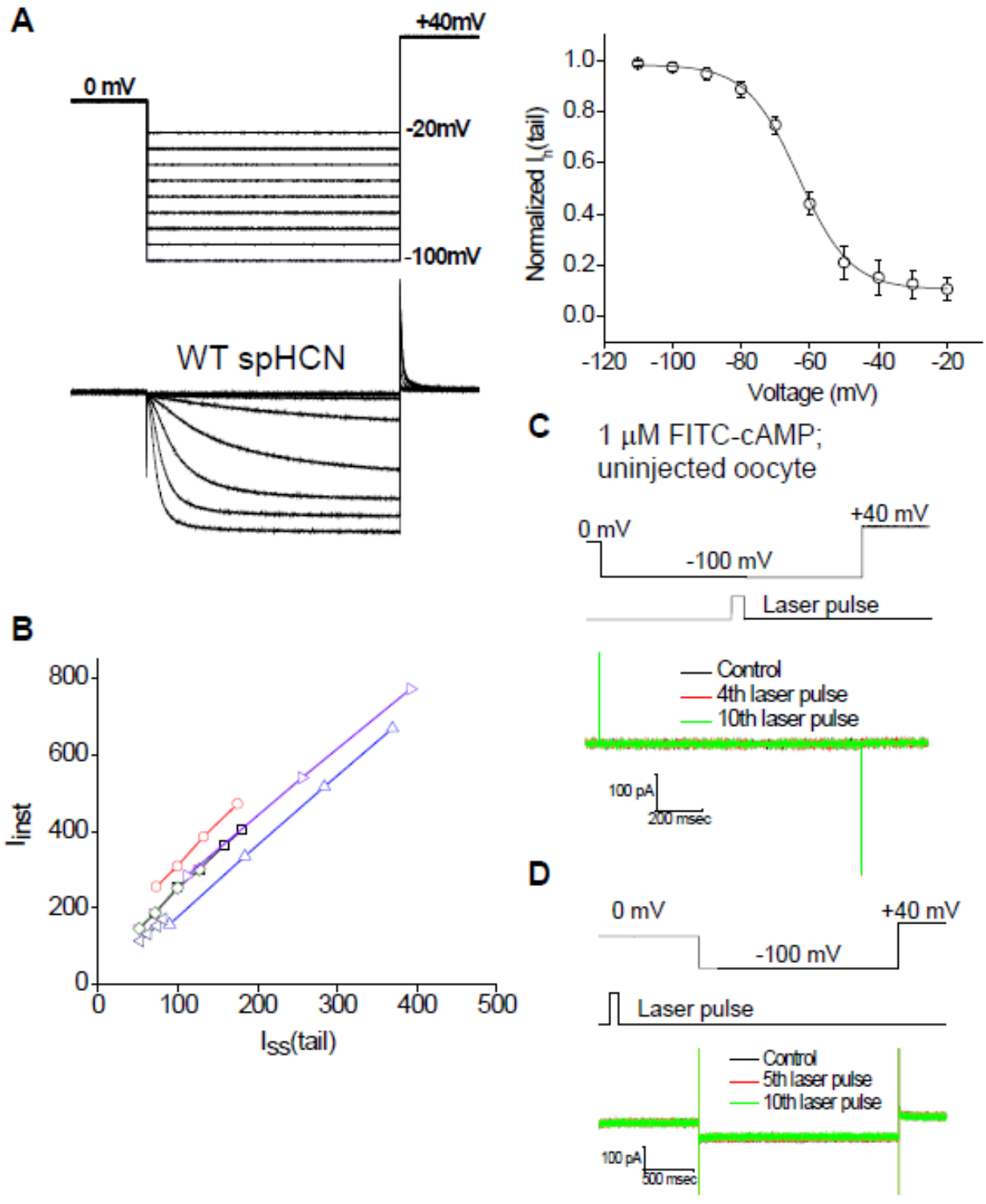
A
+40mV
0 mV
-20mV
-100mV
WT spHCN
Normalized I_h(tail)
1.0
0.8
0.6
0.4
0.2
0.0
-120
-100
-80
-60
-40
-20
Voltage (mV)
B
800
600
400
200
0
I_{inst}
0
100
200
300
400
500
I_{SS}(tail)
C
1 µM FITC-cAMP;
uninjected oocyte
0 mV
+40 mV
-100 mV
Laser pulse
Control
4th laser pulse
10th laser pulse
100 pA
200 msec
D
0 mV
+40 mV
-100 mV
Laser pulse
Control
5th laser pulse
10th laser pulse
100 pA
500 msec

Fig. 12. Characterization of the WT spHCN channel, correlation between the I_{inst} and I_{ss} (tail) after photodynamic modification, and effects of photodynamic modification on cell membrane without spHCN channel.

A. Top, voltage steps used for channel activation. Tail Currents were recorded at +40 mV. Bottom, current traces recorded in presence of 10 µM cAMP. Boltzmann Fit for the IV curve showing an average half maximal voltage ($V_{1/2}$) of 63.15 ± 0.8 mV (N=5).

B. Cross-plotting the amplitudes of I_{inst} and I_{ss} of WT spHCN channel after photodynamic modification. Four sequential laser pulses were applied in the middle of the voltage step. Each point shows amplitudes of the I_{ss} (tail) of the present current trace (measured after laser pulse at +40 mV) and the I_{inst} of the following current trace (measured before the next laser pulse at -100 mV).

C. Top, voltage command and timing of laser pulse (during voltage step). Bottom: current traces recorded from uninjected oocytes before and after laser pulse application. Black, last control current trace before laser pulses. Green, current traces in response to laser pulses.

D. Control results for laser pulses applied before voltage step.

As previously demonstrated with the mHCN2 channels[117] , laser pulses significantly prolonged the time constant for deactivation of spHCN (Fig. 11H). After photodynamic modification, the $\tau_{deactivation}$ was still less than 100 msec, much shorter than the interval between two adjacent current episodes (15 seconds). Thus, the slowdown in deactivation did not contribute to the increases in the voltage insensitive current component (Fig. 13A). The effects of photodynamic modification were long-lasting: they could still be seen 5 minutes after end of laser pulses and the washing off of FITC-cAMP (Fig. 14A). There was noticeable variability from patch to patch in terms of the extent of photodynamic modification of channel inactivation removal and the fraction of Iinst within Imacro. The geometry and position of membrane patch and the attachment of intracellular particles to the membrane are factors affecting the efficiency of the photodynamic modification.

Both Iinst (measured at -100 mV) and Iss (+40 mV) are conducted by spHCN channel:

Similar to previous study on the mHCN2 channel, laser pulses led to a prominent expression of Iss after the complete deactivation of Ih(tail) at +40 mV (Fig. 13A-13B). Because the light-activated spHCN current is long lasting, it can also be measured as Iinst in the following current trace, at the very beginning of the voltage jump from 0 to -100 mV. Importantly, the amplitudes of Iss (+40 mV; present trace) and the Iinst (-100 mV) of the subsequent trace are tightly correlated (Fig. 12B).

To confirm the Iinst and Iss are conducted by spHCN channel but not due to non-specific conductance after photodynamic modification, we applied ZD7288, a HCN channel specific blocker, to the intracellular side (bath solution) (Fig. 13A, 13B). In sequence, the current traces correspond to control trace before laser pulse and regular cAMP (black; 1), maximal current in 10 μM regular cAMP (grey; 2), current trace with the 3rd laser pulse (blue; 3), current trace after the stop of laser pulses (green; 4), and current trace in the presence of ZD7288 (red; 5). The difference

between the green trace after photodynamic modification and the red trace with ZD7288 demonstrate the block of I_{inst}, I_h, I_h (tail), and I_{ss}. Averaged results are shown in Fig. 13C, 13D. Moreover, both Iinst and Iss can be upregulated by cAMP applied to the bath solution (after the stop of laser pulses; Fig. 14A), which provides another evidence supporting the identity of spHCN channel behind Iinst and Iss.

To further test whether the I_{inst} is carried by the spHCN channels, we measured the K^+/Na^+ selectivity of I_{inst}. HCN channels are weakly selective for K^+, with P_K/P_{Na} between 3 and 4. We first measured the P_K/P_{Na} of the maximal current before laser pulses (in the presence of cAMP; Fig. 13E, 13F). With the K^+ solution in the pipette (extracellular), we measured currents with K^+ in the bath solution (intracellular) and then replaced K^+ in the bath with Na^+ to determine the reversal potentials. The shift in the reversal potential from 1.3 ± 0.3 mV (K^+_i) to -27.8 ± 1.2mV (Na^+_i) (N=4) confirmed the weak selectivity for K^+ by spHCN channels. Then we measured P_K/P_{Na} using a voltage ramp from +40 mV to -20 mV, which was chosen to minimize Ih activation (Fig. 13G, top). The current traces recorded before laser pulse (light magenta and light cyan in Fig. 13G, bottom) should correspond mostly to non-specific conductance, since both the reversal potentials and the holding current at 0 mV were close to zero with [Na+]i solution. After laser pulse treatment, there was a significant increase in current amplitude, and the reversal potential was shifted from 0.9 ± 0.2 mV (K^+_i) to -26.5 ± 0.9 mV (Na^+_i) (N=4). Therefore, the similar P_K/P_{Na} between I_h and I_{inst} provide additional evidence that after photodynamic modification I_{inst} was mainly carried by spHCN channels.

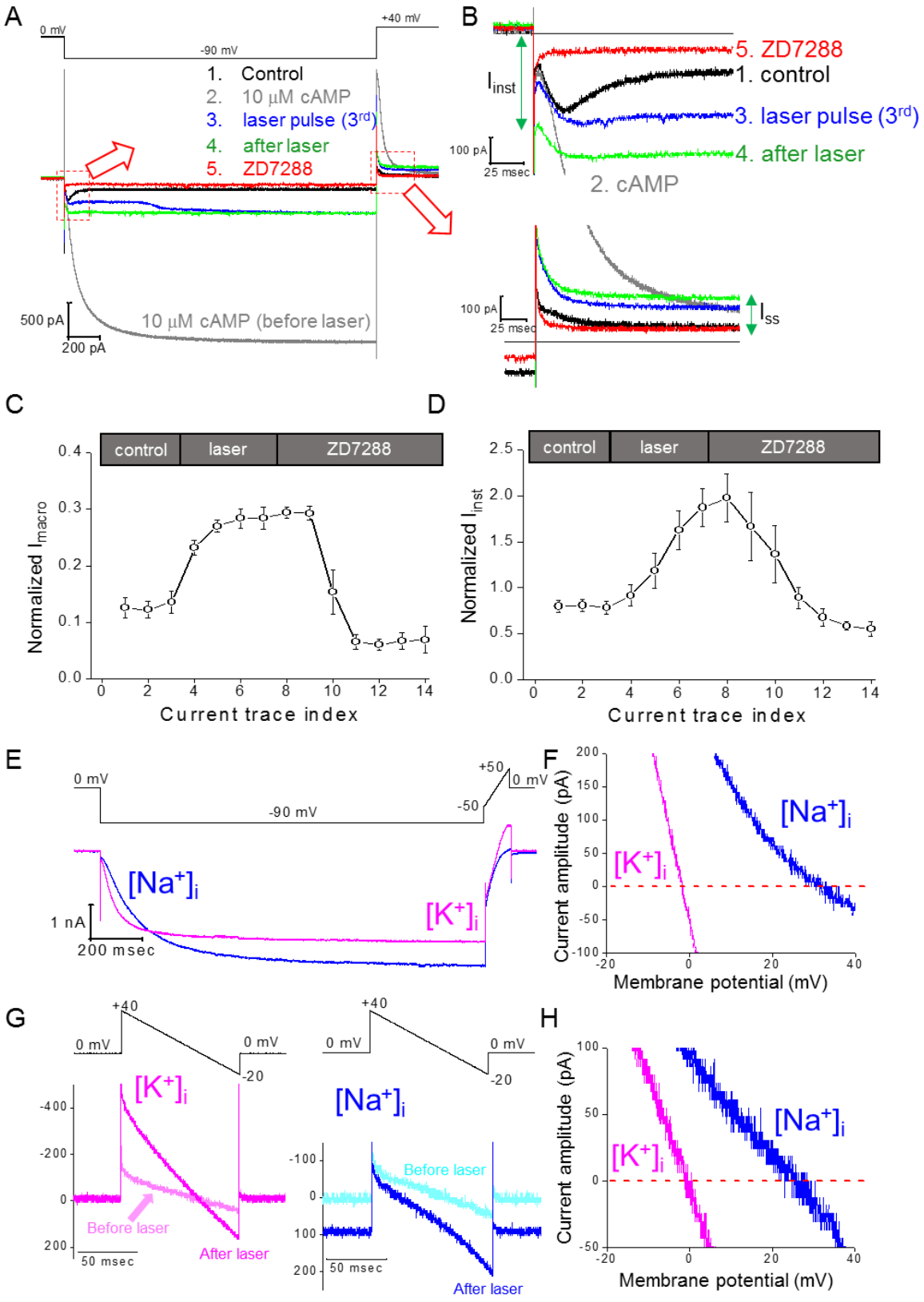
A
0 mV
-90 mV
+40 mV
1. Control
2. 10 μM cAMP
3. laser pulse (3rd)
4. after laser
5. ZD7288
500 pA
200 pA
10 μM cAMP (before laser)
B
Iinst
100 pA
25 msec
5. ZD7288
1. control
3. laser pulse (3rd)
4. after laser
2. cAMP
Iss
C
control
laser
ZD7288
Normalized Imacro
Current trace index
D
Normalized Iinst
Current trace index
E
0 mV
-90 mV
+50
0 mV
-50
[Na+]i
[K+]i
1 nA
200 msec
F
Current amplitude (pA)
Membrane potential (mV)
G
+40
0 mV
-20
[K+]i
[Na+]i
Before laser
After laser
50 msec
H
Current amplitude (pA)
Membrane potential (mV)

Figure 13. I_h and I_{inst} share similar sensitivity to ZD7288, a HCN channel specific blocker, and K+/Na+ selectivity

A. Top, voltage protocol. Bottom, four current traces in sequence showing control (no cAMP), 10 µM cAMP, the 3rd trace with laser pulse (with 1 µM FITC-cAMP), after laser pulses stopped and washing off FITC-cAMP, ZD7288 (100 µM).

B. Zoomed views showing the Iinst (top) and the Ih (tail) and Iss (bottom).

C. Averaged results showing that laser pulses applied in the presence of FTIC-cAMP increase the amplitude of Imacro, which can be blocked by ZD7288.

D. Averaged results showing that laser pulses applied in the presence of FTIC-cAMP increase the amplitude of Iinst, which can also be blocked by ZD7288.

E. Top, voltage protocol for Ih activation (0 to -90 mV) and a voltage ramp (-50 to 50 mV) used for the measurement of reversal potential. Bottom, current traces recording from the same membrane patch with symmetrical [K+]in/[K+]out (magenta) or [Na+]in/[K+]out (blue). 10 µM cAMP was added to the bath solution on the intracellular side.

F. Cross-plot of current amplitude vs. membrane potential during the voltage ramp for Ih.

G. Top, a voltage ramp (+40 to -20 mV) was used for the measurement of reversal potential of Iinst. Bottom, current traces recorded from the same membrane patch with symmetrical [K+]in/[K+]out (magenta, left) or [Na+]in/[K+]out (blue, right). Current traces in light colors are recorded before laser pulses. Current traces in dark colors are recorded after laser pulses stopped and in the absence of FITC-cAMP.

H. Cross-plot of current amplitude vs. membrane potential during the voltage ramp for the Iinst after laser pulses.

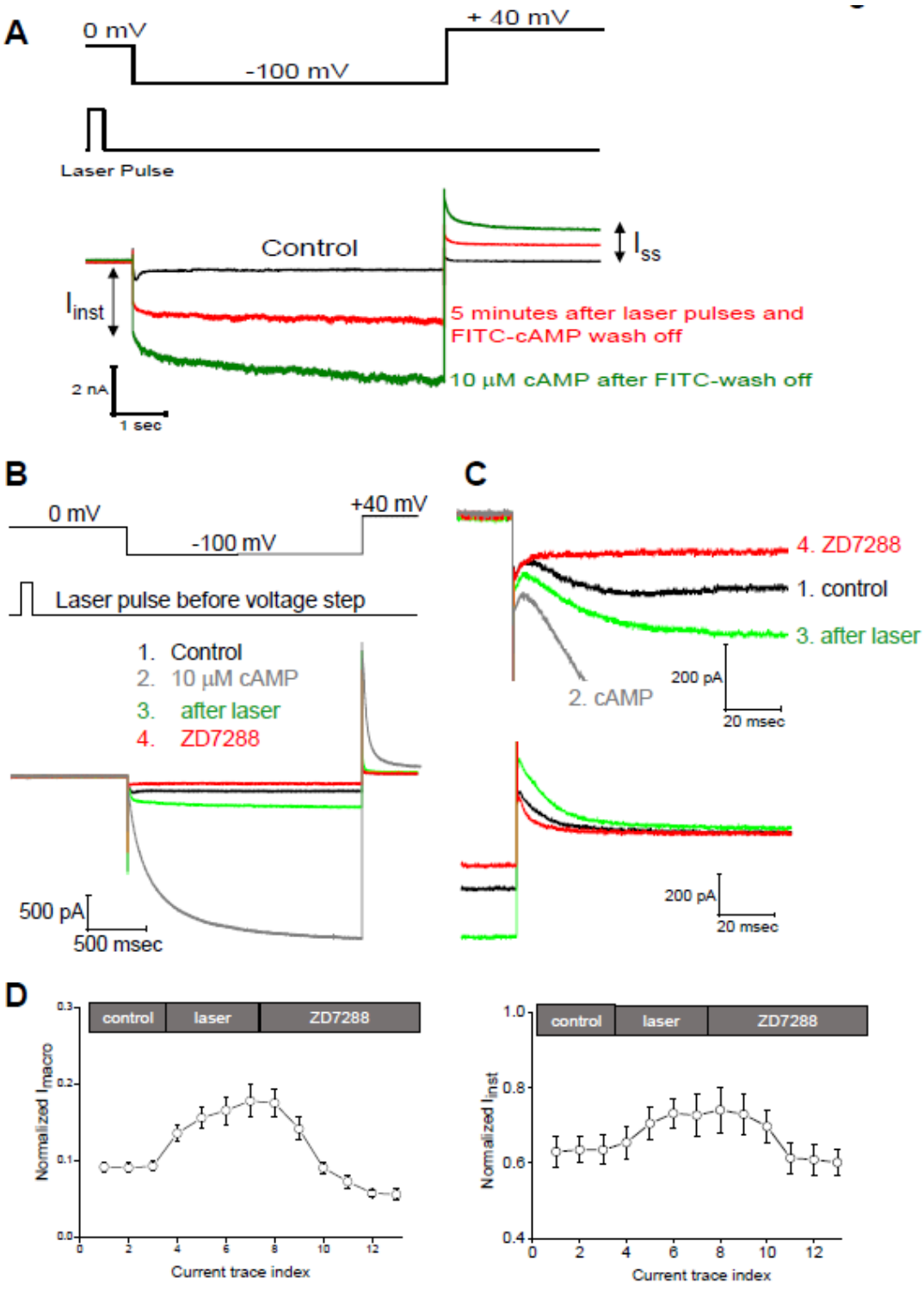
A
0 mV
+ 40 mV
-100 mV
Laser Pulse
Control
I_{ss}
I_{inst}
5 minutes after laser pulses and FITC-cAMP wash off
10 µM cAMP after FITC-wash off
2 nA
1 sec
B
0 mV
+40 mV
-100 mV
Laser pulse before voltage step
1. Control
2. 10 µM cAMP
3. after laser
4. ZD7288
500 pA
500 msec
C
4. ZD7288
1. control
3. after laser
2. cAMP
200 pA
20 msec
200 pA
20 msec
D
control
laser
ZD7288
Normalized I_{macro}
Current trace index
control
laser
ZD7288
Normalized I_{inst}
Current trace index

Fig. 14. I_{inst} and I_{ss} after photodynamic modification can be blocked by ZD7288 and be upregulated by cAMP.

A. Top, protocol of voltage step and laser pulse (before voltage step). Bottom, four current traces in sequence showing control (no cAMP; black), regular cAMP (10 μM; grey), after laser pulses stopped and washing off FITC-cAMP (green), and ZD7288 (100 μM; red).

B. Zoomed view showing the Iinst (top) or the Ih (tail) and Iss (bottom).

C. Averaged results of Imacro (left) and Iinst (right) in response to laser pulses (before voltage step) and ZD7288.

Photodynamic modification of the spHCN channel in the closed state

In the above experiments, laser pulses were applied in the middle of the hyperpolarizing voltage step, when most of the channels were in the inactivated state. Laser pulses directly initiated a time-dependent channel opening process. Next, we studied the effects of laser pulses on the channel in the closed state by applying laser pulses preceding the hyperpolarizing voltage step when most of the channel channels were in the closed state (Fig. 15A In the presence of 1 □M FITC-cAMP, laser pulses (100 msec) did not lead to immediate channel opening; however, in response to the following hyperpolarization voltage step, channel inactivation became less prominent (Fig. 15B, top). After a number of laser pulses, the inactivation was completely abolished and replaced by a continuous activation phase, similar to the activation of mammalian HCN channels or the spHCN channel in the presence of saturating concentrations of cAMP. Correspondingly, the amplitude of the macroscopic current and the I_h component increases (Fig. 15B, bottom; 15C, 15D). Interestingly, different from the laser pulses applied during the voltage step to mainly inactivated channel, laser pulses applied to closed spHCN channel results in more pronounced increase in Ih but only small increase in I_{inst} (Fig. 17).

To confirm whether the above changes in ionic current were indeed carried by the spHCN channel on the membrane, we added 100 μM ZD7288 to the bath solution or 2 mM Cs+ to the pipette solution. Similar to the results of laser pulse during voltage step, ZD7288 blocked the increases in Imacro and Iinst upon photodynamic modification with laser pulse before voltage step (Fig. 14B-14D). Alternatively, Cs+ applied to the extracellular side can effectively block the inward HCN current in a voltage-dependent manner (Fain et al., 1978; Barnes and Hille, 1989). Indeed, we observed a complete block of ionic current during the -100 mV voltage step after laser pulses,

which excluded the contribution by non-specific leak conductance to the increase in Iinst after photodynamic modification (Fig. 13E, 13F). To highlight the effects of photodynamic modification in the presence of Cs+, we monitored the current trace in response to the depolarizing voltage step from -100 to +40 mV. The significant increase in Ih (tail) and the non-deactivating Iss confirmed the impacts of the photodynamic modification. Averaged results for the application of Cs+ are shown in (Fig. 18).

A single point mutation, H462A, abolishes effects of photodynamic modification

Among the 20 amino acids, histidine is believed to be the major target of 1O2 (Matheson et al., 1975). Previously, we have identified a histidine residue critical to photodynamic modification in the mHCN2 channel, H434, which is located in the last transmembrane domain (S6) and close to the activation gate of HCN channels (Wu et al., 2012). Alanine replacement of H434 abolishes most effects of photodynamic modification on mHCN2 channels. In spHCN channels, the corresponding residue is H462. We started from a basic characterization of the spHCN/H462A mutant channel. The mutant channel behaves similarly to the WT channel, including the binding of FITC-cAMP and the response to cAMP **(16A, 16B**). In contrast to the WT spHCN channel, laser pulses applied in the presence of FITC-cAMP exerted minimal effects on the inactivation of the spHCN/H462 mutant channel and largely failed to initiate the transition of the channel from the inactivated state to the open state (**Fig. 16C**). Laser pulses applied to the closed channel do have a moderate impact on the opening of the channel, reflected in moderate increase in I_{macro} (**Fig. 16D**). Compared to the WT channel, the extent of changes in the H462A mutant channel after photodynamic modification was much smaller (**Fig. 16E, 16F**). Thus, for both spHCN and mHCN2 channels, the same conserved histidine residue in S6 appears to be critical for the photodynamic modification and the enhancement of voltage-insensitive I_{inst} and I_{ss} components.

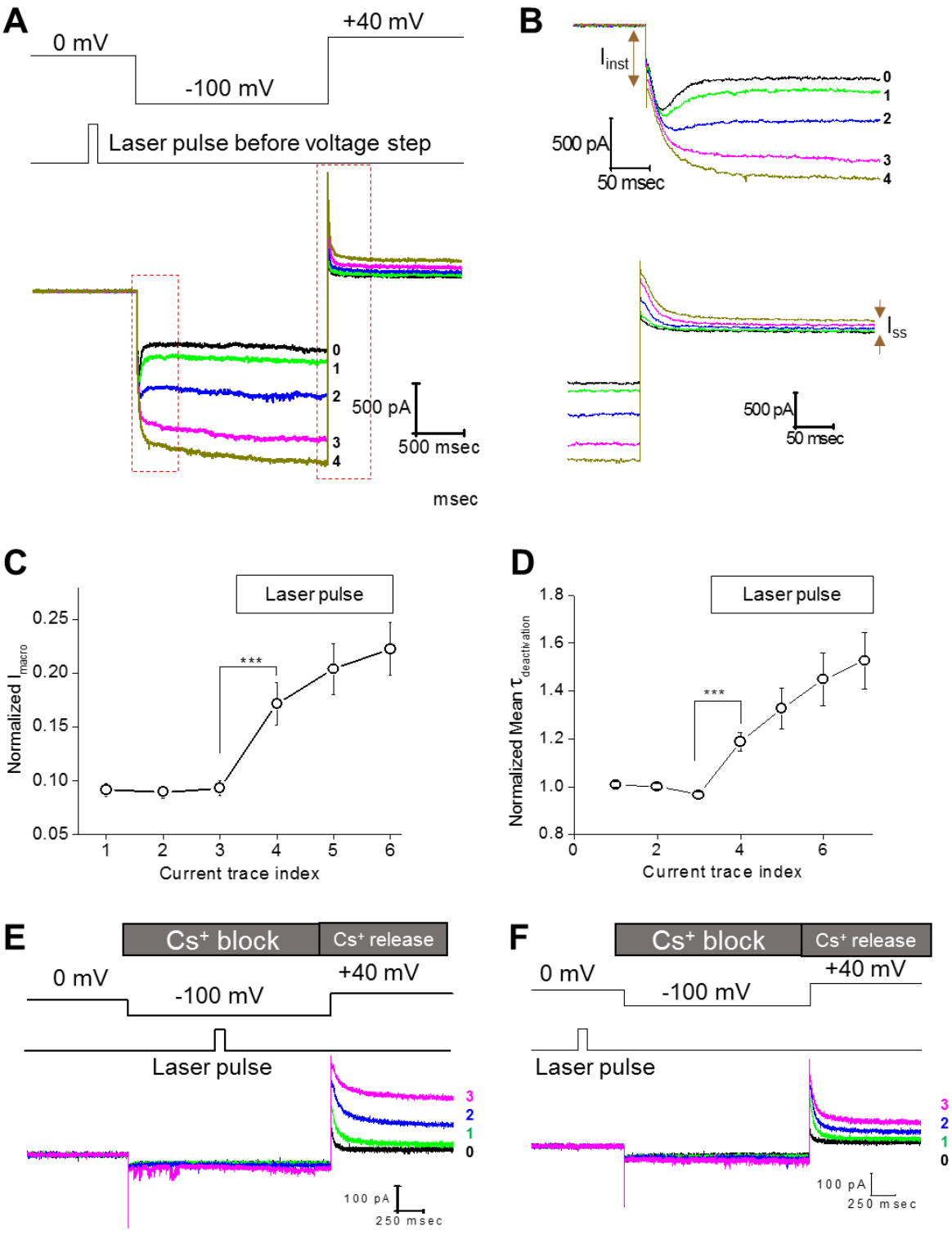
A
0 mV
+40 mV
-100 mV
Laser pulse before voltage step
0
1
2
3
4
500 pA
500 msec
msec
B
I_{inst}
500 pA
50 msec
I_{ss}
C
Laser pulse
Normalized I_{macro}
Current trace index
***
D
Laser pulse
Normalized Mean $\tau_{deactivation}$
Current trace index
***
E
Cs⁺ block
Cs⁺ release
0 mV
+40 mV
-100 mV
Laser pulse
100 pA
250 msec
F
Cs⁺ block
Cs⁺ release
0 mV
+40 mV
-100 mV
Laser pulse
100 pA
250 msec

Figure 15. Photodynamic modification of the spHCN channel in the closed state and the sensitivity of modified spHCN channels to Cs+.

A. Top, voltage command and the timing of laser pulses. Laser pulses were applied preceding the hyperpolarization voltage step when most of the channels should stay in the closed state. Bottom, current traces recorded with 1 μM FITC-cAMP in the bath solution. The last control trace before laser pulse is shown in black and labeled 0.

B. Zoomed views of the region within the red box shown in A.

C. Averaged (N=15) results showing the effect of laser pulses on the amplitude of macroscopic current.

D. Averaged (N=15) results showing the effect of laser pulses on the time constant of deactivation.

E. During the -100 mV voltage step, Cs+ applied to the extracellular side of the membrane blocks the spHCN current after photodynamic modification (laser pulse during voltage step). The following depolarizing voltage step from -100 to +40 mV released the block by Cs+ and revealed the effects of photodynamic modification. Photodynamic modification leads to slowdown in channel deactivation and increases in I_h (tail) and I_{ss}. Black, last current trace before laser pulse. Green, traces with laser pulses.

F. Laser pulses were applied preceding the hyperpolarization voltage step. Cs+ blocks the macroscopic current at -100 mV. The voltage step from -100 to +40 mV released the Cs+ block and revealed the effects of photodynamic modification.

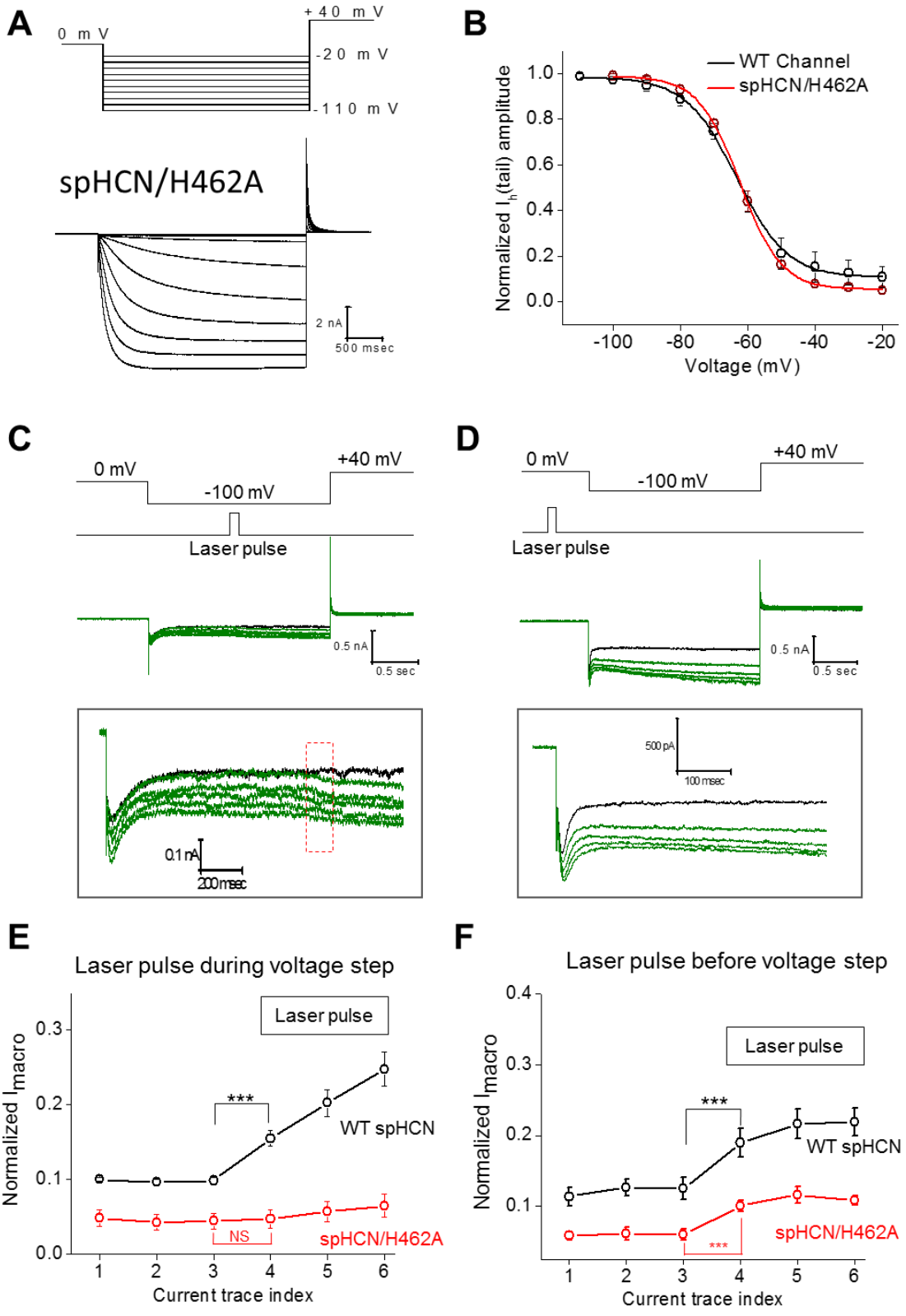
A
0 m V
+ 4 0 m V
-2 0 m V
-1 1 0 m V
spHCN/H462A
2 nA
500 msec
B
WT Channel
spHCN/H462A
Normalized I_h(tail) amplitude
1.0
0.8
0.6
0.4
0.2
0.0
-100
-80
-60
-40
-20
Voltage (mV)
C
0 mV
-100 mV
+40 mV
Laser pulse
0.5 nA
0.5 sec
0.1 nA
200msec
D
0 mV
-100 mV
+40 mV
Laser pulse
0.5 nA
0.5 sec
500 pA
100 msec
E
Laser pulse during voltage step
Laser pulse
Normalized I_macro
0.3
0.2
0.1
0.0
***
WT spHCN
NS
spHCN/H462A
1
2
3
4
5
6
Current trace index
F
Laser pulse before voltage step
Laser pulse
Normalized I_macro
0.4
0.3
0.2
0.1
***
WT spHCN
***
spHCN/H462A
1
2
3
4
5
6
Current trace index

Figure 16. spHCN/H462A mutant channel shows minimal responses to photodynamic modification. **A.** Top, voltage steps used for channel activation. Tail currents were recording at +40 mV. Bottom, current traces recorded in the presence of 10 μM cAMP. **B.** Averaged voltage-dependent activation curve of WT (black, N=5, V1/2 63.15±1.8 mV) and spHCN/H462A mutant (red, N=6, V1/2 63.15± 2.1 mV) channels. **C.** SpHCN/H462A mutant channel shows almost no responses to laser pulses applied in the middle of the -100 mV voltage step. A zoomed view shows the current trace at the moment when laser pulses are applied (inside the box). **D.** Laser pulses applied proceeding the -100 mV voltage step leads to small increases in macroscopic current but have no effect on channel inactivation. A zoomed view shows the current trace near the start of the -100 mV voltage step (inside the box). **E**. Averaged results showing the effect of laser pulses (applied in the middle of the -100 mV voltage step) on the macroscopic current amplitude of the WT (N=8, black) and spHCN/H462A mutant (N=5, red) channels. The first trace after laser pulse with FITC-cAMP is already significantly different from the last control trace (P= 0.017, Paired T-test) in Wild type channel compared to spHCN/H462A mutant channel. NS, not significant (P-value 0.33, paired T-test). **F.** Averaged results showing the effect of laser pulses (applied before the -100 mV voltage step) on the macroscopic current amplitude of the WT (N=7, black) and spHCN/H462A mutant (N=5, red) channels. The first trace after laser pulse with FITC-cAMP is already significantly different from the last control trace (P= 0.017, Paired T-test) in Wild type channel and spHCN/H462A mutant channel. (P-value 0.0008, paired T-test), but the mutant channel still shows inactivation.

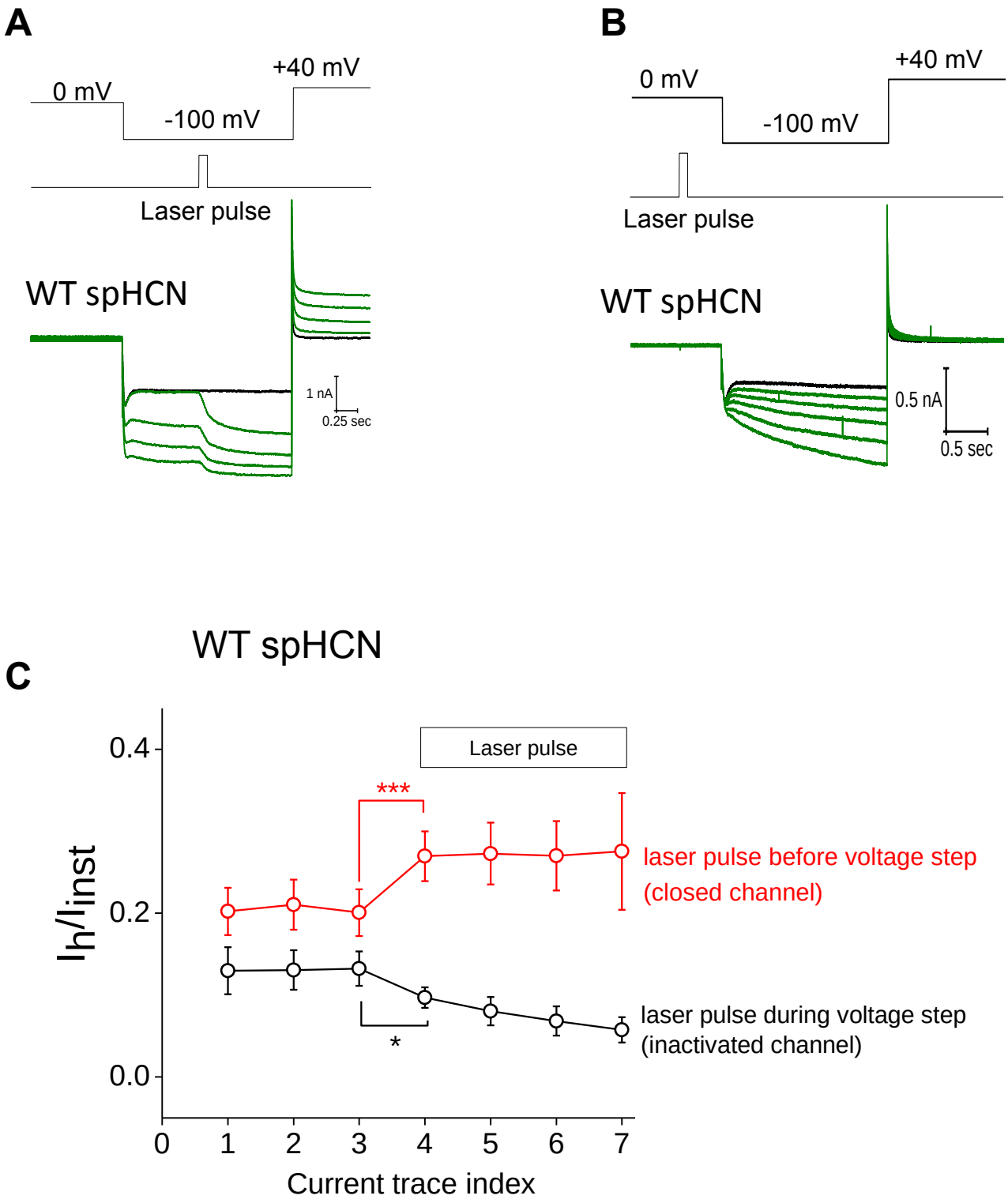
A
0 mV
+40 mV
-100 mV
Laser pulse
WT spHCN
1 nA
0.25 sec
B
0 mV
+40 mV
-100 mV
Laser pulse
WT spHCN
0.5 nA
0.5 sec
C
WT spHCN
Laser pulse
***
*
laser pulse before voltage step
(closed channel)
laser pulse during voltage step
(inactivated channel)
I_h/I_{inst}
0.4
0.2
0.0
0
1
2
3
4
5
6
7
Current trace index

Fig. 17. Laser pulses applied before and in the middle of the hyperpolarizing voltage step have different impact on I_{inst} and I_h (tail).

A. Top, voltage command and timing of laser pulse (during voltage step). Bottom: current traces before and after laser pulses. Black, current trace before the 1st laser pulse. Green, current traces in response to laser pulses.

B. Top, voltage command and timing of laser pulse (during voltage step). Bottom: current traces before and after laser pulses. Black, current trace before the 1st laser pulse. Green, current traces in response to laser pulses.

C. Ratio of I_h/I_{inst} plotted as a function of current trace index. Laser pulses started from the fourth episode. Red, laser pulse before voltage step (N=16). Black, laser pulse after laser pulse (N=10).

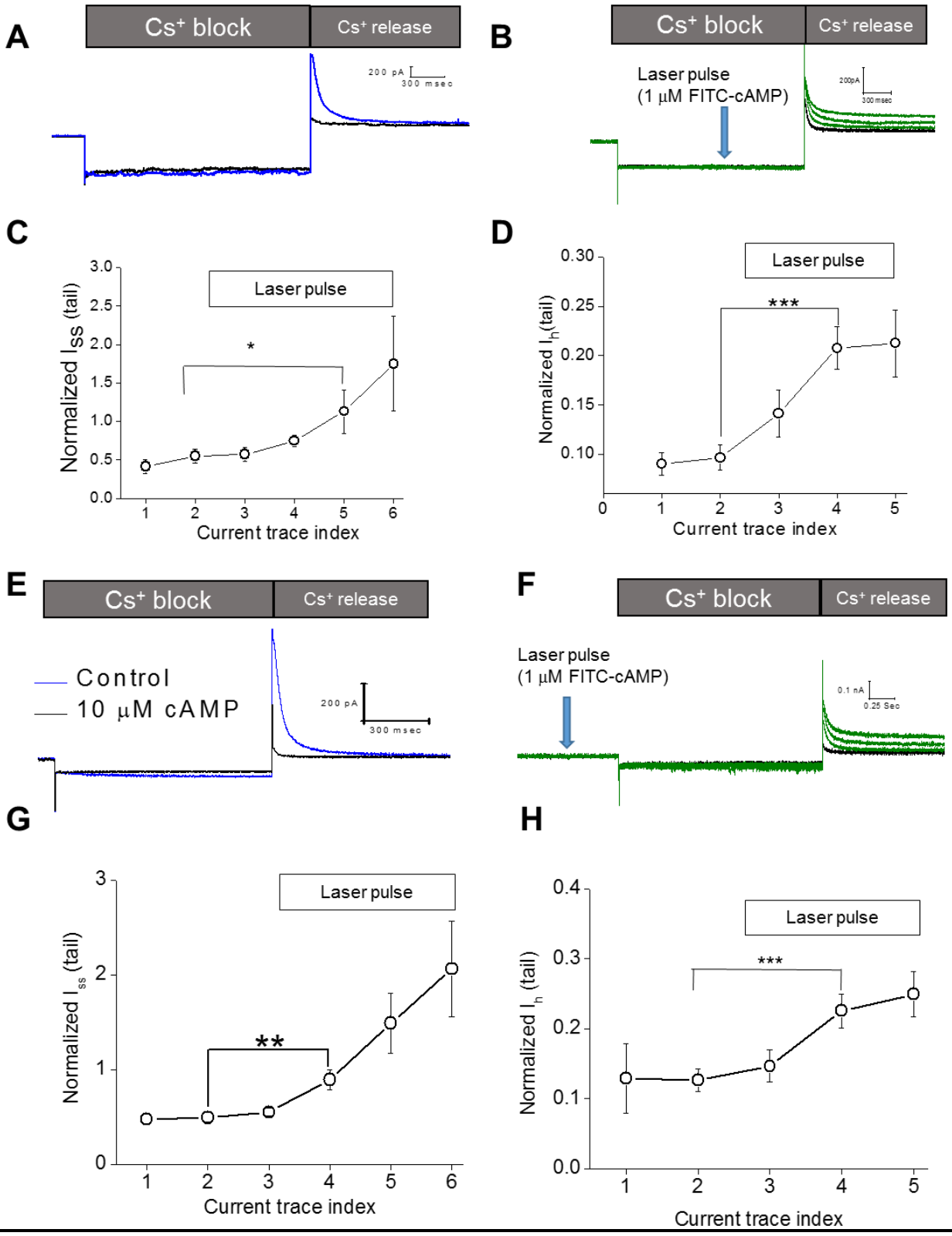
A
Cs+ block
Cs+ release
200 pA
300 msec
B
Cs+ block
Cs+ release
Laser pulse
(1 μM FITC-cAMP)
200pA
300 msec
C
Laser pulse
*
Normalized Iss (tail)
Current trace index
D
Laser pulse
***
Normalized Ih (tail)
Current trace index
E
Cs+ block
Cs+ release
Control
10 μM cAMP
200 pA
300 msec
F
Cs+ block
Cs+ release
Laser pulse
(1 μM FITC-cAMP)
0.1 nA
0.25 Sec
G
Laser pulse
**
Normalized Iss (tail)
Current trace index
H
Laser pulse
***
Normalized Ih (tail)
Current trace index

Fig. 18. Cs^+ blocks I_{inst} and I_h after photodynamic modification.

A. WT spHCN current traces recorded before laser pulses. Black, control; blue, 10 μM cAMP. 2 mM Cs^+ applied to the glass pipette or the extracellular side of the membrane blocks spHCN currents at -100 mV. The block by Cs^+ can be released by a depolarizing voltage step from -100 to +40 mV.

B. Current traces showing the effect of laser pulse (during voltage step) on the WT spHCN channel in the presence of Cs^+. Black, last control current trace before the 1st laser pulse. Green, current traces in response to laser pulses.

C. Averaged results showing the effect of laser pulses (during voltage step) on I_{ss} (tail) (N=6).

D. Averaged results showing the effect of laser pulses (during voltage step) on I_h (tail) (N=5).

E. Current traces recorded with 2 mM Cs^+ added to the pipette solution. Black, control; blue, 10 μM cAMP.

Application of Rose Bengal and $^1O_2$ quenchers/generator supports the involvement of $^1O_2$

To confirm the above observations are the result of a photodynamic process, we chose Rose Bengal, a popular photosensitizer, in the absence of FITC-cAMP or regular cAMP. 100 nm Rose Bengal was applied to the bath solution in inside-out excised patch clamp experiments from cells expressing spHCN (Fig. 20A). We found that laser pulses during the hyperpolarization voltage step triggered an increase in I_{macro}, I_{ss}, and I_{inst}, similar to our observation with FITC-cAMP in the bath solution (Fig. 20B, 20D). When applied before voltage step to closed channels, laser pulses removed channel inactivation and introduced a prominent increase in Imacro (Fig. 20C; 20E). In contrast, the spHCN/H462A mutant channel showed minimal responses to laser pulses with Rose Bengal in the bath, which is comparable to results with FITC-cAMP (Fig. 21).

To further confirm the involvement of 1O2 in the photodynamic modification of spHCN channel, we separately tested $^1O_2$ quenchers including sodium azide (1 mM) and Trolox-C (1 mM). In the presence of these 1O2 quenchers, the effects of photodynamic modification were significantly diminished (Fig. 20F, FITC-cAMP; 20G, Rose Bengal; Fig. 22, Rose Bengal; laser pulses during voltage step; Fig. 23, Rose Bengal; laser pulse before voltage step). In addition, we tested the effects on Rose Bengal on membrane patches pulled from uninjected oocytes. No obvious effects on the leak conductance was detected even with higher concentration of Rose Bengal (200 nM) and more laser pulses (up to 10) (Fig. 19). Taken together, these results provide further support for the identity of 1O2 as the critical player in the modification of the spHCN channel.

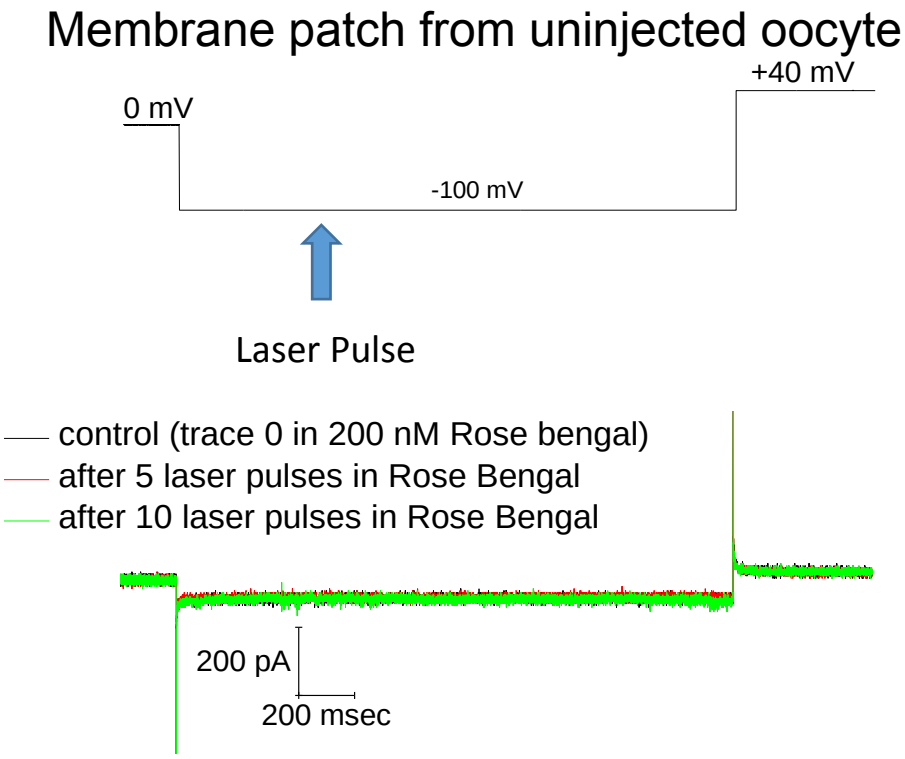

Fig. 19 Rose Bengal with laser pulses has no effects on empty membrane patch without spHCN channel.

Top, protocol of voltage and laser pulse (during voltage step). 100 msec laser pulse duration Bottom, leak currents recorded from membrane patches pulled from uninjected Xenopus oocyte. Rose Bengal (200 nM) was applied to the bath solution. Black, control trace before laser pulse. Red, current trace with the 5^{th} laser pulse. Green, current trace with the 10^{th} laser pulse.

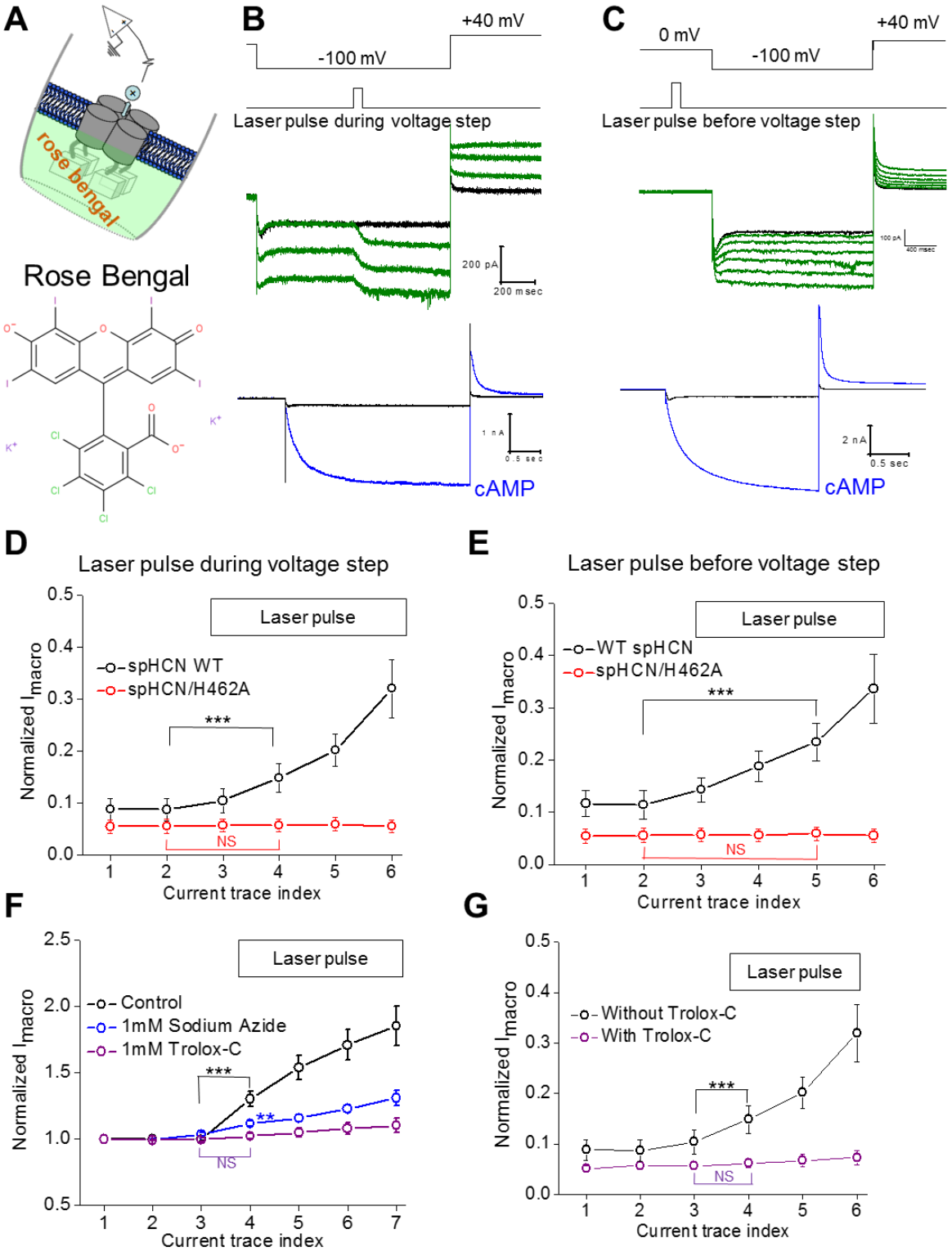
A
rose bengal
Rose Bengal
B
+40 mV
-100 mV
Laser pulse during voltage step
200 pA
200 msec
1 nA
0.5 sec
cAMP
C
0 mV
+40 mV
-100 mV
Laser pulse before voltage step
100 pA
400 msec
2 nA
0.5 sec
cAMP
D
Laser pulse during voltage step
Laser pulse
spHCN WT
spHCN/H462A
***
NS
Normalized Imacro
Current trace index
E
Laser pulse before voltage step
Laser pulse
WT spHCN
spHCN/H462A
***
NS
Normalized Imacro
Current trace index
F
Laser pulse
Control
1mM Sodium Azide
1mM Trolox-C
***
**
NS
Normalized Imacro
Current trace index
G
Laser pulse
Without Trolox-C
With Trolox-C
***
NS
Normalized Imacro
Current trace index

Figure 20. Application of a general photosensitizer (Rose bengal) and 1O2 quenchers (sodium azide and Trolox C) support the involvement of 1O2.

A. Schematic drawing of the experiment configuration. Rose Bengal was applied to the bath solution which is contact with the intracellular side of the channel. **B.** 100 nM Rose Bengal was applied to the bath solution. Laser pulses applied in the middle of -100 mV voltage step abolishes WT channel inactivation. **C.** Reponses of WT spHCN channel in the presence of Rose Bengal to laser pulses applied proceeding the voltage step. **D.** Averaged results showing the effect of laser pulses (in the middle of the -100 mV voltage step) on the macroscopic current amplitude of the WT (N=8, black) and spHCN/H462A mutant (N= 8 , red) channels. The first trace after laser pulse with Rose Bengal is already significantly different from the last control trace (P= 0.001, Paired T-test) in Wild type channel, but not in the spHCN/H462A mutant channel (P= 0.38, Paired T-test) **E**. Averaged results showing the effect of laser pulses (before the voltage step) on the macroscopic current amplitude of the WT (N=5, black) and spHCN/H462A mutant (N=5, red) channels. The first trace after laser pulse with Rose Bengal is already significantly different from the last control trace (P= 0.01, Paired T-test) in Wild type channel, but not in the spHCN/H462A mutant channel (P= 0.38, Paired T-test) **F.** Averaged results showing the effect of Sodium Azide (N=7, blue) and Trolox C (N=8, purple) on the photodynamic modification (FITC-cAMP) of WT spHCN channels. The first trace after laser pulse with FITC-cAMP is already significantly different from the last control trace (P= 0.001, Paired T-test) in the absence of quenchers, but not in the presence of 1mM Sodium Azide (P= 0.07, Paired T-test) channel still shows inactivation. G. Averaged results showing the effect of Trolox C (purple) on the photodynamic modification (N=11, Rose Bengal) of WT spHCN mutant (N=7, red) channels. The first trace after laser pulse with Rose Bengal is already significantly different from the last control trace (P= 0.001, Paired T-test) in the absence of quencher, but not in the presence of the quencher (P= 0.08, Paired T-test).

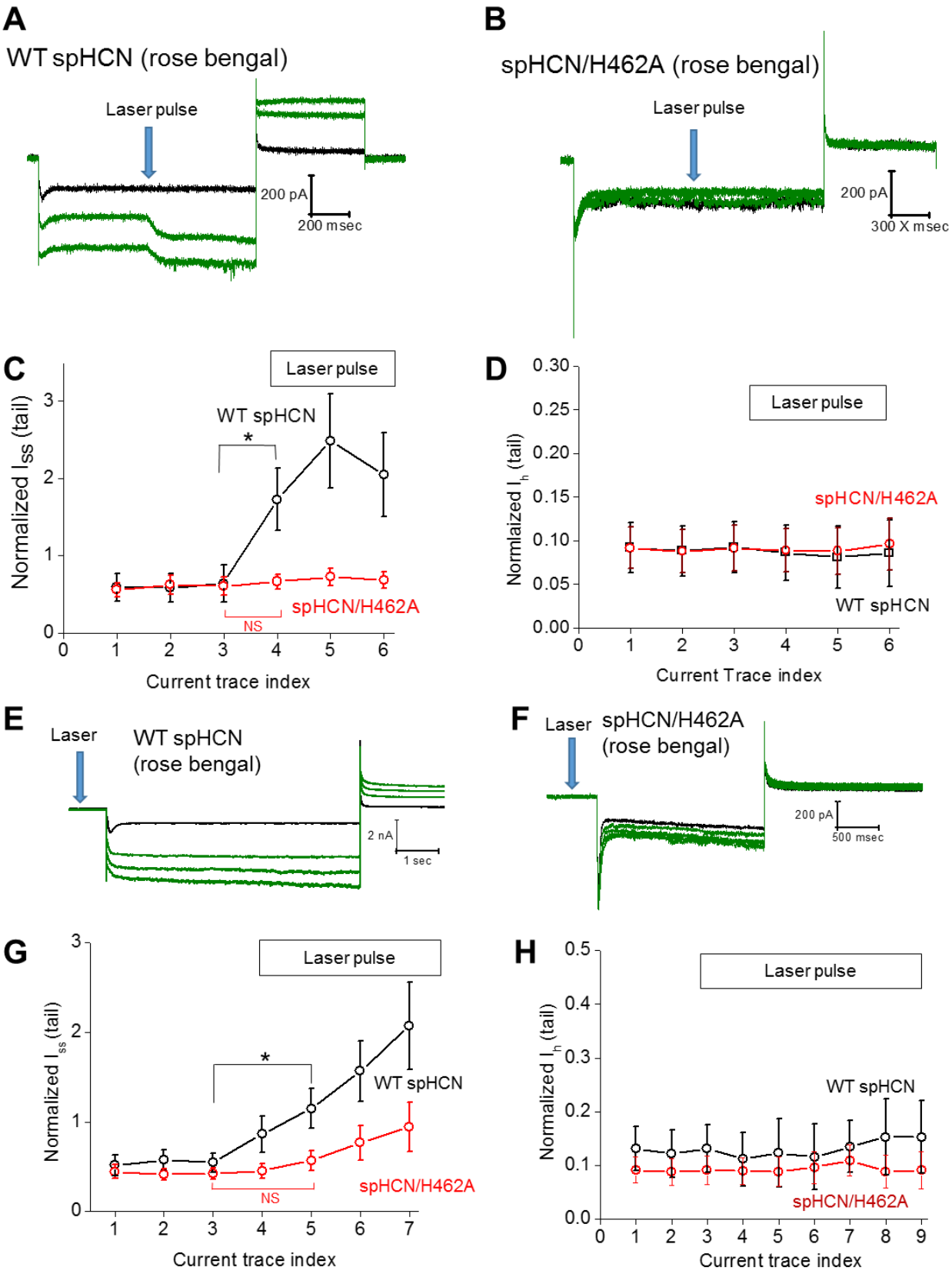
A
WT spHCN (rose bengal)
Laser pulse
200 pA
200 msec
B
spHCN/H462A (rose bengal)
Laser pulse
200 pA
300 X msec
C
Laser pulse
WT spHCN
*
spHCN/H462A
NS
Normalized Iss (tail)
Current trace index
D
Laser pulse
spHCN/H462A
WT spHCN
Normlaized Ih (tail)
Current Trace index
E
Laser
WT spHCN
(rose bengal)
2 nA
1 sec
F
Laser
spHCN/H462A
(rose bengal)
200 pA
500 msec
G
Laser pulse
*
WT spHCN
spHCN/H462A
NS
Normalized Iss (tail)
Current trace index
H
Laser pulse
WT spHCN
spHCN/H462A
Normalized Ih (tail)
Current trace index

Fig. 21. Rose Bengal mediated photodynamic modification of WT spHCN and spHCN/H472A mutant channels.

A. Representative current traces showing the effect of laser pulses (during voltage step) on the WT spHCN channel in the presence of 100 nM Rose Bengal. Black, last control current trace before the 1st laser pulse. Green, current traces with laser pulses.

B. Representative current traces showing the effect of laser pulses (during voltage step) on the spHCN/H462A channel in the presence of 100 nM Rose Bengal. Black, last control current trace before the 1st laser pulse. Green, current traces in response to laser pulses.

C. Averaged results showing the effect of laser pulses (during voltage step) on the I_{ss} (tail) of the WT (N=6, black) and spHCN/H462A mutant (N=7, red) channels.

D. Averaged results showing the effect of laser pulses (during voltage step) on the Ih current of the WT (N=6, black) and spHCN/H462A mutant (N=8, red) channels.

E. Representative current traces showing the effect of photodynamic modification on the WT spHCN channel (before voltage step) in the presence of 100 nM Rose Bengal. Black, last control current trace before the 1st laser pulse. Green, current traces in response to laser pulses.

F. Representative current trace showing the effect of photodynamic modification on spHCN/H462A channel (before voltage step) in the presence of 100 nM Rose Bengal. Black, last control current trace before the 1st laser pulse. Green, current traces in response to laser pulses.

G. Averaged results showing the effect of laser pulses (before voltage step) on the Iss (tail) of the WT (N=7, black) and spHCN/H462A mutant (N=5, red) channels.

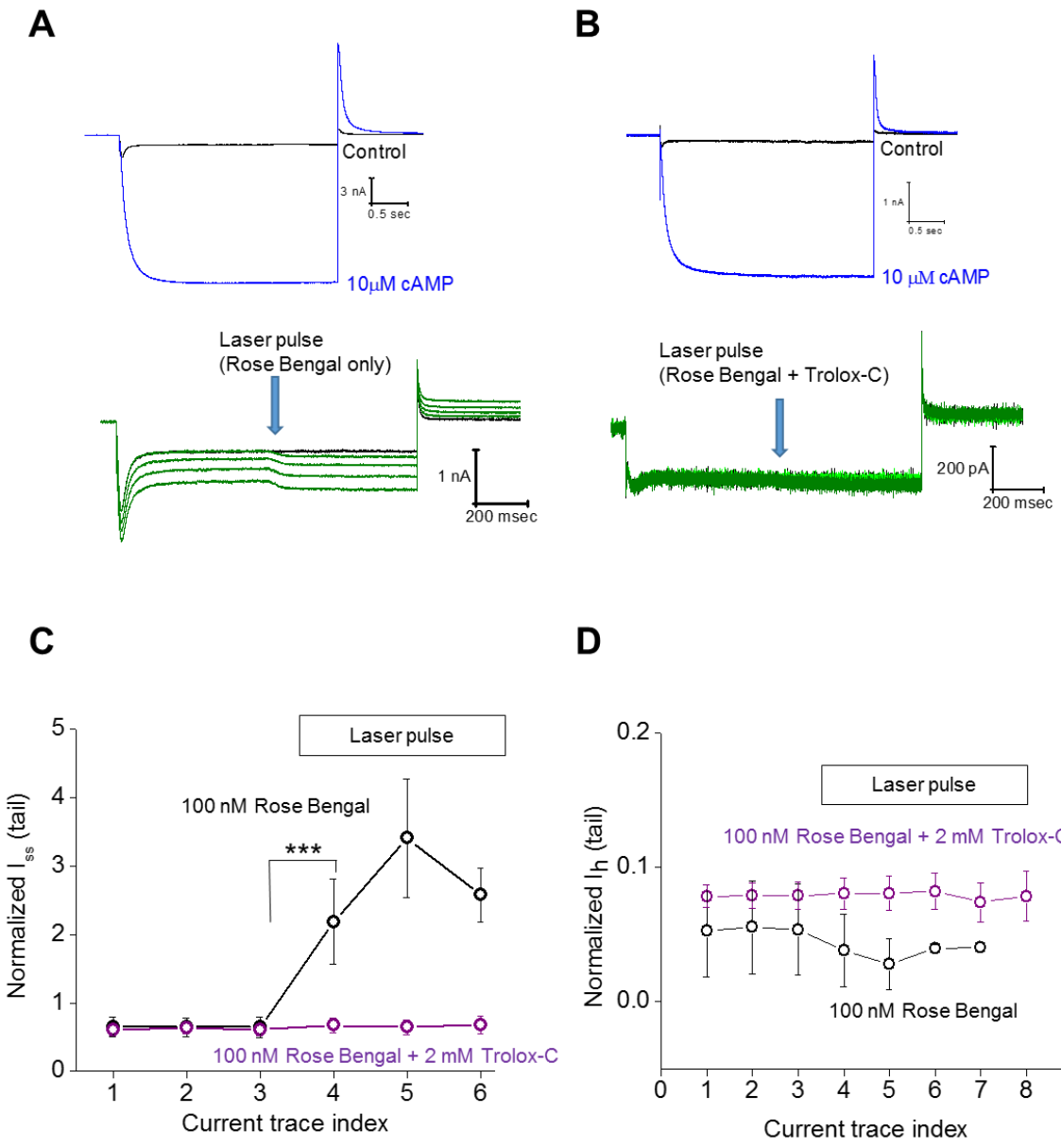
A
Control
3 nA
0.5 sec
10μM cAMP
Laser pulse
(Rose Bengal only)
1 nA
200 msec
B
Control
1 nA
0.5 sec
10 μM cAMP
Laser pulse
(Rose Bengal + Trolox-C)
200 pA
200 msec
C
Laser pulse
100 nM Rose Bengal
***
100 nM Rose Bengal + 2 mM Trolox-C
Normalized I_{ss} (tail)
Current trace index
D
Laser pulse
100 nM Rose Bengal + 2 mM Trolox-C
100 nM Rose Bengal
Normalized I_h (tail)
Current trace index

Fig. 22. Effect of singlet oxygen quencher Trolox-C on the photodynamic modification of inactivated spHCN channels mediated by Rose Bengal.

A. Top, current traces of the WT spHCN channel before (black) and after adding (blue) 10 µM cAMP. Bottom, responses of the WT spHCN channel to laser pulses (during voltage step) in the presence of 100 nM rose Bengal (green).

B. Top, current trace recorded from the WT spHCN channel before (black) and after adding 10 µM cAMP (blue). Bottom, responses of WT spHCN channel to laser pulses (during voltage step) in the presence of Rose Bengal and 2 mM Trolox-C (green).

C. Averaged results showing the effect of laser pulses on I_{ss} (tail) without (N=11, black) or with (N=6, purple) 2 mM Trolox-C.

D. Averaged results showing the effect of laser pulses on I_h (tail) without (N=11, black) or with (N=6, purple) 2 mM Trolox-C.

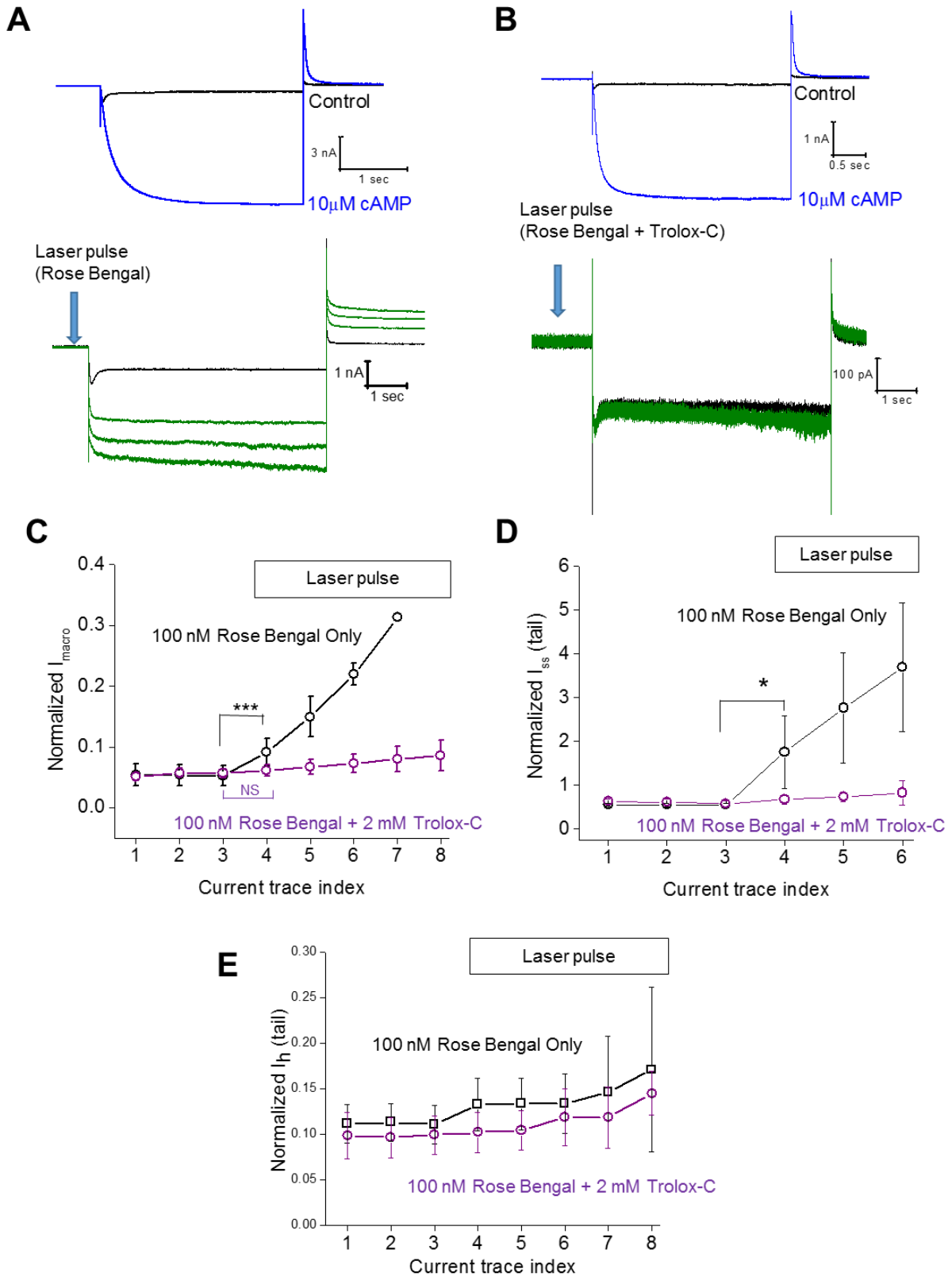
A
Control
3 nA
1 sec
10μM cAMP
Laser pulse
(Rose Bengal)
1 nA
1 sec
B
Control
1 nA
0.5 sec
10μM cAMP
Laser pulse
(Rose Bengal + Trolox-C)
100 pA
1 sec
C
Laser pulse
100 nM Rose Bengal Only
***
NS
100 nM Rose Bengal + 2 mM Trolox-C
Normalized I_macro
Current trace index
D
Laser pulse
100 nM Rose Bengal Only
*
100 nM Rose Bengal + 2 mM Trolox-C
Normalized I_ss (tail)
Current trace index
E
Laser pulse
100 nM Rose Bengal Only
100 nM Rose Bengal + 2 mM Trolox-C
Normalized I_h (tail)
Current trace index

Fig. 23. Effect of Trolox-C on the photodynamic modification of closed spHCN channels mediated by Rose Bengal.

A. Top, current traces of the WT spHCN channel before (black) and after adding 10 µM cAMP (blue). Bottom, responses of the WT spHCN channel to laser pulses (before voltage step) in the presence of 100 nM Rose Bengal (green).

B. Top, current traces recorded from the WT spHCN channel before (black) and after adding 10 µM cAMP (blue). Bottom, responses of the WT spHCN channel to laser pulses (before voltage step) in the presence of Rose Bengal and 2 mM Trolox-C (green).

C. Averaged results showing the effect of laser pulses on I_{macro} without (N=9, black) and with (N=6, purple) 2 mM Trolox-C.

D. Averaged results showing the effect of laser pulses on I_{ss} (tail) without (N=9, black) and with (N=6, purple) 2 mM Trolox-C.

E. Averaged results showing the effect of laser pulses on I_h (tail) without (N=9, black) and with (N=6, purple) 2 mM Trolox-C.

Chemically generated $^1O_2$ modifies WT spHCN but not spHCN/H462A mutant channel

To further confirm the involvement of 1O2 and exclude the involvement of other reactive oxygen species, we tested the effect of H2O2 alone, ClO- alone, or H2O2 together with ClO-, a chemical reaction that has been widely used to generate 1O2 (Fig. 24A). Separately applying H2O2 or ClO- had no obvious effects on the function of the spHCN channel. In contrast, exposing the membrane patch to freshly mixed H2O2 and ClO- leads to an immediate increase in macroscopic current amplitude (Fig. 24B; 24D). To make the modification effects more observable, we noticed that the isolated membrane patch has to be mounted near the opening of the double-barrel glass pipette where H2O2 and ClO- solutions flow out and mix (Fig. 25A). This is consistent with the fact that 1O2 has a very short life time in microseconds. Again, we repeated the same experiments on the spHCN/H462A mutant channel and observed no obvious responses to the chemical mixture of H_2O_2 and ClO^- (Fig. 24C; 24D). Thus, for both WT and H462A mutant spHCN channels, the chemically generated 1O2 reproduced modifications effects by photodynamic processes but in the absence of light stimulation and photosensitizer.

Finally, we set out to study the sensitivity of the spHCN channel to hydroxyl radical and superoxide, the other two reactive oxygen species (Fig. 24E). We applied hydrogen peroxide and iron sulfate to the bath solution. After 6 minutes of incubation, we didn't observe any obvious changes in the function of the channel (Fig. 24F). To test the involvement of superoxide, we added Xanthine and Xanthine oxidase to the bath solution (Fig. 24G). Again, no obvious changes in the current traces were detected. Averaged results are shown in Fig. 25B-25C. Taken together, in conjunction with the results of 1O2 quenchers and generators, these observations support the involvement of $^1O_2$ in the photodynamic modification of spHCN channel and exclude the contribution from other reactive oxygen species.

A

$$H_2O_2 + ClO^- \rightarrow H_2O + Cl^- + {}^1O_2$$

B

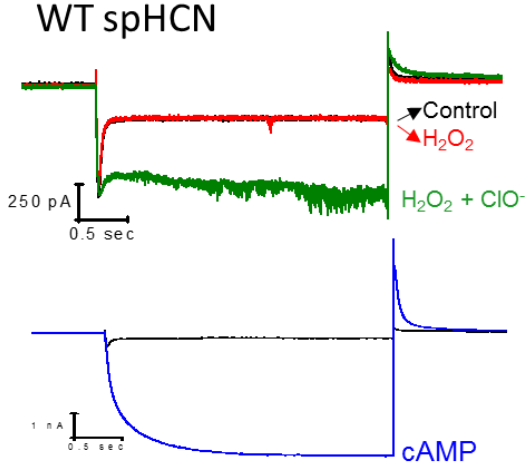

C

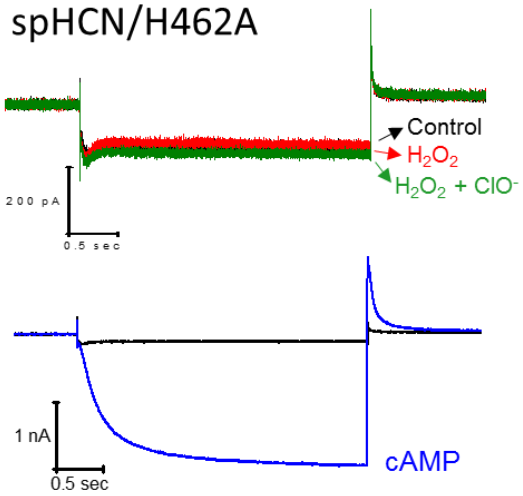

D

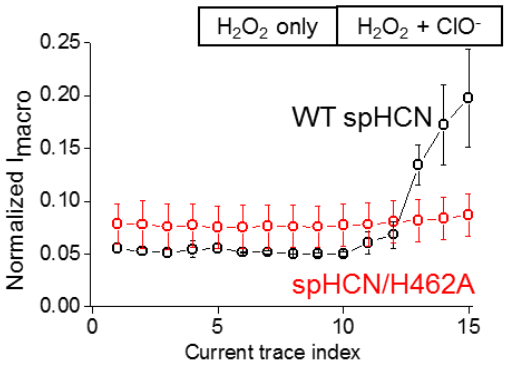

E

$$H_2O_2 + Fe^{2+} \rightarrow Fe^{3+} + OH^- + \cdot OH$$

$$Xanthine + 2O_2 + H_2O \rightarrow uric\ acid + 2O_2^{\cdot -} + 2H^+$$

F

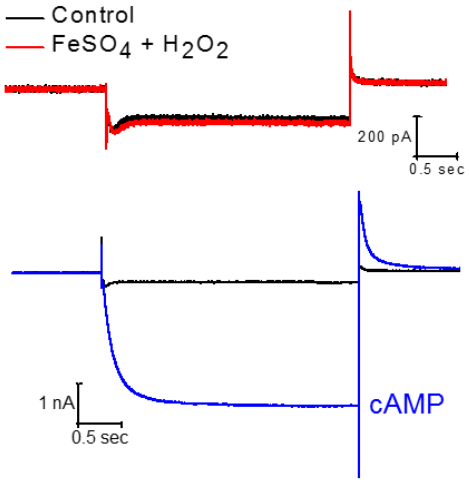

G

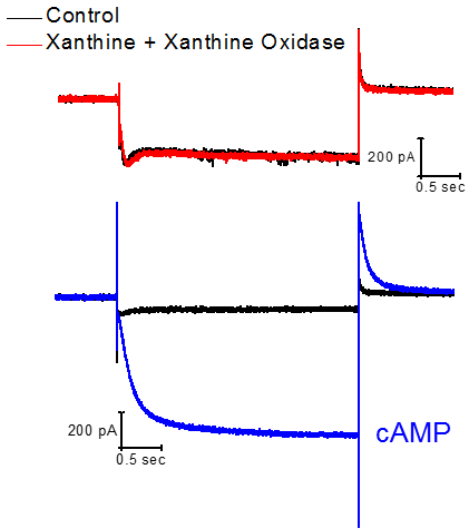

Figure 24. The WT spHCN (not spHCN/H462A) channel responds to chemically generated 1O2 but not to other reactive oxygen species.

A. Chemical generation of 1O2 by mixing hydrogen peroxide and sodium hypochlorite. **B.** Top, current traces of WT spHCN channel recorded under control condition (black), in the presence of 10 mM H_2O_2 only (red), or 10 mM H2O2 and 10 mM NaClO (green). Bottom, current trace recording before and after 10 µM cAMP illustrating the maximal current. **C.** The spHCN/H462A mutant channel shows no response to H2O2+NaClO. **D.** Averages results showing the responses to H_2O_2 only followed by H_2O_2+NaClO by WT (N=3, black) or H462A mutant (N=3, red) spHCN channel. **E**. Reaction schemes for the generation of hydroxyl or superoxide radicals. **F.** WT spHCN channel shows no response (N=3) to mixture of FeSO4 (1 mM) and H_2O_2 (15 mM) which generates hydroxyl radical. G.WT spHCN channel shows no response (N=3) to mixture of xanthine (5 mM) and xanthine oxidase (20 mU; 6 minutes of incubation) which generates superoxide.

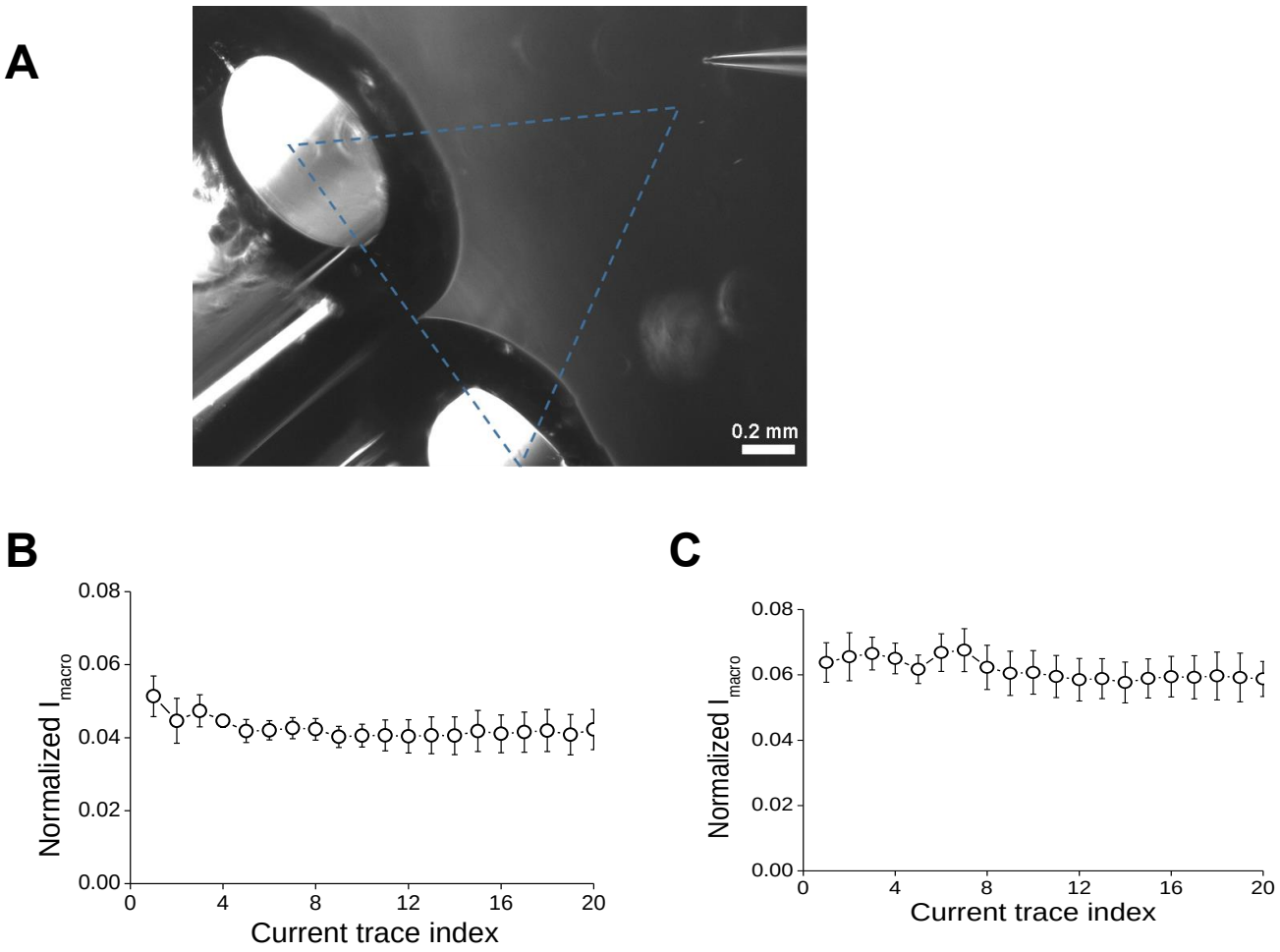

Fig. 25. Configuration of the perfusion system for H_2O_2 and ClO^- and averaged results of effects of hydroxyl and superoxide radicals.

A. Top, configuration of the perfusion system and positioning of the recording pipette. A double-barrel glass pipette was used to deliver H_2O_2 and ClO^- in each of its tube to the membrane patch. The X-Y position of membrane patch was adjusted according to the picture. The membrane patch was lowered to the same focal plane of the lower edge of the double-barrel pipette.

B. Averaged results showing the effect of 1 mM $FeSO_4$ + 15 mM H_2O_2 on I_{macro}.

C. Averaged results showing the effect of 5 mM Xanthine + 15 mU Xanthine oxidase on I_{macro}.

3.5 DISCUSSION:

Here we studied the modification of the spHCN channel by singlet oxygen, which had been generated through either a canonical photodynamic process or a chemical process in the absence of light. In the absence of cAMP, photodynamic modification of the spHCN channel abolishes the voltage-dependent channel inactivation and increases the hyperpolarization-activated Ih and the voltage-insensitive Iinst. These modification effects can be reproduced by exposing the spHCN channel to a chemical mixture of hypochlorite and hydrogen peroxide, which together with a consortium of chemicals including $^1O_2$ quenchers and generators of other ROS, help establish $^1O_2$ as a critical player in the photodynamic modification of the spHCN channel.

Remarkably, for both spHCN and mHCN2 channels, a highly conserved histidine residue located near the activation gate in S6 appears to be critical for the photodynamic modification. Both mHCN2/H434A and spHCN/H462A mutant channels show minimal responses to the light pulses applied during the hyperpolarization voltage command. For the spHCN/H462A channel, light pulses applied to the channel in the closed state moderately increase current amplitude but largely failed to remove the inactivation of the channel. This difference between the WT and the H462A mutant channel should not be attributed to the binding of FITC-cAMP, which shows no obvious difference between WT and H462A mutant channels (Fig. S11). Moreover, the spHCN/H462A mutant channel shows minimal responses to the $^1O_2$ generated through another photosensitizer (Rose Bengal) or through a chemical process (H_2O_2+ClO-). Therefore, H462 in the spHCN channel could be the major substrate being modified by $^1O_2$. It is known that the imidazole ring in histidine reacts with $^1O_2$ at a very fast reaction rate (5 x 107 M-1s-1) [182,183]. The pair of electrons occupying the highest molecular orbital in 1O2 show high reactivity towards electro-rich chemical structure, especially those with conjugated double bonds[170]. It is possibly

that the $^1O_2$-Histidine reaction involves the formation of endo-peroxide as an intermediate and ends in a complex mixture of products, of which the mechanism are being investigated by both experimental and theoretical approaches[183]. Further studies are needed to pinpoint the chemical nature of the reaction between $^1O_2$ and H462. Alternatively, it is possible that H462 is only one of several residues targeted by singlet oxygen whereas the histidine to alanine mutation limits the express of I_{inst} and I_{ss} (tail). Other than histidine, tyrosine, methionine, cysteine, and tryptophan can also react with $^1O_2$ (Kim et al., 2012).

Previously we had shown that the photodynamic modification of the mHCN2 channel in the open state slows down the channel deactivation and increases the instantaneous component, whereas the major effect on the closed channel is the decrease in the I_h amplitude [117]. For the spHCN channel, photodynamic modifications on both closed and inactivated channels abolish the channel inactivation. Photodynamic modification of closed spHCN channel leads to more pronounced increases in Ih but only slight increase in Iinst. These state-dependent responses to photodynamic modification for both mHCN2 and spHCN channel could be attributed to the difference in the accessibility of the critical residues to $^1O_2$ at different conformations and might reflects subtle but critical structural reorganizations during the gating process. For the spHCN channel, the inactivation has been attributed to the re-closure of the same activation gate, due to a loose coupling or slippage between the voltage-sensor and the gate[43,146]. Notably, H462 in spHCN and H434 in mHCN2 are located in S6 and very close to the activation gate in both channels.

$^1O_2$ is one of the least understood ROS, partially due to its volatile chemical nature and the complex cross-interactions with signal transduction pathways [172]. It is often difficult to pinpoint whether the contribution is truly mediated by $^1O_2$ but not by other ROS. Here to confirm $^1O_2$ as the major player behind the photodynamic modifications, we applied a popularly used photosensitizer (Rose

Bengal) and a chemical process to generate $^1O_2$ (hydrogen peroxide and hypochlorite), which produced comparable changes in channel behavior especially in terms of removing the channel inactivation. The involvement of $^1O_2$ is further supported by the application of $^1O_2$ quenchers (Sodium azide and Trolox-C) which effectively abolish the photodynamic modification effects. Moreover, we used a consortium of chemicals to exclude the direct involvement of hydrogen peroxide, superoxide, and hydroxyl radicals. Taken together, this study helps provide further insights into the modification of ion channels by $^1O_2$, a ubiquitous but still mysterious signaling molecule.

CHAPTER 4

ONGOING STUDIES, GENERAL DISCUSSION, FUTURE DIRECTIONS AND CONCLUSIONS

Ongoing studies: Photodynamic transformation of retinal CNGA1 channel:

Role of singlet oxygen in the eye: The physiological role of singlet oxygen is still relatively unexplored and thus possesses a tremendous research potential. To this end we have studied how singlet oxygen modifies CNGA1 channel. Cyclic nucleotide gated ion channels (CNG channels) belong to the superfamily of voltage-gated potassium channels and play a central role in the photo-transduction pathway in the photoreceptors of the retina[184]. Photoactive chromophores including all-trans retinal are abundantly present in the eye and are effective photosensitizers. When exposed to light including UV radiation, retinal or other intracellular photosensitizers, can generate reactive oxygen species including singlet oxygen. As protective mechanisms against these reactive species, the eye tissue is equipped with robust antioxidant species like lutein, zeaxanthin and other carotenoids[185]. But, an age related decline in the function of antioxidant mechanisms and thereby gradual loss of vision has been long known but the underlying molecular mechanism remain elusive[186–188]. Earlier we have shown that mHCN2 and spHCN channels are sensitive to modification by singlet oxygen ($^1O_2$). Considering the potential abundance of singlet oxygen production in the eye, the evolutionary closeness and structural similarity of CNG channels to HCN channels[23,184], we hypothesized that singlet oxygen can modify CNG channels. Our preliminary results show that bovine CNGA1 channels undergo photodynamic transformation in a state dependent manner. Brief light stimulation of Rose-Bengal, a popularly used singlet oxygen generator, could enhance the opening of bovine CNGA1 channels, both in presence or absence of the ligand cyclic guanosine monophosphate). The effects of singlet oxygen seem to be more pronounced when the concentration of cGMP is below saturating level. We would like to extend this study to understand the mechanistic effects of singlet oxygen at single molecule level. Some potential directions that can be explored to this end are:

Preliminary results:

We used the inside-out configuration of the patch-clamp technique to record currents from bovine CNGA1 channels expressed in Xenopus oocytes. Unlike the HCN channel isoforms, CNGA1 channels are not strongly voltage gated. CNGA1 channels are ligand gated channels with cGMP being the primary ligand. We measured the dose-response relationship between CNGA1 channels and its ligand cGMP and the EC50 was found to be 32.6μM (Fig 26). We then tested the effects of singlet oxygen on CNGA1 channels. We generated singlet oxygen using a popular photosensitizer called Rose Bengal. Interestingly, we found that singlet oxygen generated by photo activation of Rose Bengal could modify the channel biophysical properties (Fig 27a). In the presence of 100nM Rose Bengal and sub-saturating concentrations of ligand, after the laser pulse, we observed an increase in the current amplitude. This laser induced increase in current amplitude was not washable as opposed to the ligand induced current, suggesting that the photo-dynamically generated singlet oxygen can modify the channel irreversibly. Furthermore, the effects of singlet oxygen seem to be not voltage dependent (Fig 27b). Similar effects were also observed when we generated singlet oxygen in the absence of the ligand cGMP (data not shown). We then measured the effects of singlet oxygen in the presence of saturating concentrations of cGMP. Surprisingly, we found that singlet oxygen generated in the presence of saturating cGMP concentrations decreased the current amplitude through CNGA1 channel (Fig 28). Moreover, some of the channels remained in the open state even after cGMP has been washed away. Further studies are needed to exactly pinpoint the effects of singlet oxygen on the CNGA1 channel.

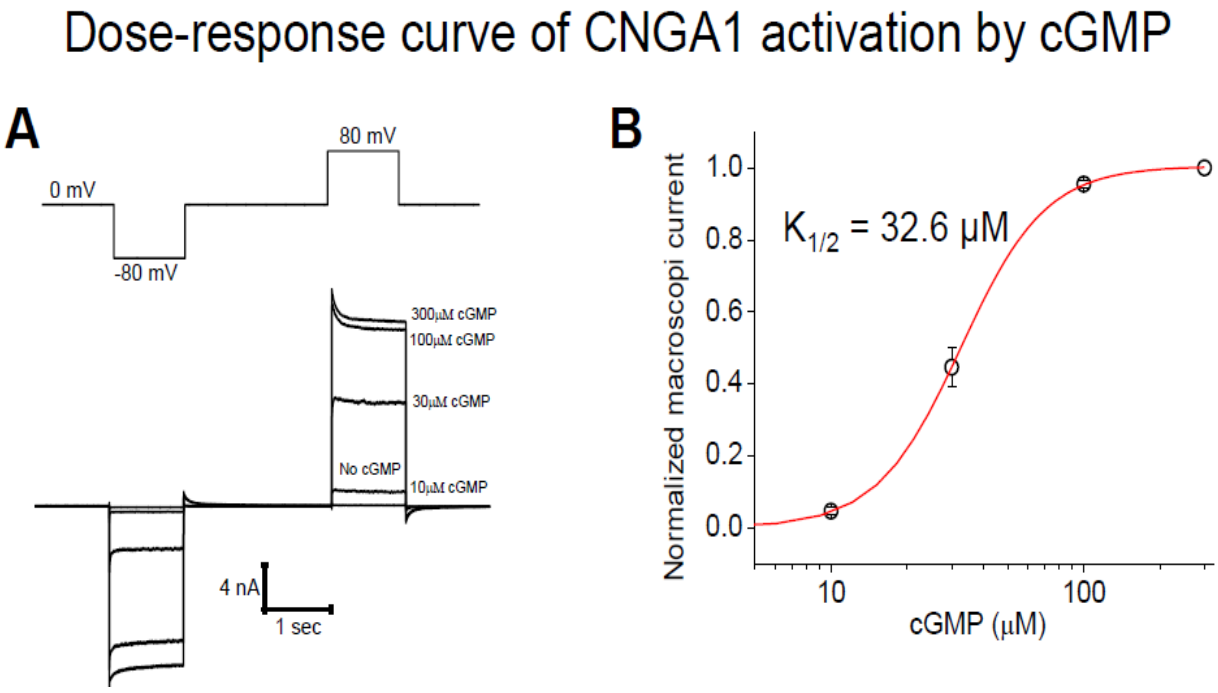

Fig 26 Dose-response curve of CNGA1 activation by cGMP

A. Top, Voltage protocol. Bottom, raw current traces recorded under different cGMP concentration.

B. Dose response, curve is fitted by Hill equation. K1/2, 32.6 ±0.6 μM

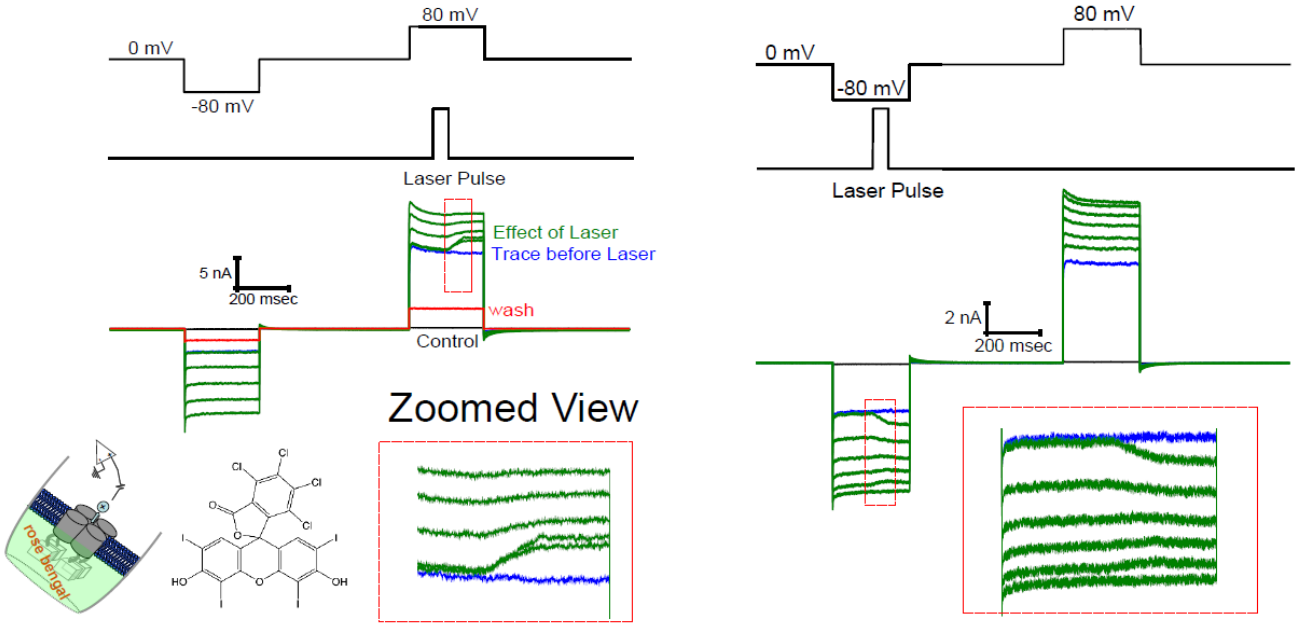

Fig 27 Singlet oxygen generated using Rose Bengal modifies CNGA1 channel in presence of 30 µM cGMP

A. Top, voltage step protocol and the timing of laser pulses (applied at +80 mV). Bottom: the last current trace before (blue) and current traces after laser pulses (green). After washing off Rose Bengal and cGMP, remaining currents (red) indicate permanent modifications left on the channel.

B. Laser pulses were applied at the holding potential of -80 mV**.** Top, voltage and laser pulse protocol. Bottom, current traces before (blue) and after laser pulses (green).

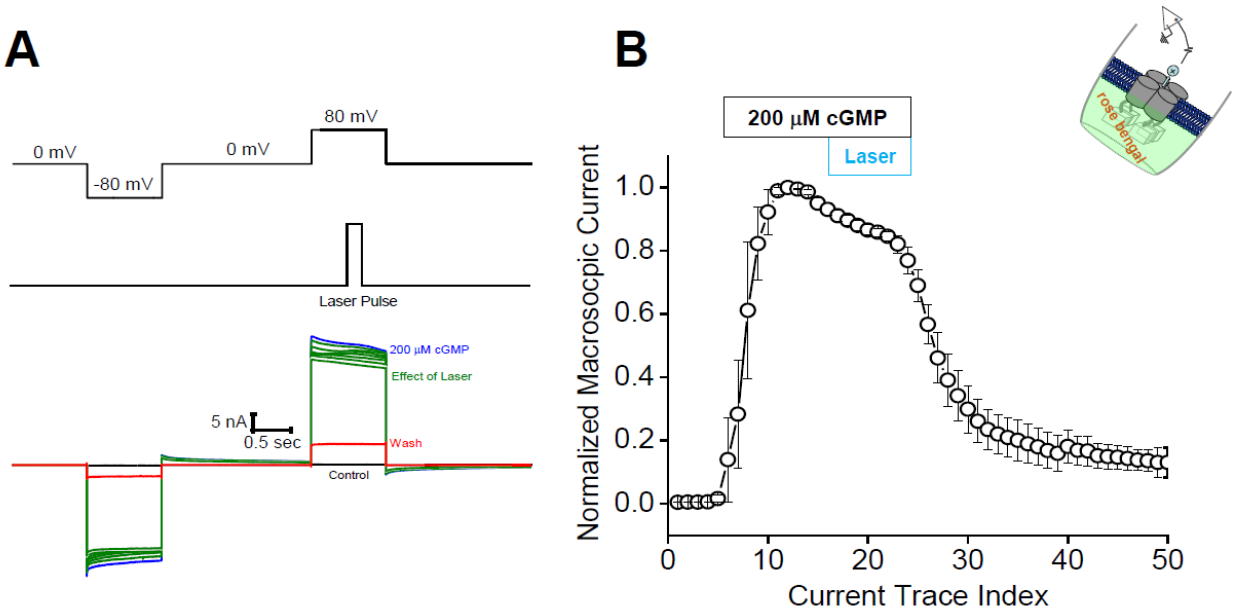

Fig 28 Singlet oxygen generated using Rose Bengal modifies CNGA1 channel in the presence of 200 µM cGMP

A. Top, voltage step protocol and the timing of laser pulse. Bottom: the last current trace before (blue) and current traces after (green) laser pulse application in the presence of 200 nM Rose Bengal in the 200 mM (saturating) cGMP. Some of the channels remain in persistently open state after wash (red trace).

B. Averaged results showing a decrease in the current amplitude subsequent to the laser pulse application. The current amplitude was normalized to the traces before the application of laser

4.2. General Discussion:

The precise mechanism of how ligands or regulatory proteins bind to and activate their receptors has been an area of debate for many years. The central hypothesis has been that ligand binding begets a conformational change in the receptor, but whether the corresponding conformational change is induced by the ligand (Induced Fit model) or the ligand preferentially chooses one of the many infinite number of microstates that the receptor fluctuates in and then stabilizes this conformation (Conformational selection) is not yet clear [136,189]. Technical advances in NMR, X-ray crystallography and also MD simulations have shown that the proteins are dynamic in nature undergoing many conformations with different levels of potential energies. This ensemble of various levels of conformational energies gives rise to an energy landscape of proteins[189,190] . Ligand binding is believed to shift the equilibrium of this conformational ensemble towards a particular conformation. Furthermore, the ligand binding at one region leads to a conformational change or a functional consequence at a distant site in the protein; a mechanism known as allostery. Much progress has been made in understanding protein structure and function but the mechanism of how proteins achieve allostery is still under intense scrutiny. Crystal structures which provide a snapshot of one of the many conformations adopted by the protein do not provide enough information pertaining to the protein's function, especially to understand complicated aspects such as protein allostery, therefore functional assays are need of the hour. Techniques such as patch clamp fluorometry (PCF) provides one such opportunity to test both the receptor/channel function and the conformational changes associated with it simultaneously.

Ligand dependent gating in HCN channels is a classic example of an allosteric effect of ligand on the receptor. Binding of cAMP to the CNBD opens the channels gate located further away from the ligand binding pocket. Much work has been done on the mammalian HCN channels,

especially mHCN2 and many interesting aspects of ligand dependent gating have been uncovered. Previous studies have shown that cAMP binding to the HCN channel in the resting/deactivated state is not as strong as that of the activated state, in other words ligand binds preferentially to the open channel and thus stabilizes it in the open conformation. This idea that the ligand binding depends on the functional state of entire protein but not just the conformation of an isolated domain (CNBD) could be the most appropriate argument to explain the protein allostery.

Currently, the information related with the ligand binding to an inactivated channel/receptor is lacking. Studying cAMP binding in spHCN channel using fluorescent cAMP analogues is an ideal way to address this gap in the knowledge. Our research shows that cAMP binding to the inactivated spHCN channels is significantly weaker compared to the closed state suggesting that the inactivated state in spHCN channel could be a state distinct from the closed state. The original line of thought was that the inactivated state occurs due to closure of the activation gate of the channel[43], but our results support the notion that the inactivated state could be yet another distinct state with potential alterations resting in the other parts of the channel such as CNBD. Using the lock open state and the spHCN/F459L mutant channels, we show that the open channel has higher cAMP binding compared to that of the closed state. Thus, the three distinct states of spHCN exhibit starkly different ligand binding profiles with the cAMP binding preference decreases in the order active/open state > deactivated state/closed state > inactivated state. To circumvent the argument that the differential binding was due to changes in local environment (including the alterations in fluorophore properties upon binding to the membrane, changes in the lipid environment of the membrane) that indirectly affects quantum efficiency of fluorescence release, we choose FITC or Alexa conjugated cAMP as the marker for cAMP binding.

As shown above, studying ligand binding using fluorescently labelled cAMP analogues in HCN channels has given valuable information. Nevertheless, caution should be exercised when the photosensitizer tagged molecules are used. Other than the release of fluorescent light, many photosensitizers generate singlet oxygen molecules a phenomenon known as photodynamic effect (PDT). Singlet oxygen can modify the protein molecule under study and thereby can be a caveat in interpreting the data. spHCN channel can be modified by singlet oxygen, where it removes the inactivation of the channel. Thus, we had to take extreme caution in our data interpretation. To circumvent this issue we repeated our cAMP binding studies in the presence of Trolox-C which can quench singlet oxygen molecules. The binding profile of spHCN channel was similar both in the presence and absence of the quencher Trolox-C suggesting that the changes in cAMP binding we observed are not artefacts of photodynamic transformation. Furthermore, a photodynamic effect a mutant spHCN channel which is resistant to the photodynamic effect, shows similar cAMP binding profile to that of WT spHCN further strengthening the argument that the results we obtained were not a result of the singlet oxygen effect on the channel. Finally, the effects of singlet oxygen on bio-macromolecules should be taken into consideration and if possible ruled out wherever fluorescently labelled compounds are used in the experiments and especially when performing functional studies.

Future Directions:

1. Further establish the effects of singlet oxygen on CNG channels at various cGMP concentrations. Also test whether modified channels show altered sensitivity to cGMP.
2. To test whether singlet oxygen has an effect on the open probability of CNGA1 channels. We will employ either single channel recordings or Non stationary Noise Analysis (NSNA).
3. To tease out the residues that underlie the channel modification, we would like to target candidate residues through site directed mutagenesis.
4. To test if naturally occurring singlet oxygen quenchers like beta carotene and other Xanthophylls have protective effects on the channels under physiological conditions.
5. Furthermore, it would be interesting to study the effects in primary cells like rods and cones from mouse retina.

4.4 Conclusion:

Ligand binding to the receptor is at the core of most signal transduction events. Understanding the molecular determinants and the mechanistic details underlying ligand binding could be important in designing new drugs that either facilitate or impede the corresponding channel/receptor function. Fluorescently labelled cAMP analogues can be used as probes to study ligand binding in HCN channels. On the other hand, care should be taken in designing and interpreting these experiments, photodynamically generated singlet oxygen can modify properties of bio-macromolecules such as HCN channel in a spatially and temporally specific manner. Photo modification of native channels in neurons by singlet oxygen can be developed into a useful biophotonics/optigenetics tool.

Appendix

SHANK3 encodes a scaffolding protein that is highly enriched in the post-synaptic density (PSD) of excitatory synapses [191–193]. The full-length Shank3 protein contains 1,731 amino acids (a.a.) which fold into highly conserved domains that mediate protein-protein interactions: an Ankyrin repeat domain, a SH3 domain, a PDZ domain, a proline-rich domain, and a sterile alpha motif (SAM) domain [194]. Due to multiple intragenic promoters and alternative splicing, a complex array of Shank3 isoforms exists. These isoforms are often differentially affected by mutations and deletions in the Shank3 gene discovered from human patients, which have been modelled by over a dozen knockout or transgenic mouse lines [195–201]. Most of these knockout mice reproduced key features of ASD, including obsessive-compulsive disorders, deficits in social interaction, and increased levels of anxiety [197]. At the synapse level, the affected neurons show morphological defects including thinner and shorter PSD, sparse spine density, and impaired synaptic transmission [198,202–204]. However, crucial gaps still remain in the understanding of the impacts of Shank3 deficiency on the cellular physiology, especially the basic electrical properties of affected neurons.

Biophysical basis of SHANK3 and HCN Channel Interactions:

The increase in HCN channel expression when co-expressed with SHANK3 is an intriguing observation, with numerous open questions yet to be answered. Further investigation on other HCN channel isoforms is necessary, at the same time the mechanistic details underlying the increased expression have to be explored. Considering the fact that the increased expression at protein did not correlate with an increase in mRNA levels, post translational modifications and protein trafficking of the protein to and from the membrane should be studied. Whether SHANK3

stabilizes HCN channels on the membrane or increases the trafficking to the membrane or slows down the channel recycling from the membrane are open questions. Yet another interesting aspect of SHANK3 regulation is whether SHANK3 interaction with HCN channel affects the cAMP binding of the channel, to this end the HCN/R591E mutant that does not bind the cAMP will be necessary to tease out these differences in the absence of cAMP. To test these interesting questions the following experiments will be planned:

RESULTS

To study the impact of Shank3 on the expression of HCN2 channel, we started from the heterologous expression system of Xenopus oocyte and co-injected the cRNAs encoding HCN2 and Shank3. We separately tested two isoforms, Shank3A and Shank3C (Fig. 29A), of which the related knockout mice, Shank3Δ4-9 and Shank3ΔΔΔ-16, respectively, are characterized later in this study [198,205]. Two-electrode voltage clamp (TEVC) measurements were used to measure the whole-cell HCN current. As shown in Fig. 29B-C, co-expressing either Shank3A or Shank3C significantly increases the HCN current amplitude (20.4 ± 5.8% for Shank3C and 30.1 ± 6.5% for Sahnk3A). Shank3C or Shank3A has minimal effects on the gating kinetics but shifted the V1/2 value – the voltage step that leads to half maximal opening - towards hyperpolarization by ~4mV (Fig. 29D). To check the surface expression of HCN2, we co-expressed EGFP-tagged HCN2 channel with Shank3 and subjected the injected cells to confocal microscopy (Fig. 29E). The presence of Shank3A or Shank3C clearly increases the fluorescence intensity of HCN2-EGFP. However, under the whole-cell configuration, the arc of fluorescence signals does not exclusively correspond to the signal from the membrane but also the HCN2-EGFP molecules in the vicinity. To further clarify the membrane expression, we applied patch-clamp fluorometry on isolated

membrane patches pulled from the cell surface and obtained direct support for the enhancement of HCN channel surface expression upon co-expression with Shank3 (Fig.29F).

Future Directions:

1. Express HCN1 in *Xenopus* oocytes with or without SHANK3 and measure the currents using two electrode voltage clamp, to see if SHANK3 can affect the surface expression of other isoforms of HCN channels.
2. Express the R591E mutants and see whether the increased expression in HCN channels is consistent with the WT channels.
3. Determine the exact physical location of the interaction between SHANK3 and HCN channel, using a combination of yeast two hybrid system and site directed mutagenesis.

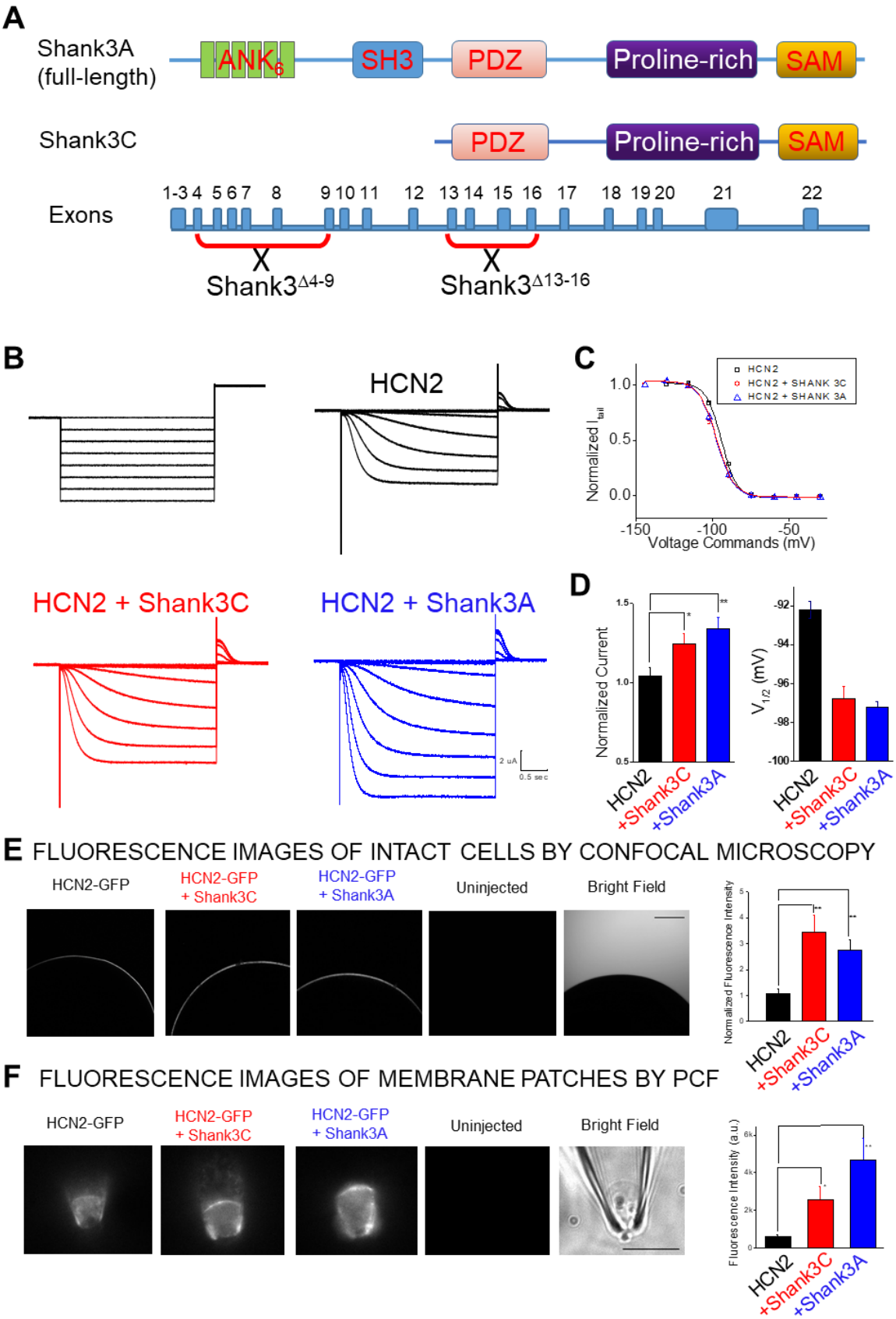
A
Shank3A
(full-length)
ANK6
SH3
PDZ
Proline-rich
SAM
Shank3C
PDZ
Proline-rich
SAM
Exons
1-3 4 5 6 7 8 9 10 11 12 13 14 15 16 17 18 19 20 21 22
X
Shank3Δ4-9
X
Shank3Δ13-16
B
HCN2
HCN2 + Shank3C
HCN2 + Shank3A
2 uA
0.5 sec
C
HCN2
HCN2 + SHANK 3C
HCN2 + SHANK 3A
Normalized I tail
1.0
0.5
0.0
-150
-100
-50
Voltage Commands (mV)
D
Normalized Current
1.5
1.0
0.5
*
**
HCN2
+Shank3C
+Shank3A
V1/2 (mV)
-92
-94
-96
-98
-100
HCN2
+Shank3C
+Shank3A
E FLUORESCENCE IMAGES OF INTACT CELLS BY CONFOCAL MICROSCOPY
HCN2-GFP
HCN2-GFP
+ Shank3C
HCN2-GFP
+ Shank3A
Uninjected
Bright Field
Normalized Fluorescence Intensity
HCN2
+Shank3C
+Shank3A
F FLUORESCENCE IMAGES OF MEMBRANE PATCHES BY PCF
HCN2-GFP
HCN2-GFP
+ Shank3C
HCN2-GFP
+ Shank3A
Uninjected
Bright Field
Fluorescence Intensity (a.u.)
HCN2
+Shank3C
+Shank3A

Figure 29. Effect of SHANKA and SHANK3C co-expression with HCN channels

Shank3 isoforms improve the surface expression of recombinant HCN2 channel in *Xenopus* oocyte. A. Schematic drawings of the genomic structure of Shank3 gene and two splicing isoforms, Shank3A (full-length) and Shank3C (missing Ankyrin and SH3 domains in the N-terminus). B. Representative HCN2 current (top; no Shank3) recording from whole oocytes by TEVC. A series of hyperpolarizing voltage steps (bottom) were used to activate the channel. C. HCN2 current recorded from oocytes co-injected with Shank3A (top) or Shank3C (bottom). D. Summary of Shank3 effects on the function of HCN2 channel. Values of V1/2, HCN2: -92.2 ± 1.1 mV; HCN2 + Shank3C, -96.0 ± 1.5 mV; HCN2 + Shank3A, -97.2 ± 0.6 mV. E. Confocal images of whole oocyte expressing (from left to right) HCN2 alone, HCN2+Shank3A, HCN2+Shank3C, and un-injected cell. F. Fluorescence images of membrane fractions pulled from oocyte surface and held within the glass patch-clamp pipette in the inside-out configuration. Statistics are shown in the right.

REFERENCES

1. WEIDMANN, S. Effect of current flow on the membrane potential of cardiac muscle. *J. Physiol.* **115,** 227–236 (1951).
2. Noble, D. & Tsien, R. W. Outward membrane currents activated in the plateau range of potentials in cardiac Purkinje fibres. *J. Physiol.* **200,** 205–231 (1969).
3. McAllister, R. E. & Noble, D. The time and voltage dependence of the slow outward current in cardiac Purkinje fibres. *J. Physiol.* **186,** 632–662 (1966).
4. DiFrancesco, D. & McNaughton, P. A. The effects of calcium on outward membrane currents in the cardiac Purkinje fibre. *J. Physiol.* **289,** 347–373 (1979).
5. Seyama, I. Characteristics of the rectifying properties of the sino-atrial node cell of the rabbit. *J. Physiol.* **255,** 379–397 (1976).
6. Brown, H. F., Giles, W. & Noble, S. J. Membrane currents underlying activity in frog sinus venosus. *J. Physiol.* **271,** 783–816 (1977).
7. Noma, A. & Irisawa, H. A time- and voltage-dependent potassium current in the rabbit sinoatrial node cell. *Pflugers Arch.* **366,** 251–258 (1976).
8. Brown, H. & Difrancesco, D. Voltage-clamp investigations of membrane currents underlying pace-maker activity in rabbit sino-atrial node. *J. Physiol.* **308,** 331–351 (1980).
9. Brown, H. F., DiFrancesco, D. & Noble, S. J. How does adrenaline accelerate the heart? *Nature* **280,** 235–236 (1979).
10. Yanagihara, K. & Irisawa, H. Inward current activated during hyperpolarization in the rabbit sinoatrial node cell. *Pflugers Arch.* **385,** 11–19 (1980).
11. Brown, H. F., DiFrancisco, D. & Noble, S. J. Adrenaline action on rabbit sino-atrial node [proceedings]. *J. Physiol.* **290,** 31P–32P (1979).
12. DiFrancesco, D. & Mangoni, M. Modulation of single hyperpolarization-activated channels (i(f)) by cAMP in the rabbit sino-atrial node. *J. Physiol.* **474,** 473–482 (1994).
13. Bobker, D. H. & Williams, J. T. Serotonin augments the cationic current Ih in central neurons. *Neuron* **2,** 1535–1540 (1989).
14. DiFrancesco, D. & Tromba, C. Muscarinic control of the hyperpolarization-activated current (if) in rabbit sino-atrial node myocytes. *J. Physiol.* **405,** 493–510 (1988).

15. McCormick, D. A. & Pape, H. C. Properties of a hyperpolarization-activated cation current and its role in rhythmic oscillation in thalamic relay neurones. *J. Physiol.* **431,** 291–318 (1990).
16. DiFrancesco, D. & Tortora, P. Direct activation of cardiac pacemaker channels by intracellular cyclic AMP. *Nature* **351,** 145–147 (1991).
17. DiFrancesco, D. A new interpretation of the pace-maker current in calf Purkinje fibres. *J. Physiol.* **314,** 359–376 (1981).
18. DiFrancesco, D. A study of the ionic nature of the pace-maker current in calf Purkinje fibres. *J. Physiol.* **314,** 377–393 (1981).
19. Mayer, M. L. & Westbrook, G. L. A voltage-clamp analysis of inward (anomalous) rectification in mouse spinal sensory ganglion neurones. *J. Physiol.* **340,** 19–45 (1983).
20. Pape, H. C. Queer current and pacemaker: the hyperpolarization-activated cation current in neurons. *Annu. Rev. Physiol.* **58,** 299–327 (1996).
21. Luthi, A. & McCormick, D. A. Periodicity of thalamic synchronized oscillations: the role of Ca2+-mediated upregulation of Ih. *Neuron* **20,** 553–563 (1998).
22. Bader, C. R. & Bertrand, D. Effect of changes in intra- and extracellular sodium on the inward (anomalous) rectification in salamander photoreceptors. *J. Physiol.* **347,** 611–631 (1984).
23. Biel, M., Wahl-Schott, C., Michalakis, S. & Zong, X. Hyperpolarization-activated cation channels: from genes to function. *Physiol. Rev.* **89,** 847–885 (2009).
24. Santoro, B., Grant, S. G., Bartsch, D. & Kandel, E. R. Interactive cloning with the SH3 domain of N-src identifies a new brain specific ion channel protein, with homology to eag and cyclic nucleotide-gated channels. *Proc. Natl. Acad. Sci. U. S. A.* **94,** 14815–14820 (1997).
25. Santoro, B. *et al.* Identification of a gene encoding a hyperpolarization-activated pacemaker channel of brain. *Cell* **93,** 717–729 (1998).
26. Ludwig, A., Zong, X., Jeglitsch, M., Hofmann, F. & Biel, M. A family of hyperpolarization-activated mammalian cation channels. *Nature* **393,** 587–591 (1998).
27. Ishii, T. M., Takano, M., Xie, L. H., Noma, A. & Ohmori, H. Molecular characterization of the hyperpolarization-activated cation channel in rabbit heart sinoatrial node. *J. Biol. Chem.* **274,** 12835–12839 (1999).

28. Gauss, R., Seifert, R. & Kaupp, U. B. Molecular identification of a hyperpolarization-activated channel in sea urchin sperm. *Nature* **393,** 583–587 (1998).
29. Seifert, R. *et al.* Molecular characterization of a slowly gating human hyperpolarization-activated channel predominantly expressed in thalamus, heart, and testis. *Proc. Natl. Acad. Sci. U. S. A.* **96,** 9391–9396 (1999).
30. Vaccari, T. *et al.* The human gene coding for HCN2, a pacemaker channel of the heart. *Biochim. Biophys. Acta* **1446,** 419–425 (1999).
31. Krieger, J., Strobel, J., Vogl, A., Hanke, W. & Breer, H. Identification of a cyclic nucleotide- and voltage-activated ion channel from insect antennae. *Insect Biochem. Mol. Biol.* **29,** 255–267 (1999).
32. Yang, Q. *et al.* Hyperpolarization-activated, cyclic nucleotide-gated cation channels in Aplysia: Contribution to classical conditioning. *Proc. Natl. Acad. Sci. U. S. A.* **112,** 16030–16035 (2015).
33. Ludwig, A. *et al.* Two pacemaker channels from human heart with profoundly different activation kinetics. *EMBO J.* **18,** 2323–2329 (1999).
34. Soltesz, I. *et al.* Two inward currents and the transformation of low-frequency oscillations of rat and cat thalamocortical cells. *J. Physiol.* **441,** 175–197 (1991).
35. Altomare, C. *et al.* Heteromeric HCN1-HCN4 channels: a comparison with native pacemaker channels from the rabbit sinoatrial node. *J. Physiol.* **549,** 347–359 (2003).
36. Chen, S., Wang, J. & Siegelbaum, S. A. Properties of hyperpolarization-activated pacemaker current defined by coassembly of HCN1 and HCN2 subunits and basal modulation by cyclic nucleotide. *J. Gen. Physiol.* **117,** 491–504 (2001).
37. McKay, D. B. & Steitz, T. A. Structure of catabolite gene activator protein at 2.9 A resolution suggests binding to left-handed B-DNA. *Nature* **290,** 744–749 (1981).
38. Shabb, J. B. & Corbin, J. D. Cyclic nucleotide-binding domains in proteins having diverse functions. *J. Biol. Chem.* **267,** 5723–5726 (1992).
39. Santoro, B. & Tibbs, G. R. The HCN gene family: molecular basis of the hyperpolarization-activated pacemaker channels. *Ann. N. Y. Acad. Sci.* **868,** 741–764 (1999).
40. Zhou, L. & Siegelbaum, S. A. Gating of HCN channels by cyclic nucleotides: residue contacts that underlie ligand binding, selectivity, and efficacy. *Structure* **15,** 655–670

(2007).

41. Su, Y. *et al.* Regulatory subunit of protein kinase A: structure of deletion mutant with cAMP binding domains. *Science* **269,** 807–813 (1995).
42. Weber, I. T. & Steitz, T. A. Structure of a complex of catabolite gene activator protein and cyclic AMP refined at 2.5 A resolution. *J. Mol. Biol.* **198,** 311–326 (1987).
43. Shin, K. S., Maertens, C., Proenza, C., Rothberg, B. S. & Yellen, G. Inactivation in HCN channels results from reclosure of the activation gate: desensitization to voltage. *Neuron* **41,** 737–744 (2004).
44. Akimoto, M. *et al.* A mechanism for the auto-inhibition of hyperpolarization-activated cyclic nucleotide-gated (HCN) channel opening and its relief by cAMP. *J. Biol. Chem.* **289,** 22205–22220 (2014).
45. Wainger, B. J., DeGennaro, M., Santoro, B., Siegelbaum, S. A. & Tibbs, G. R. Molecular mechanism of cAMP modulation of HCN pacemaker channels. *Nature* **411,** 805–810 (2001).
46. Wang, J., Chen, S. & Siegelbaum, S. A. Regulation of hyperpolarization-activated HCN channel gating and cAMP modulation due to interactions of COOH terminus and core transmembrane regions. *J. Gen. Physiol.* **118,** 237–250 (2001).
47. Barbuti, A., Baruscotti, M., Altomare, C., Moroni, A. & DiFrancesco, D. Action of internal pronase on the f-channel kinetics in the rabbit SA node. *J. Physiol.* **520 Pt 3,** 737–744 (1999).
48. Zagotta, W. N. *et al.* Structural basis for modulation and agonist specificity of HCN pacemaker channels. *Nature* **425,** 200–205 (2003).
49. Flynn, G. E., Black, K. D., Islas, L. D., Sankaran, B. & Zagotta, W. N. Structure and rearrangements in the carboxy-terminal region of SpIH channels. *Structure* **15,** 671–682 (2007).
50. Lolicato, M. *et al.* Cyclic dinucleotides bind the C-linker of HCN4 to control channel cAMP responsiveness. *Nat. Chem. Biol.* **10,** 457–462 (2014).
51. Hayoz, S., Tiwari, P. B., Piszczek, G., Uren, A. & Brelidze, T. I. Investigating cyclic nucleotide and cyclic dinucleotide binding to HCN channels by surface plasmon resonance. *PLoS One* **12,** e0185359 (2017).
52. Edman, A. & Grampp, W. Ion permeation through hyperpolarization-activated membrane

channels (Q-channels) in the lobster stretch receptor neurone. *Pflugers Arch.* **413,** 249–255 (1989).

53. Ho, W. K., Brown, H. F. & Noble, D. Internal K ions modulate the action of external cations on hyperpolarization-activated inward current in rabbit isolated sinoatrial node cells. *Pflugers Arch.* **424,** 308–314 (1993).
54. Guo, J., Ono, K. & Noma, A. A sustained inward current activated at the diastolic potential range in rabbit sino-atrial node cells. *J. Physiol.* **483 (Pt 1,** 1–13 (1995).
55. Mercuri, N. B., Bonci, A., Calabresi, P., Stefani, A. & Bernardi, G. Properties of the hyperpolarization-activated cation current Ih in rat midbrain dopaminergic neurons. *Eur. J. Neurosci.* **7,** 462–469 (1995).
56. Wollmuth, L. P. & Hille, B. Ionic selectivity of Ih channels of rod photoreceptors in tiger salamanders. *J. Gen. Physiol.* **100,** 749–765 (1992).
57. Fain, G. L., Quandt, F. N., Bastian, B. L. & Gerschenfeld, H. M. Contribution of a caesium-sensitive conductance increase to the rod photoresponse. *Nature* **272,** 466–469 (1978).
58. Hestrin, S. The properties and function of inward rectification in rod photoreceptors of the tiger salamander. *J. Physiol.* **390,** 319–333 (1987).
59. Frace, A. M., Maruoka, F. & Noma, A. External K+ increases Na+ conductance of the hyperpolarization-activated current in rabbit cardiac pacemaker cells. *Pflugers Arch.* **421,** 97–99 (1992).
60. Yu, X. *et al.* Calcium influx through If channels in rat ventricular myocytes. *Am. J. Physiol. Cell Physiol.* **292,** C1147-55 (2007).
61. Yu, X., Duan, K.-L., Shang, C.-F., Yu, H.-G. & Zhou, Z. Calcium influx through hyperpolarization-activated cation channels (I(h) channels) contributes to activity-evoked neuronal secretion. *Proc. Natl. Acad. Sci. U. S. A.* **101,** 1051–1056 (2004).
62. Young, E. C. Will the real single HCN channel please stand up? *Biophys. J.* **105,** 1549–1550 (2013).
63. Kole, M. H. P., Brauer, A. U. & Stuart, G. J. Inherited cortical HCN1 channel loss amplifies dendritic calcium electrogenesis and burst firing in a rat absence epilepsy model. *J. Physiol.* **578,** 507–525 (2007).
64. Dekker, J. P. & Yellen, G. Cooperative gating between single HCN pacemaker channels.

J. Gen. Physiol. **128,** 561–567 (2006).

65. Thon, S., Schmauder, R. & Benndorf, K. Elementary functional properties of single HCN2 channels. *Biophys. J.* **105,** 1581–1589 (2013).
66. Johnson, J. P. J. & Zagotta, W. N. The carboxyl-terminal region of cyclic nucleotide-modulated channels is a gating ring, not a permeation path. *Proc. Natl. Acad. Sci. U. S. A.* **102,** 2742–2747 (2005).
67. Michels, G. *et al.* Single-channel properties support a potential contribution of hyperpolarization-activated cyclic nucleotide-gated channels and If to cardiac arrhythmias. *Circulation* **111,** 399–404 (2005).
68. Simeone, T. A., Rho, J. M. & Baram, T. Z. Single channel properties of hyperpolarization-activated cation currents in acutely dissociated rat hippocampal neurones. *J. Physiol.* **568,** 371–380 (2005).
69. Liu, C. *et al.* Patch-clamp fluorometry-based channel counting to determine HCN channel conductance. *J. Gen. Physiol.* **148,** 65–76 (2016).
70. Suh, B.-C. & Hille, B. Regulation of ion channels by phosphatidylinositol 4,5-bisphosphate. *Curr. Opin. Neurobiol.* **15,** 370–378 (2005).
71. Suh, B.-C. & Hille, B. PIP2 is a necessary cofactor for ion channel function: how and why? *Annu. Rev. Biophys.* **37,** 175–195 (2008).
72. Logothetis, D. E., Petrou, V. I., Adney, S. K. & Mahajan, R. Channelopathies linked to plasma membrane phosphoinositides. *Pflugers Arch.* **460,** 321–341 (2010).
73. Pian, P., Bucchi, A., Decostanzo, A., Robinson, R. B. & Siegelbaum, S. A. Modulation of cyclic nucleotide-regulated HCN channels by PIP(2) and receptors coupled to phospholipase C. *Pflugers Arch.* **455,** 125–145 (2007).
74. Pian, P., Bucchi, A., Robinson, R. B. & Siegelbaum, S. A. Regulation of gating and rundown of HCN hyperpolarization-activated channels by exogenous and endogenous PIP2. *J. Gen. Physiol.* **128,** 593–604 (2006).
75. Zolles, G. *et al.* Pacemaking by HCN channels requires interaction with phosphoinositides. *Neuron* **52,** 1027–1036 (2006).
76. Flynn, G. E. & Zagotta, W. N. Molecular mechanism underlying phosphatidylinositol 4,5-bisphosphate-induced inhibition of SpIH channels. *J. Biol. Chem.* **286,** 15535–15542 (2011).

77. Zong, X. *et al.* A novel mechanism of modulation of hyperpolarization-activated cyclic nucleotide-gated channels by Src kinase. *J. Biol. Chem.* **280,** 34224–34232 (2005).
78. Arinsburg, S. S., Cohen, I. S. & Yu, H.-G. Constitutively active Src tyrosine kinase changes gating of HCN4 channels through direct binding to the channel proteins. *J. Cardiovasc. Pharmacol.* **47,** 578–586 (2006).
79. Yu, H.-G., Lu, Z., Pan, Z. & Cohen, I. S. Tyrosine kinase inhibition differentially regulates heterologously expressed HCN channels. *Pflugers Arch.* **447,** 392–400 (2004).
80. Li, C.-H. *et al.* Src tyrosine kinase alters gating of hyperpolarization-activated HCN4 pacemaker channel through Tyr531. *Am. J. Physiol. Cell Physiol.* **294,** C355-62 (2008).
81. Poolos, N. P. h-Channels and seizures: less is more. *Epilepsy Curr.* **5,** 89–90 (2005).
82. Munsch, T. & Pape, H. C. Modulation of the hyperpolarization-activated cation current of rat thalamic relay neurones by intracellular pH. *J. Physiol.* **519 Pt 2,** 493–504 (1999).
83. Munsch, T. & Pape, H. C. Upregulation of the hyperpolarization-activated cation current in rat thalamic relay neurones by acetazolamide. *J. Physiol.* **519 Pt 2,** 505–514 (1999).
84. Zong, X., Stieber, J., Ludwig, A., Hofmann, F. & Biel, M. A single histidine residue determines the pH sensitivity of the pacemaker channel HCN2. *J. Biol. Chem.* **276,** 6313–6319 (2001).
85. Stevens, D. R. *et al.* Hyperpolarization-activated channels HCN1 and HCN4 mediate responses to sour stimuli. *Nature* **413,** 631–635 (2001).
86. Santoro, B., Wainger, B. J. & Siegelbaum, S. A. Regulation of HCN channel surface expression by a novel C-terminal protein-protein interaction. *J. Neurosci.* **24,** 10750–10762 (2004).
87. Magee, J. C. Dendritic hyperpolarization-activated currents modify the integrative properties of hippocampal CA1 pyramidal neurons. *J. Neurosci.* **18,** 7613–7624 (1998).
88. Lorincz, A., Notomi, T., Tamas, G., Shigemoto, R. & Nusser, Z. Polarized and compartment-dependent distribution of HCN1 in pyramidal cell dendrites. *Nat. Neurosci.* **5,** 1185–1193 (2002).
89. Lewis, A. S. *et al.* Alternatively spliced isoforms of TRIP8b differentially control h channel trafficking and function. *J. Neurosci.* **29,** 6250–6265 (2009).
90. Lewis, A. S. *et al.* Deletion of the hyperpolarization-activated cyclic nucleotide-gated channel auxiliary subunit TRIP8b impairs hippocampal Ih localization and function and

promotes antidepressant behavior in mice. *J. Neurosci.* **31,** 7424–7440 (2011).

91. Han, Y. *et al.* Method for Identifying Small Molecule Inhibitors of the Protein-protein Interaction Between HCN1 and TRIP8b. *J. Vis. Exp.* (2016). doi:10.3791/54540
92. Lyman, K. A. *et al.* Allostery between two binding sites in the ion channel subunit TRIP8b confers binding specificity to HCN channels. *J. Biol. Chem.* **292,** 17718–17730 (2017).
93. Yi, F. *et al.* Autism-associated SHANK3 haploinsufficiency causes Ih channelopathy in human neurons. *Science* **352,** aaf2669 (2016).
94. Grabrucker, A. M. *et al.* Amyloid beta protein-induced zinc sequestration leads to synaptic loss via dysregulation of the ProSAP2/Shank3 scaffold. *Mol. Neurodegener.* **6,** 65 (2011).
95. Betancur, C. & Buxbaum, J. D. SHANK3 haploinsufficiency: a 'common' but underdiagnosed highly penetrant monogenic cause of autism spectrum disorders. *Mol. Autism* **4,** 17 (2013).
96. Leblond, C. S. *et al.* Meta-analysis of SHANK Mutations in Autism Spectrum Disorders: a gradient of severity in cognitive impairments. *PLoS Genet.* **10,** e1004580 (2014).
97. Rosti, R. O., Sadek, A. A., Vaux, K. K. & Gleeson, J. G. The genetic landscape of autism spectrum disorders. *Dev. Med. Child Neurol.* **56,** 12–18 (2014).
98. Carbonetto, S. A blueprint for research on Shankopathies: a view from research on autism spectrum disorder. *Dev. Neurobiol.* **74,** 85–112 (2014).
99. Zhu, M. *et al.* Shank3-deficient thalamocortical neurons show HCN channelopathy and alterations in intrinsic electrical properties. *J. Physiol.* (2018). doi:10.1113/JP275147
100. Wahl-Schott, C., Baumann, L., Zong, X. & Biel, M. An arginine residue in the pore region is a key determinant of chloride dependence in cardiac pacemaker channels. *J. Biol. Chem.* **280,** 13694–13700 (2005).
101. Yu, H. *et al.* MinK-related peptide 1: A beta subunit for the HCN ion channel subunit family enhances expression and speeds activation. *Circ. Res.* **88,** E84-7 (2001).
102. Decher, N., Bundis, F., Vajna, R. & Steinmeyer, K. KCNE2 modulates current amplitudes and activation kinetics of HCN4: influence of KCNE family members on HCN4 currents. *Pflugers Arch.* **446,** 633–640 (2003).
103. Qu, J. *et al.* MiRP1 modulates HCN2 channel expression and gating in cardiac myocytes. *J. Biol. Chem.* **279,** 43497–43502 (2004).

104. Gravante, B. *et al.* Interaction of the pacemaker channel HCN1 with filamin A. *J. Biol. Chem.* **279,** 43847–43853 (2004).
105. Much, B. *et al.* Role of subunit heteromerization and N-linked glycosylation in the formation of functional hyperpolarization-activated cyclic nucleotide-gated channels. *J. Biol. Chem.* **278,** 43781–43786 (2003).
106. Zha, Q., Brewster, A. L., Richichi, C., Bender, R. A. & Baram, T. Z. Activity-dependent heteromerization of the hyperpolarization-activated, cyclic-nucleotide gated (HCN) channels: role of N-linked glycosylation. *J. Neurochem.* **105,** 68–77 (2008).
107. Hegle, A. P., Nazzari, H., Roth, A., Angoli, D. & Accili, E. A. Evolutionary emergence of N-glycosylation as a variable promoter of HCN channel surface expression. *Am. J. Physiol. Cell Physiol.* **298,** C1066-76 (2010).
108. Lee, C.-H. & MacKinnon, R. Structures of the Human HCN1 Hyperpolarization-Activated Channel. *Cell* **168,** 111–120.e11 (2017).
109. Xu, X., Vysotskaya, Z. V, Liu, Q. & Zhou, L. Structural basis for the cAMP-dependent gating in the human HCN4 channel. *J. Biol. Chem.* **285,** 37082–37091 (2010).
110. Angstadt, J. D. & Calabrese, R. L. A hyperpolarization-activated inward current in heart interneurons of the medicinal leech. *J. Neurosci.* **9,** 2846–2857 (1989).
111. Hagiwara, N. & Irisawa, H. Modulation by intracellular Ca2+ of the hyperpolarization-activated inward current in rabbit single sino-atrial node cells. *J. Physiol.* **409,** 121–141 (1989).
112. Mitcheson, J. S., Chen, J. & Sanguinetti, M. C. Trapping of a methanesulfonanilide by closure of the HERG potassium channel activation gate. *J. Gen. Physiol.* **115,** 229–240 (2000).
113. Chen, J., Mitcheson, J. S., Lin, M. & Sanguinetti, M. C. Functional roles of charged residues in the putative voltage sensor of the HCN2 pacemaker channel. *J. Biol. Chem.* **275,** 36465–36471 (2000).
114. Chen, J., Mitcheson, J. S., Tristani-Firouzi, M., Lin, M. & Sanguinetti, M. C. The S4-S5 linker couples voltage sensing and activation of pacemaker channels. *Proc. Natl. Acad. Sci. U. S. A.* **98,** 11277–11282 (2001).
115. Proenza, C., Angoli, D., Agranovich, E., Macri, V. & Accili, E. A. Pacemaker channels produce an instantaneous current. *J. Biol. Chem.* **277,** 5101–5109 (2002).

116. Proenza, C. & Yellen, G. Distinct populations of HCN pacemaker channels produce voltage-dependent and voltage-independent currents. *J. Gen. Physiol.* **127,** 183–190 (2006).
117. Gao, W., Su, Z., Liu, Q. & Zhou, L. State-dependent and site-directed photodynamic transformation of HCN2 channel by singlet oxygen. *J. Gen. Physiol.* **143,** 633–644 (2014).
118. Nolan, M. F., Dudman, J. T., Dodson, P. D. & Santoro, B. HCN1 channels control resting and active integrative properties of stellate cells from layer II of the entorhinal cortex. *J. Neurosci.* **27,** 12440–12451 (2007).
119. Endo, T. *et al.* Dendritic Ih ensures high-fidelity dendritic spike responses of motion-sensitive neurons in rat superior colliculus. *J. Neurophysiol.* **99,** 2066–2076 (2008).
120. Doan, T. N. & Kunze, D. L. Contribution of the hyperpolarization-activated current to the resting membrane potential of rat nodose sensory neurons. *J. Physiol.* **514 (Pt 1,** 125–138 (1999).
121. Nolan, M. F. *et al.* A behavioral role for dendritic integration: HCN1 channels constrain spatial memory and plasticity at inputs to distal dendrites of CA1 pyramidal neurons. *Cell* **119,** 719–732 (2004).
122. Nolan, M. F. *et al.* The hyperpolarization-activated HCN1 channel is important for motor learning and neuronal integration by cerebellar Purkinje cells. *Cell* **115,** 551–564 (2003).
123. Stieber, J. *et al.* The hyperpolarization-activated channel HCN4 is required for the generation of pacemaker action potentials in the embryonic heart. *Proc. Natl. Acad. Sci. U. S. A.* **100,** 15235–15240 (2003).
124. Ludwig, A. *et al.* Absence epilepsy and sinus dysrhythmia in mice lacking the pacemaker channel HCN2. *EMBO J.* **22,** 216–224 (2003).
125. Chaplan, S. R. *et al.* Neuronal hyperpolarization-activated pacemaker channels drive neuropathic pain. *J. Neurosci.* **23,** 1169–1178 (2003).
126. Yao, H., Donnelly, D. F., Ma, C. & LaMotte, R. H. Upregulation of the hyperpolarization-activated cation current after chronic compression of the dorsal root ganglion. *J. Neurosci.* **23,** 2069–2074 (2003).
127. Dalle, C. & Eisenach, J. C. Peripheral block of the hyperpolarization-activated cation current (Ih) reduces mechanical allodynia in animal models of postoperative and

neuropathic pain. *Reg. Anesth. Pain Med.* **30,** 243–248 (2005).

128. Luo, L. *et al.* Role of peripheral hyperpolarization-activated cyclic nucleotide-modulated channel pacemaker channels in acute and chronic pain models in the rat. *Neuroscience* **144,** 1477–1485 (2007).
129. Jiang, Y.-Q., Sun, Q., Tu, H.-Y. & Wan, Y. Characteristics of HCN channels and their participation in neuropathic pain. *Neurochem. Res.* **33,** 1979–1989 (2008).
130. Takasu, K., Ono, H. & Tanabe, M. Spinal hyperpolarization-activated cyclic nucleotide-gated cation channels at primary afferent terminals contribute to chronic pain. *Pain* **151,** 87–96 (2010).
131. Emery, E. C., Young, G. T., Berrocoso, E. M., Chen, L. & McNaughton, P. A. HCN2 ion channels play a central role in inflammatory and neuropathic pain. *Science* **333,** 1462–1466 (2011).
132. Momin, A., Cadiou, H., Mason, A. & McNaughton, P. A. Role of the hyperpolarization-activated current Ih in somatosensory neurons. *J. Physiol.* **586,** 5911–5929 (2008).
133. Huang, H. & Trussell, L. O. Presynaptic HCN channels regulate vesicular glutamate transport. *Neuron* **84,** 340–346 (2014).
134. Goh, C.-S., Milburn, D. & Gerstein, M. Conformational changes associated with protein-protein interactions. *Curr. Opin. Struct. Biol.* **14,** 104–109 (2004).
135. Kern, D. & Zuiderweg, E. R. P. The role of dynamics in allosteric regulation. *Curr. Opin. Struct. Biol.* **13,** 748–757 (2003).
136. Csermely, P., Palotai, R. & Nussinov, R. Induced fit, conformational selection and independent dynamic segments: an extended view of binding events. *Trends Biochem. Sci.* **35,** 539–546 (2010).
137. Ma, B. & Nussinov, R. Enzyme dynamics point to stepwise conformational selection in catalysis. *Curr. Opin. Chem. Biol.* **14,** 652–659 (2010).
138. Changeux, J.-P. & Edelstein, S. Conformational selection or induced fit? 50 years of debate resolved. *F1000 Biol. Rep.* **3,** 19 (2011).
139. Biskup, C. *et al.* Relating ligand binding to activation gating in CNGA2 channels. *Nature* **446,** 440–443 (2007).
140. Kusch, J. *et al.* Interdependence of receptor activation and ligand binding in HCN2 pacemaker channels. *Neuron* **67,** 75–85 (2010).

141. Wu, S. *et al.* State-dependent cAMP binding to functioning HCN channels studied by patch-clamp fluorometry. *Biophys. J.* **100,** 1226–1232 (2011).
142. Wu, S. *et al.* Inner activation gate in S6 contributes to the state-dependent binding of cAMP in full-length HCN2 channel. *J. Gen. Physiol.* **140,** 29–39 (2012).
143. Mannikko, R., Pandey, S., Larsson, H. P. & Elinder, F. Hysteresis in the voltage dependence of HCN channels: conversion between two modes affects pacemaker properties. *J. Gen. Physiol.* **125,** 305–326 (2005).
144. Mannikko, R., Elinder, F. & Larsson, H. P. Voltage-sensing mechanism is conserved among ion channels gated by opposite voltages. *Nature* **419,** 837–841 (2002).
145. Bruening-Wright, A., Elinder, F. & Larsson, H. P. Kinetic relationship between the voltage sensor and the activation gate in spHCN channels. *J. Gen. Physiol.* **130,** 71–81 (2007).
146. Ryu, S. & Yellen, G. Charge movement in gating-locked HCN channels reveals weak coupling of voltage sensors and gate. *J. Gen. Physiol.* **140,** 469–479 (2012).
147. BoSmith, R. E., Briggs, I. & Sturgess, N. C. Inhibitory actions of ZENECA ZD7288 on whole-cell hyperpolarization activated inward current (If) in guinea-pig dissociated sinoatrial node cells. *Br. J. Pharmacol.* **110,** 343–349 (1993).
148. Rothberg, B. S., Shin, K. S., Phale, P. S. & Yellen, G. Voltage-controlled gating at the intracellular entrance to a hyperpolarization-activated cation channel. *J. Gen. Physiol.* **119,** 83–91 (2002).
149. Shin, K. S., Rothberg, B. S. & Yellen, G. Blocker state dependence and trapping in hyperpolarization-activated cation channels: evidence for an intracellular activation gate. *J. Gen. Physiol.* **117,** 91–101 (2001).
150. Barnes, S. & Hille, B. Ionic channels of the inner segment of tiger salamander cone photoreceptors. *J. Gen. Physiol.* **94,** 719–743 (1989).
151. DiFrancesco, D. Block and activation of the pace-maker channel in calf purkinje fibres: effects of potassium, caesium and rubidium. *J. Physiol.* **329,** 485–507 (1982).
152. Denyer, J. C. & Brown, H. F. Pacemaking in rabbit isolated sino-atrial node cells during Cs+ block of the hyperpolarization-activated current if. *J. Physiol.* **429,** 401–409 (1990).
153. Rothberg, B. S., Shin, K. S. & Yellen, G. Movements near the gate of a hyperpolarization-activated cation channel. *J. Gen. Physiol.* **122,** 501–510 (2003).

154. del Camino, D., Holmgren, M., Liu, Y. & Yellen, G. Blocker protection in the pore of a voltage-gated K+ channel and its structural implications. *Nature* **403,** 321–325 (2000).
155. Hackos, D. H., Chang, T.-H. & Swartz, K. J. Scanning the intracellular S6 activation gate in the shaker K+ channel. *J. Gen. Physiol.* **119,** 521–532 (2002).
156. Webster, S. M., Del Camino, D., Dekker, J. P. & Yellen, G. Intracellular gate opening in Shaker K+ channels defined by high-affinity metal bridges. *Nature* **428,** 864–868 (2004).
157. Zhou, M., Morais-Cabral, J. H., Mann, S. & MacKinnon, R. Potassium channel receptor site for the inactivation gate and quaternary amine inhibitors. *Nature* **411,** 657–661 (2001).
158. Colomer, J. *et al.* Long-term improvement of slow-channel congenital myasthenic syndrome with fluoxetine. *Neuromuscul. Disord.* **16,** 329–333 (2006).
159. Piccari, V., Deflorio, C., Bigi, R., Grassi, F. & Fucile, S. Modulation of the Ca(2+) permeability of human endplate acetylcholine receptor-channel. *Cell Calcium* **49,** 272–278 (2011).
160. Engel, A. G. *et al.* New mutations in acetylcholine receptor subunit genes reveal heterogeneity in the slow-channel congenital myasthenic syndrome. *Hum. Mol. Genet.* **5,** 1217–1227 (1996).
161. Muroi, Y., Arcisio-Miranda, M., Chowdhury, S. & Chanda, B. Molecular determinants of coupling between the domain III voltage sensor and pore of a sodium channel. *Nat. Struct. Mol. Biol.* **17,** 230–237 (2010).
162. Kochevar, I. E. Singlet oxygen signaling: from intimate to global. *Sci. STKE* **2004,** pe7 (2004).
163. Ogilby, P. R. Singlet oxygen: there is still something new under the sun, and it is better than ever. *Photochem. Photobiol. Sci.* **9,** 1543–1560 (2010).
164. DeRosa, M. C. & Crutchley, R. J. Photosensitized singlet oxygen and its applications. *Coord. Chem. Rev.* **233,** 351–371 (2002).
165. Kanofsky, J. R., Hoogland, H., Wever, R. & Weiss, S. J. Singlet oxygen production by human eosinophils. *J. Biol. Chem.* **263,** 9692–9696 (1988).
166. Prasad, A., Ferretti, U., Sedlarova, M. & Pospisil, P. Singlet oxygen production in Chlamydomonas reinhardtii under heat stress. *Sci. Rep.* **6,** 20094 (2016).
167. da Silva, E. F. F. *et al.* Intracellular singlet oxygen photosensitizers: on the road to solving

the problems of sensitizer degradation, bleaching and relocalization. *Integr. Biol. (Camb).* **8,** 177–193 (2016).

168. Baier, J. *et al.* Singlet oxygen generation by UVA light exposure of endogenous photosensitizers. *Biophys. J.* **91,** 1452–1459 (2006).
169. Baumler, W., Regensburger, J., Knak, A., Felgentrager, A. & Maisch, T. UVA and endogenous photosensitizers--the detection of singlet oxygen by its luminescence. *Photochem. Photobiol. Sci.* **11,** 107–117 (2012).
170. Mano, C. M. *et al.* Excited singlet molecular O(2)((1)Deltag) is generated enzymatically from excited carbonyls in the dark. *Sci. Rep.* **4,** 5938 (2014).
171. Steinbeck, M. J., Khan, A. U. & Karnovsky, M. J. Intracellular singlet oxygen generation by phagocytosing neutrophils in response to particles coated with a chemical trap. *J. Biol. Chem.* **267,** 13425–13433 (1992).
172. Klotz, L.-O., Kroncke, K.-D. & Sies, H. Singlet oxygen-induced signaling effects in mammalian cells. *Photochem. Photobiol. Sci.* **2,** 88–94 (2003).
173. Tour, O., Meijer, R. M., Zacharias, D. A., Adams, S. R. & Tsien, R. Y. Genetically targeted chromophore-assisted light inactivation. *Nat. Biotechnol.* **21,** 1505–1508 (2003).
174. Liao, J. C., Roider, J. & Jay, D. G. Chromophore-assisted laser inactivation of proteins is mediated by the photogeneration of free radicals. *Proc. Natl. Acad. Sci. U. S. A.* **91,** 2659–2663 (1994).
175. Agostinis, P. *et al.* Photodynamic therapy of cancer: an update. *CA. Cancer J. Clin.* **61,** 250–281 (2011).
176. Schweitzer, C. & Schmidt, R. Physical mechanisms of generation and deactivation of singlet oxygen. *Chem. Rev.* **103,** 1685–1757 (2003).
177. Valenzeno, D. P. & Tarr, M. Membrane photomodification of cardiac myocytes: potassium and leakage currents. *Photochem. Photobiol.* **53,** 195–201 (1991).
178. Eisenman, L. N. *et al.* Anticonvulsant and anesthetic effects of a fluorescent neurosteroid analog activated by visible light. *Nat. Neurosci.* **10,** 523–530 (2007).
179. Babes, A. *et al.* Photosensitization in Porphyrias and Photodynamic Therapy Involves TRPA1 and TRPV1. *J. Neurosci.* **36,** 5264–5278 (2016).
180. Jiang, H. N., Li, Y. & Cui, Z. J. Photodynamic Physiology-Photonanomanipulations in Cellular Physiology with Protein Photosensitizers. *Front. Physiol.* **8,** 191 (2017).

181. Robinson, R. B. & Siegelbaum, S. A. Hyperpolarization-activated cation currents: from molecules to physiological function. *Annu. Rev. Physiol.* **65,** 453–480 (2003).
182. Bisby, R. H., Morgan, C. G., Hamblett, I. & Gorman, A. A. Quenching of singlet oxygen by Trolox C, ascorbate, and amino acids: effects of pH and temperature. *J. Phys. Chem. A* **103,** 7454–7459 (1999).
183. Mendez-Hurtado, J., Lopez, R., Suarez, D. & Menendez, M. I. Theoretical study of the oxidation of histidine by singlet oxygen. *Chemistry* **18,** 8437–8447 (2012).
184. Craven, K. B. & Zagotta, W. N. CNG and HCN channels: two peas, one pod. *Annu. Rev. Physiol.* **68,** 375–401 (2006).
185. Roberts, J. E. & Dennison, J. The Photobiology of Lutein and Zeaxanthin in the Eye. *J. Ophthalmol.* **2015,** 687173 (2015).
186. Krishna, C. M., Uppuluri, S., Riesz, P., Zigler, J. S. J. & Balasubramanian, D. A study of the photodynamic efficiencies of some eye lens constituents. *Photochem. Photobiol.* **54,** 51–58 (1991).
187. Zigler, J. S. J. & Goosey, J. D. Singlet oxygen as a possible factor in human senile nuclear cataract development. *Curr. Eye Res.* **3,** 59–65 (1984).
188. Li, B., Lin, L., Lin, H. & Wilson, B. C. Photosensitized singlet oxygen generation and detection: Recent advances and future perspectives in cancer photodynamic therapy. *J. Biophotonics* **9,** 1314–1325 (2016).
189. Nussinov, R. Introduction to Protein Ensembles and Allostery. *Chemical reviews* **116,** 6263–6266 (2016).
190. Ferreiro, D. U., Hegler, J. A., Komives, E. A. & Wolynes, P. G. On the role of frustration in the energy landscapes of allosteric proteins. *Proceedings of the National Academy of Sciences of the United States of America Proc Natl Acad Sci U S A 108:3504.* **108,** 3499–3503 (2011).
191. Durand, C. M. *et al.* Mutations in the gene encoding the synaptic scaffolding protein SHANK3 are associated with autism spectrum disorders. *Nat. Genet.* **39,** 25–27 (2007).
192. Monteiro, P. & Feng, G. SHANK proteins: roles at the synapse and in autism spectrum disorder. *Nat. Rev. Neurosci.* **18,** 147–157 (2017).
193. Naisbitt, S. *et al.* Shank, a novel family of postsynaptic density proteins that binds to the NMDA receptor/PSD-95/GKAP complex and cortactin. *Neuron* **23,** 569–582 (1999).

194. Wang, X. *et al.* Altered mGluR5-Homer scaffolds and corticostriatal connectivity in a Shank3 complete knockout model of autism. *Nat. Commun.* **7,** 11459 (2016).
195. Han, Q. *et al.* SHANK3 Deficiency Impairs Heat Hyperalgesia and TRPV1 Signaling in Primary Sensory Neurons. *Neuron* **92,** 1279–1293 (2016).
196. Hulbert, S. W. & Jiang, Y.-H. Monogenic mouse models of autism spectrum disorders: Common mechanisms and missing links. *Neuroscience* **321,** 3–23 (2016).
197. Jiang, Y.-H. & Ehlers, M. D. Modeling autism by SHANK gene mutations in mice. *Neuron* **78,** 8–27 (2013).
198. Peca, J. *et al.* Shank3 mutant mice display autistic-like behaviours and striatal dysfunction. *Nature* **472,** 437–442 (2011).
199. Shcheglovitov, A. *et al.* SHANK3 and IGF1 restore synaptic deficits in neurons from 22q13 deletion syndrome patients. *Nature* **503,** 267–271 (2013).
200. Wang, X., Xu, Q., Bey, A. L., Lee, Y. & Jiang, Y.-H. Transcriptional and functional complexity of Shank3 provides a molecular framework to understand the phenotypic heterogeneity of SHANK3 causing autism and Shank3 mutant mice. *Mol. Autism* **5,** 30 (2014).
201. Zhou, Y. *et al.* Mice with Shank3 Mutations Associated with ASD and Schizophrenia Display Both Shared and Distinct Defects. *Neuron* **89,** 147–162 (2016).
202. Arons, M. H. *et al.* Shank3 Is Part of a Zinc-Sensitive Signaling System That Regulates Excitatory Synaptic Strength. *J. Neurosci.* **36,** 9124–9134 (2016).
203. Bariselli, S. *et al.* SHANK3 controls maturation of social reward circuits in the VTA. *Nat. Neurosci.* **19,** 926–934 (2016).
204. Peixoto, R. T., Wang, W., Croney, D. M., Kozorovitskiy, Y. & Sabatini, B. L. Early hyperactivity and precocious maturation of corticostriatal circuits in Shank3B(-/-) mice. *Nat. Neurosci.* **19,** 716–724 (2016).
205. Bozdagi, O. *et al.* Haploinsufficiency of the autism-associated Shank3 gene leads to deficits in synaptic function, social interaction, and social communication. *Mol. Autism* **1,** 15 (2010).

VITA

VINAY KUMAR IDIKUDA
idikudav@vcu.edu

EDUCATION

Ph.D. Neuroscience- Virginia Commonwealth University, 2013-Current
M.S Pharmacology- Idaho State University, January 2011 - July 2013
B.S Pharmacy- Osmania University, October 2007 - July 2010

SELECTED PUBLICATIONS:

1. **Mengye Zhu*, Vinay Idikuda*,** Jianbing Wang, Virang Kumar, Nikhil Shah, Qinglian Liu, Lei Zhou. HCN Channelopathy causes major alterations in intrinsic electrical properties of Shank3-deficient neurons. 2017 **(**equal contribution**, Journal of Physiology., 2018)**
2. **Vinay Idikuda***, Weihua Gao, Zhuocheng Su, Khade Grant, Qinglian Liu, and Lei Zhou. Singlet oxygen mediated modification of sea urchin hyperpolarization activated cyclic nucleotide gated (spHCN) Channel. 2017 **(submitted to Journal of General Physiology Under Review)**
3. **Vinay Idikuda***, **Weihua Gao*,** Zhuocheng Su, Qinglian Liu, and Lei Zhou. Unique ligand binding profile of sea urchin HCN channel in its inactivated state. 2017 **(Submitted to Journal of General Physiology, Under review)**
4. Tadinada SM, Lai MB**, Idikuda VK**, Mukka K, Singh MRM, Pfau J, Bhushan A, Leung SW & Lai JCK (2013) Zinc Oxide Nanoparticles Induced Apoptosis and Necrosis in Hepatocellular Carcinoma HepG2 Cells. In Technical Proceedings of the 2013 NSTI Nanotechnology Conference & Expo – Nanotech 2013, Vol. 3, Chapter 5. Environmental Health & Safety, pp. 433-436.
5. **Idikuda VK**, Jaiswal AR, Wong YYW, Bhushan A, Leung SW & Lai JCK (2012) Cytotoxicity of Magnesium Oxide Nanoparticles in Schwann Cells. In Technical Proceedings of the 2012 NSTI Nanotechnology Conference & Expo – Nanotech 2012, Vol. 3, Chapter 5: Environmental Health & Safety, pages 342-345.

PRESENTATIONS:

1. **Idikuda V**, Tammy Zhao, Qinglian Liu, Lei Zhou. Photodynamic modification of rod CNGA1 channel. Poster presentation, 2018, Biophysical society meeting, San Francisco, CA.
2. **Idikuda V**, Christopher Waite, Khade Grant, Lei Zhou. Scaffolding protein SHANK3 modulates HCN channel expression and function. Poster Presentation, 2017, Biophysical Society Meeting, New Orleans, LA.
3. **Idikuda V**, Zhuocheng Su, Weihua Gao, Lei Zhou. Photodynamic transformation of spHCN channel. Poster Presentation, 2014 Biophysical Society Meeting, Baltimore, MD.
4. **Vinay K. Idikuda**, Alfred O. Isaac, Alok Bhushan and James C.K. Lai. Differential Effects of Chronic Mitochondrial DNA depletion on Schwann Cells and DRG Neurons. Poster presentation 2012 Society for Neuroscience, New Orleans LA.
5. **Vinay K. Idikuda**, Ashvin R. Jaiswal, Yin Yin W. Wong, Alok Bhushan, Solomon W Leung, and James C.K. Lai. Cytotoxicity of Magnesium Oxide Nanoparticles in Schwann Cells. Poster presentation 2012 Nanotech Conference and Expo, Santa Clara CA.
6. **Vinay Kumar Idikuda**, Ashvin R. Jaiswal, Yin Yin W. Wong, Solomon W. Leung, Christopher K. Daniels, and James C.K. Lai. Magnesium Oxide Nanoparticles induce Cytotoxic and

Proinflammatory effects in Schwann Cells and DRG neurons. Poster presentation 2012 Experimental Biology, San Diego CA.

SERVICE:

Treasurer and Executive Committee member - Tiranga Indian Nationals at VCU, 2014-2015

- Tiranga is one of the largest student organizations at VCU. As a treasurer and executive member my Responsibilities included Annual budget management and review, event management, coordinating various committees and delegating responsibilities.

Adviser and Risk Management Chair- Tiranga Indian Nationals at VCU, 2015-2017

- Roles included supervising the executive committee on the event planning.
- Assisting in team building by serving on the recruitment panel and hosting orientation workshops.

Co-founding Member and Treasurer- Cricket club at VCU, 2014-2015

- Initiated the Cricket club at VCU with interested candidates from all over VCU.
- Formulated the constitution of the organization.

Adviser- Cricket Club at VCU, 2015-2016

- Roles included assisting the executive committee on the event planning, decision making and serving on the recruitment panel.

Treasurer- Associated Graduate Students of Pharmacy, 2012-2013

- Annual budget preparation, accounting and presenting the budget to the whole committee.
- Proposing budget to the university appropriations committee.

Member of editorial board- "PHARMERA-2008", 2008-2009

- Collected and evaluated the scientific articles written by students on current global issues and selected the best ones to be published in the yearly college magazine.

Co-ordination committee member "INDO-U.S. Pharmaceutical Regulatory Symposium"

- Co-ordinated various committees and helped in conflict resolution between various teams to ensure efficient hosting of the pharmaceutical regulatory symposium held by Nalanda College of pharmacy in October-2009.